RESULTS & DISCUSSION

Results and Discussion

PART (I)

Design and synthesis of aromatic enone and dienone analogues of curcumin

Curcumin [1,7-bis(4-hydroxy-3-methoxy-phenyl)-hepta-1,6-diene-3,5-dione] **(1)** is a natural yellow-orange dye extracted from the rhizomes of the plant *Curcuma Longa L. (zingiberaceal).*[133] A variety of pharmacological properties such as antitumer,[76] and anticancer,[134] activities were reported. It has also been used as a photodynamic agent useful for the destruction of bacteria,[135] and tumer cells.[136] from the toxicological studies, however, curcumin is non-toxic even at high dosage.[137] Attempts to use it as an antioxidant additive for lubricants and motor oils,[138] photoresists,[139]and sunscreen compounds,[140] have also been made.

On the other hand, derivatives of hydroxy arylazobenzene are well known as dyes.[141-143] Consequently, the author decided to couple the diazonium salt of different aromatic amines with curcumin **(1)** with a view to synthesis new azodisperse dyes to explore the possibility of finding some new azodyes capable of dyeing different fibres and with highly expected wide spectrum of biological activity.

In the present investigation some new arylazo curcumin **(2a-f)** were prepared. The effect of the nature of substituents on the colour of the azodyes is discussed.

Diazonium salts undergo a coupling reaction with [1,7-bis(4-hydroxy-3-methoxy-phenyl)-hepta-1,6-diene-3,5-dione] **(1)** to give the corresponding 4-arylazo derivatives **(2a-f)**. However, to our knowledge, no details regarding the synthesis, biological evaluation and dyeing behaviour

of such dyes as disperse dyes for dyeing different fibres have been reported so far.

In accordance with the nomenclature of arylazo curcumin, the general structure formula for 1,7-bis-(4-hydroxy-3-methoxy-phenyl)-hepta-1,6-diene-4-arylazo-3,5-dione **(2a-f)** should be as follows:

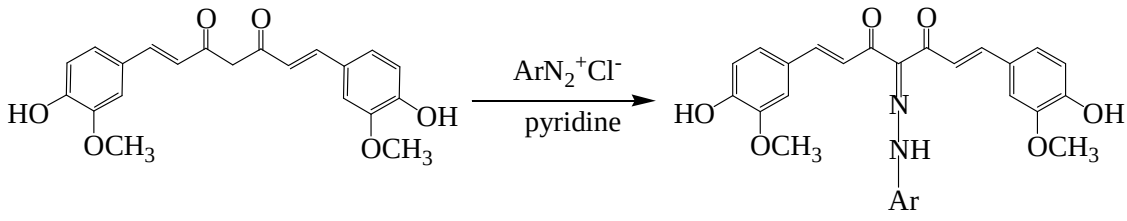

1 **2a-f**

2a , Ar = C_6H_4- OCH_3-p
2b , Ar = C_6H_4- CH_3-p
2c , Ar = C_6H_5
2d , Ar = C_6H_4- Cl-p
2e , Ar = C_6H_4- NO_2-p
2f , Ar = C_6H_4 -N=N-Ph-p

Scheme 1

It was, therefore considered worth while to prepare azodisperse dyes containing curcumin moiety for dyeing of cellulose, other synthestic fibres and/or biological evalutation. In the present investigation, six 4-arylazo curcumin **(2a-f)** have been prepared by coupling curcumin with the appropriate diazonium salt in pyridine. These dyes have been characterized by elemental analysis and assessment of their spectra in the ultra-violet, visible and infrared regions, in addition to their H^1-NMR and mass spectra. Compound **(2a-f)** can be exist in the following tautomeric form:

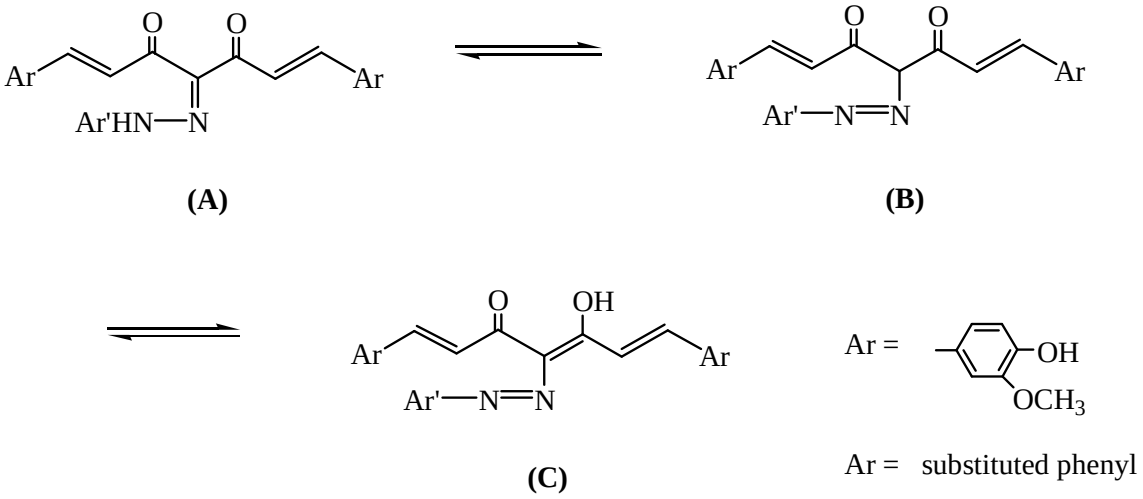

(cf. Scheme 1)

From the infrared measurements of the prepared arylazo derivatives **(2a-f)**, presence of strong bands in the region 1550-1580 cm^{-1} indicating the (–N=N–) stretching frequency and the (NH) absorption was recorded at 3250 cm^{-1} besides the (OH) stretching at 3400 cm^{-1}, and in a tautomeric mixture,[141] as well. Furthermore, the *α,β*-unsaturated carbonyl function appeared at 1690 cm^{-1}.

Generally, variation in colour of these dyes results from the alternation in the diazonium components.

The UV spectra of the diazonium coupling products of **(1)** provide additional evidence that such compounds have the tautomeric relation with azo-hydrazo system.

Most of the dyes show four absorption bands in the region 196-438 nm. The relatively small differences in λ_{max} may be due to the polarity change of the absorbing system caused by solvent interactions due to the general solvent effect.[142] It has been reported that UV spectra of monophenyl azo compounds differ from those of monophenyl hydrazones. The azo compounds generally show two absorption bands at 400-410 and

290-300 nm corresponding to n-π* and π-π* transitions respectively.[143] On the other hand, monophenyl hydrazones show three intense bands at 220-230, 250-280, and 330-390 nm regions.[142]

The UV spectra of compounds **(2a-f)** investigated can be interpreted in terms of the tautomeric mixture as well.

It is clear that these dyes exhibit four bands, of these, the medium and the high wavelength bands seem to be affected by the nature of the polar substituents in the arylazo group, and the low wavelength bands is unaffected.

In general, the presence of electrondonating and electronwithdrowing groups has not brought about any marked increase or decrease in λ_{max}. in the visible region and log € has nearly remained constant. This does point towards the presence also of hydrazone structure **(A)** where the resonance interactions with the substituents in the diazo component are minimal due to steric factors.

The H^1-NMR spectrum of compounds **(2a-f)**, in general, showed signals at 3.95 (s, 6H, 2×OCH_3), 5.8 (s, 1H, CH), 5.86 (s, 2H, 2×OH), 6.43 (d, j= 13 HZ, 2H, CH=CH), 6.91 (m, 6H, 2×C_6H_3), 7.55 (d, j= 13 HZ, 2H, CH=CH). In the H^1-NMR of **(2)**, the absence of signal in the region of (NH) protons gives an additional evidences to this structure. And suggested the presence of two trans-cinnamoyl groups.

The mass spectra of curcumin and its dyes **(2a-f)** showed in **fig 1-7**. (see experimental part). In general, **Scheme 2** showed a typical mass fragmentation route of curcumin **(1)** and its dyes derivatives **(2a-f)**.

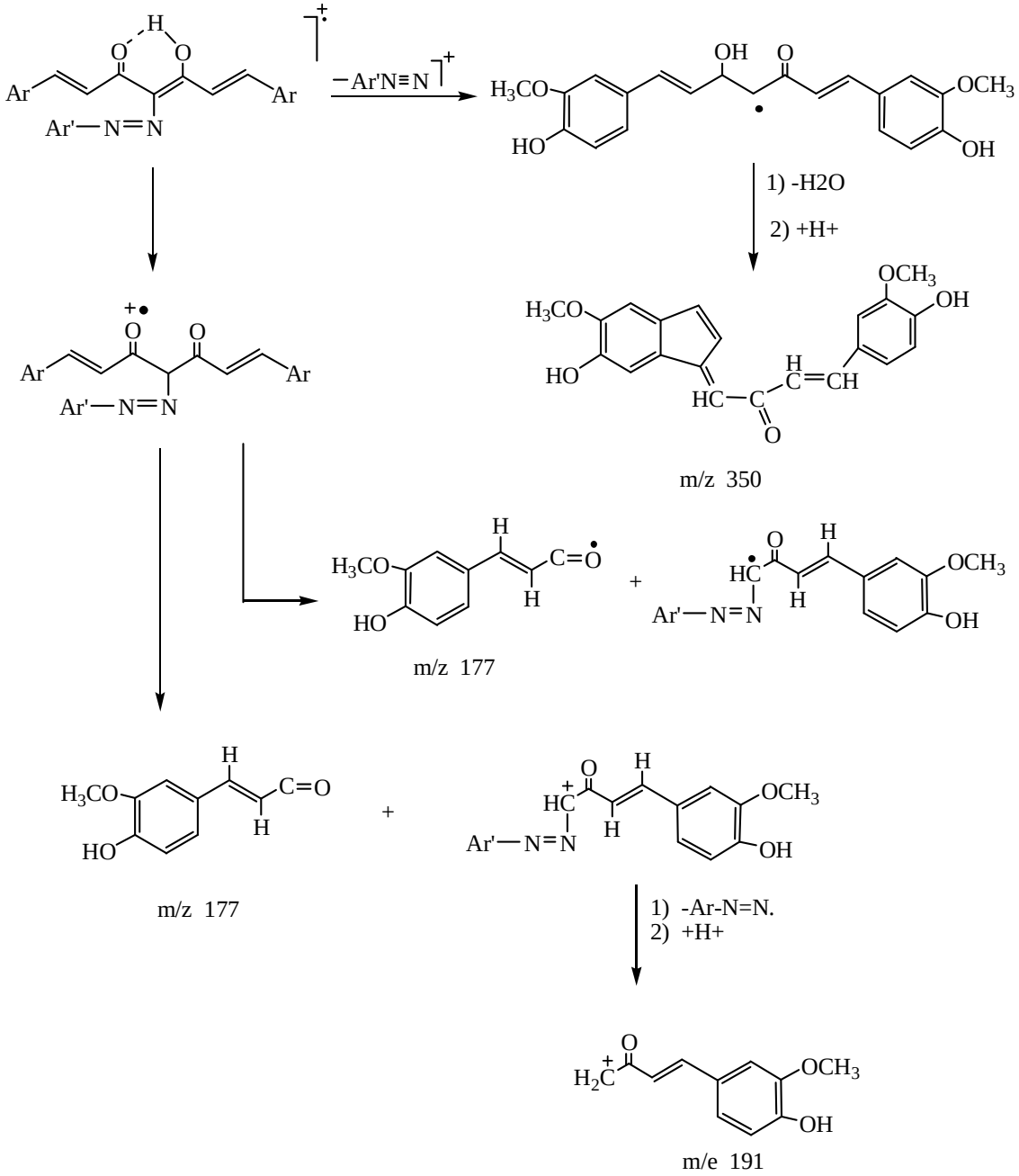

Scheme 2

On the other hand, it was studied also the coupling reaction of curcumin **(1)** with diazonium salt in sodium hydroxide medium (10%). Thus, it was found that, *p*-chlorophenyl diazonium chloride was coupled

with curcumin **(1)** in the ratio (2:1), respectively, in sodium hydroxide solution to give the corresponding bisarylazo derivative **(3)** in good yield.

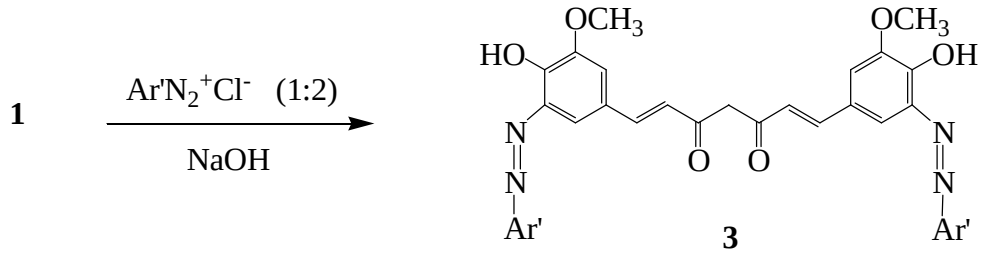

3

Ar' = C_6H_4.Cl-p

1,7-bis-[3-(4-chloro-phenylazo)-4-hydroxy-5-methoxy-phenyl]-hepta-1,6-diene-3,5-dione.**(3)**

Structure **(3)** was established on the basis of both elemental and spectral analysis. So, the IR of this compound indicates the azo-hydrazo tautomerism of such compounds and showed characteristic absorption bands at 3420, 1700, 1600, and 1580 cm^{-1} corresponding to the stretching frequencies to (OH), (C=O), (C=C) and (N=N) groups , respectively.

More over, the structure of compounds **(3)** were more confirmed by the mass spectrophotometric measurement which showed the molecular ion peak at m/e 644 (M^+-1). **(Fig 8)**

In continuation of our research program to synthesis some new antibacterial and antiviral agents, and the fact that some bromo and bromoketone compounds possess significant antibacterial activity.[144-147] These facts prompted us to synthesis the dibromo derivative **(4)**. Thus, treatment of 1,7-bis-[3-(4-nitrophenylazo)-4-hydroxy-5-methoxy)]hepta-1,6-diene-3,5-dione **(2e)** with bromine in the presence of glacial acetic acid afforded the corresponding 6,7-dibromo-1,7-bis-[3-(4-nitrophenylazo)-4-hydroxy-5-methoxy]hepta-1-ene-3,5-dione **(4)**.

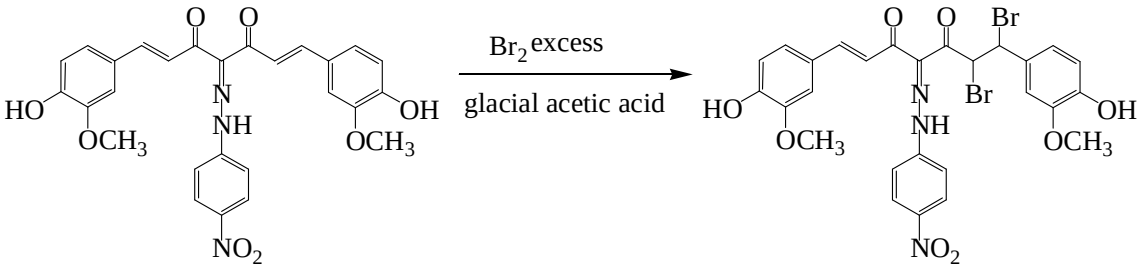

2e **4**

The structure of compound **(4)** was elucidated on the basis of both analytical and spectral data. The IR spectra of **(4)** in general showed absorption bands at 3425, 1665, 1581 and 700 cm^{-1} due to (OH), (C=O), (N=N) and (C-Br) groups, respectively. Moreover, the mass spectrum of **(4)** showed the molecular ion peak at m/e at 678 (M^{+}+1). **(Fig 9)**

The continuing search for molecules that possess the sedative-hypnotic properties of the barbiturates but show a better pharmacologic ratio has taken many directions.[148] Compound **(2e)** represents an adaptable starting material for the introduction of heterocyclic moieties in its 3- & 5-positions, and for the synthesis of some new heterocyclic binary system which have demonstrated biological activity in different areas of chemotherapy.

Thus, condensation of **(2e)** with thiourea was carried out in molar ratio (1:2), respectively, in boiling ethanolic sodium ethoxide to give the corresponding (*Z*)-4-(4-hydroxy-3-methoxy-phenyl)-6-[{6-(4-hydroxy-3-methoxy-phenyl)-2-thioxo-1,2,5,6-tetrahydro-pyrimidine-4-yl}(2-(4-nitrophenyl)hydrazono)methyl]-5,6-dihydropyrimidine-2*(1H)*-thione **(5)**.

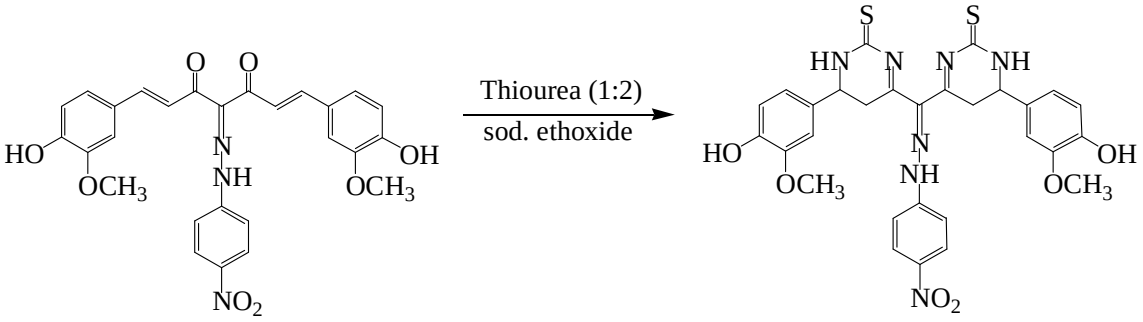

2e **5**

The structure of **(5)** was confirmed by its IR spectrum which showed the absence of spectrum band in the region of 1600 and 1690 cm^{-1}, i.e. the *α,β*-unsaturated ketone was involved in the cyclocondensation process, and in the same time the IR spectrum showed new bands at 3220, 1620 and 1273 cm^{-1} due to cyclic (NH), (C=N) and (C=S) functions, respectively. The H^1-NMR revealed bands at δ 1.7, 1.5 (m, CH_2), 1.8, 2.0 (m, CH_2), 2.6 (t, CH), 3.8 (s, 2×OCH_3), 3.9 (t, CH), 6.68-8.0(m, Ar-H), 9.8 (s, 2×OH), 10.6 (s, NH), the cyclic (NH) protons may be at δ 2.0, it is difficult to be observed. Moreover, the mass spectrum gave an additional evidence for the proposed structure, which showed fragments at m/e 632 (M^+-1), 630, 612, 496, 478, 393, 315, 227, 155 and 57. **(Fig. 10)**

In continuation of our interest in pyrimidinthione chemistry, and with a view directed towards preparing biological active heterocyclic compounds, we wish to broaden the scope of cyclocondensation reaction

Utilizing **(2e)** as candidates for facile synthetic route to heterocyclic pyrimidinthione resulted in the formation of new pyrimidinthione derivative **(6)**. Thus, (*1Z,3E*)-4-(4-hydroxy-3-methoxy-phenyl)-1-[6-(4-hydroxy-3-methoxy-phenyl)-2-thioxo-2,3,4,5-tetrahydro-pyrimidine-4-yl]-1-[2-(4-nitrophenyl)hydrazono]-but-3-ene-2-one **(6)** was prepared by

refluxing compound **(2e)** with thiourea (1:1) molar ratio in boiling ethanolic sodium ethoxide.

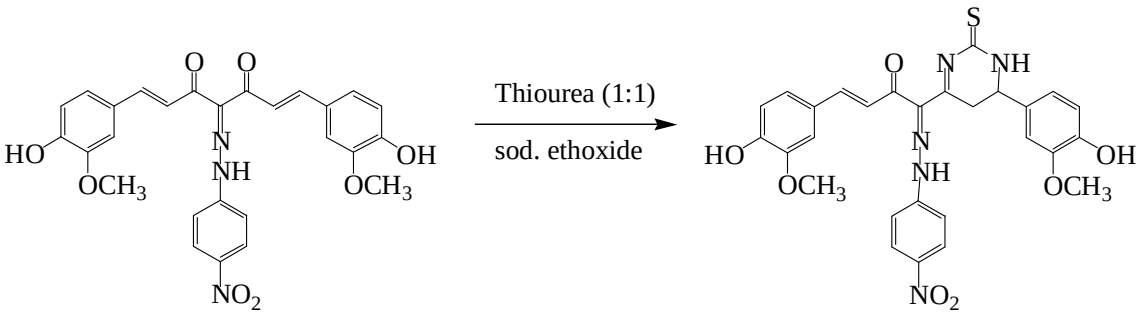

2e **6**

Structure **(6)** was deduced from both correct analytical and spectral data. The IR spectrum showed bands at 3400, 3230-3210, 2930, 1690, 1620, 1275 cm^{-1} corresponding to the absorption frequencies of (OH), (NH), (CH_2), (CO), (C=N) and (C=S), respectively. The H^1-NMR spectrum revealed the presence of doublet signals at δ 6.79, 7.7 of olefinic protons, multiplet at δ 1.5, 1.7 (CH_2), triplet at 2.6 (CH), singlet at δ 2.0 (NH pyrimidine) and 3.8 ppm (s, 2×OCH_3). In addition, the mass spectrum showed the molecular ion peak at 575 (M^+, 4%). **(Fig 11)**

Similar to the behavior of **(2e)** towards thiourea in presence of base medium, it has been found that (*Z*)-4-{5-[{5-(4-hydroxy-3-methoxy-phenyl)-2,3-dihydroisoxazol-3-yl}[2-(4-nitrophenyl)hydrazono]methyl]-2,3-dihydroisoxazole-3-yl}-2-methoxy-phenol **(7)** has been prepared by reaction of **(2e)** with hydroxylamine hydrochloride in refluxing pyridine. The structure of compound **(7)** was proved by IR spectrum which showed no absorption bands of (CO) and (C=C) groups i.e. the both *α,β*-unsaturated ketone function was involved in the ring closure, in addition to the presence

of stretching frequencies at 3400, 3240, 3220, 2929 and 1594 cm^{-1} attributable to the (OH), (2NH), (CH) and (N=N) groups, respectively.

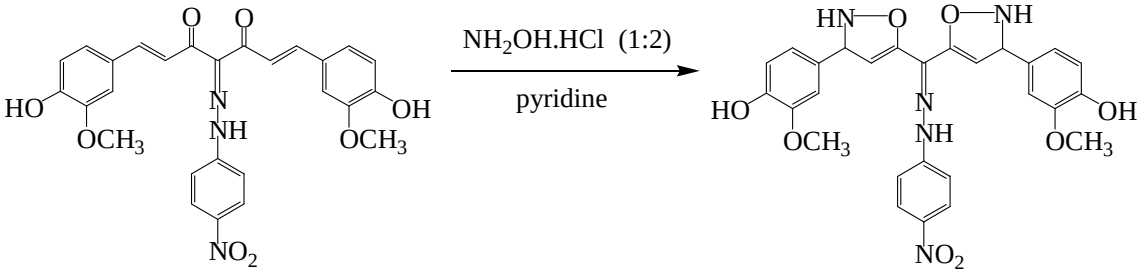

2e **7**

Moreover,the mass spectrum of **(7)** showed the molecular ion peak at m/e at 546 (M^{+}-1). **(Fig 12)**

α,β-unsaturated ketones react with hydrazine or with substituted hydrazines to yield pyrazoline derivatives.[149] In addition, pyrazoline derivatives rank some of the more venerable nonsteroidal anti-inflammatory agents. The activity of antipyrine was discovered not too long after that of aspirin. As an extension of our interest in the synthesis of new heterocycles in corporating a pyrazole nucleus,[150] we report here the behavior of **(2e)** towards hydrazine hydrate and/or its derivatives as a facile and convenient route to some heterocyclic derivatives containing a pyrazole moiety.

Therefore, the reaction of diferuloyl-(4-nitrophenyl)methane **(2e)** with hydrazine hydrate in (1:3) molar ratio in boiling mixture of ethanol-glacial acetic acid afforded the bis pyrazolyl derivative **(8)**.

The structure of **(8)** was established by both elemental and spectral data. The IR spectrum showed the absence of the carbonyl band at 1690 cm^{-1} and the olifenic (C=C) at 1600 cm^{-1}, and also showed the presence of

absorption frequencies at 3400, 3230, 3210, 2900 and 1620 due to (OH), (2NH), (CH) and (C=N) functions, respectively.

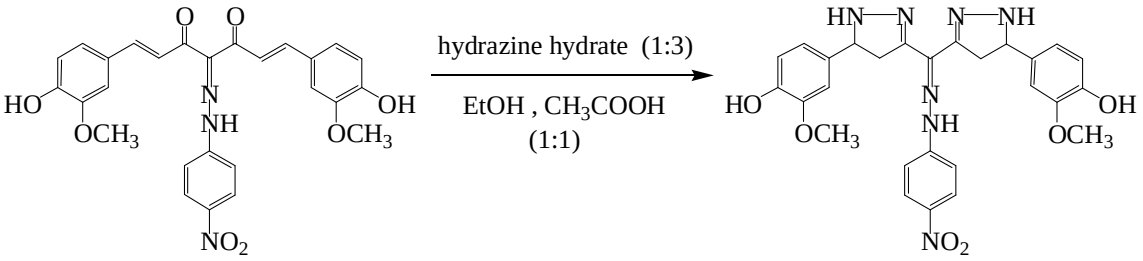

2e **8**

The H^1-NMR spectrum revealed the absence of signals at δ 6.5 and 7.5 of olifenic protons and instead appeared signal at δ 3.9 due to the methylene protons of pyrazole ring. The mass spectrum showed m/e 545 (M^+). **(Fig. 13)**

On the other hand, it was found that, when compound **(2a)** was refluxed with hydrazine hydrate in molar ratio (1:1) in refluxing mixture of ethanol-glacial acetic acid (1:1) afforded the corresponding *α,β*-unsaturated ketopyrazolinylmethane derivative **(9)**.

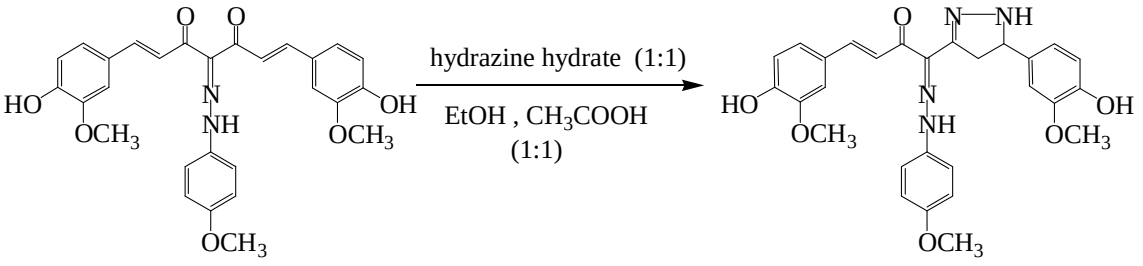

2a **9**

The formation of compound **(9)** was established on the basis of both elemental analysis and spectral data. The H^1-NMR spectrum revealed the absence of the doublet signal at δ 6.9 of the olifenic protons and showed

the other doublet signal at δ 7.5 of the other olefinic protons, and showed a new singlet signal at δ 3.9 ppm due to the methylene protons of the pyrazole ring, in addition to the other expected bands (cf. experimental part). The IR spectrum showed also an absorption bands at 3400, 3220-3230, 2900, 1690, 1620 and 1580 cm^{-1} attributable to the frequencies of (OH), (2NH), (CH_2), (CO), (C=N) and (N=N) functions, respectively.

Moreover, the mass spectrum **(Fig. 14)** gave an addition evidence to the proposed structure which showed the molecular ion peak at m/e 517 (M^++1).

Similarly, refluxing of **(2a)** with phenyl hydrazine in a molar ratio (1:1) in boiling ethanol catalyzed with few drops of glacial acetic acid, yielded the corresponding 4-(4-hydroxy-3-methoxy-phenyl)-1-[5-(4-hydroxy-3-methoxy-phenyl)-2-phenyl-2,5-dihydro-*1H*-pyrazol-3-yl]-1-[(4-methoxphenyl)-hydrazono]-but-3-ene-2-one **(10)**.

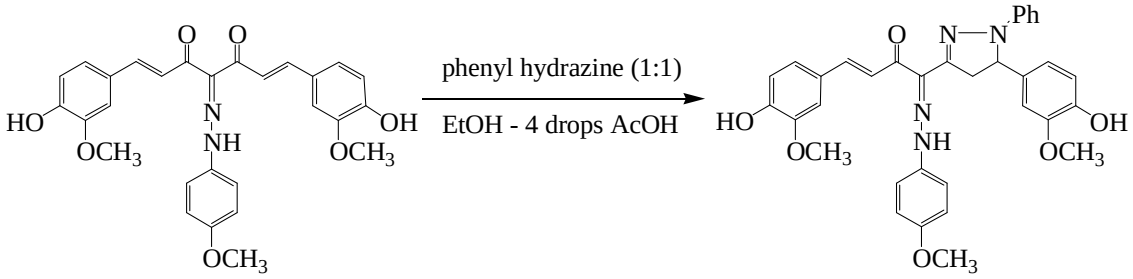

2a **10**

The structure of compound **(10)** was elucidated on the basis of both analytical and spectral data. The IR spectrum showed absorption bands at 3425, 3300, 1690, 1620 and 1582 cm^{-1} due to the frequencies of (OH), (NH), (C=O), (C=N) and (N=N) functions, respectively. In addition, the mass spectrum showed the molecular ion peak at m/e 592 (M^+). **(Fig 15)**

It has been reported that some pyridine derivatives possess considerable antimicrobial activities.[151,152] In the main time, it is well known that bis compounds are more potent than the corresponding mono derivatives. In connection of our search towards the design and synthesis of heterocyclic analogues of curcumin as potential chemotherapeutic agents, it was decided to take 4-[(4-chlorophenyl)-hydrazono]-1,7-bis-(4-hydroxy-3-methoxy-phenyl)hepta-1,6-diene-3,5-dione **(2d)** as adaptable starting material for the synthesis of new heterocyclic binary system with the hope that the new compounds may exert more potent effect. We report here the synthesis of a new bis byridyl derivative. Thus, it was found that, compound **(2d)** reacted with ethyl acetoacetate in boiling ethanolic sodium ethoxide in (1:2) molar ratio, respectively, afforded the Michael adduct 2,10-diacetyl-6-[(4-chloro-phenyl)-hydrazono]-3,9-bis-(4-hydroxy-3-methoxy-phenyl)-5,7-dioxo-undecanedioic acid diethyl ester **(11)**.

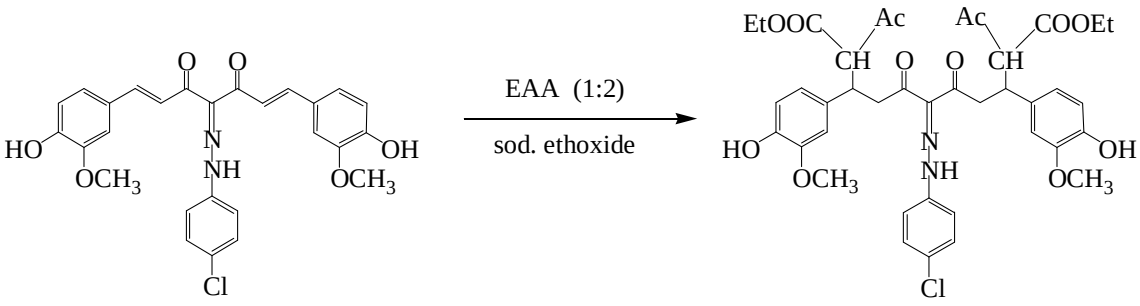

2d **11**

The structure of compound **(11)** was established based on both analytical and spectral analyses. The IR spectrum showed absorption bands assignable to two sets of frequencies at 3424, 3220, 3100-2900, 1735, 1730, 1710 and 1581 cm^{-1} due to (OH), (NH), (CH_3, CH_2, CH), (CO), (acetyl CO), (ester CO) and (N=N) functions, respectively.

The structure of **(11)** was further confirmed from its mass-spectrum which showed the molecular ion peak at m/e 768 (M^++1). **(Fig 16)**

The Michael adduct **(11)** was further subjected to react with excess ammonium acetate in boiling glacial acetic acid to give the corresponding (*Z*)-ethyl-6-{2-(4-chloro-phenyl)hydrazono}[4-(4-hydroxy-3-methoxy-phenyl)-6-1,4-dihydropyridin-2-yl]-4-(4-hydroxy-3-methoxy-phenyl)-2-methyl-1,4-dihydropyridine-3-carboxylate **(12)**.

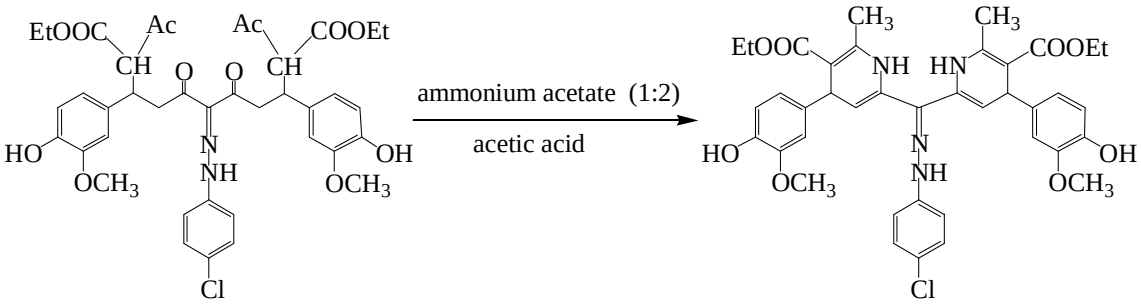

11 **12**

The IR spectrum of **(12)** showed absorption bands at 3400, 3300, 2900-3000, 1720, 1595 and 1580 cm^{-1} due to the frequencies of (OH), (NH), (CH_3), (CH), (CO ester), (C=C) and (N=N) functions. The H^1-NMR revealed signals at δ 1.3 (t, 2×CH_3CH_2), 2.26 (s, 2×CH_3), 3.83 (s, 2×OCH_3), 4.2 (q, 2CH_2CH_3), 4.4 (s, 2×CH), 6.6-7.5 (m, Ar-H), 9.83 (s, 2×OH) and 13.2 (s, =N-NH), while the mass spectrum showed molecular ion peak at m/e 729 (M^+). **(Fig 17)**

Extensive studies on the structure-activity relationship of curcuminoids have revealed that phenol ring structures of the compound may be essential for the antioxidant activity,[153] and diketone moiety of THC also involves antioxidative mechanism of the compound.[154] In addition, phenolic hydroxyl or methoxyl groups were modified to enhance

the potency of other biological activities of curcumin including the induction of phase 2 detoxification enzymes and the inhibition of HIV-1 integrase.[155,156] These studies suggest that diketone moiety of curcumin may be essentially involved in its broad-range biological activities. We have developed several new synthetic derivatives of curcumin to enhance the biological activity, especially, anti-angiogenic activity of the compound.

Thus, it was found that, diketone moieties of curcumin was replaced with hydrazine hydrate in refluxing glacial acetic acid. One step coupling of **(1)** with hydrazinium dihydrochloride gave compound **(13)**. The compound was purified by crystallization from ethanol to give a pall yellow crystals which was analyzed for $C_{21}H_{20}N_2O_4$ by elemental analysis. Our procedure for the synthesis of **(13)** is considered the best one reported still now.[28,29,157] (optimum reaction time and the highest yield).

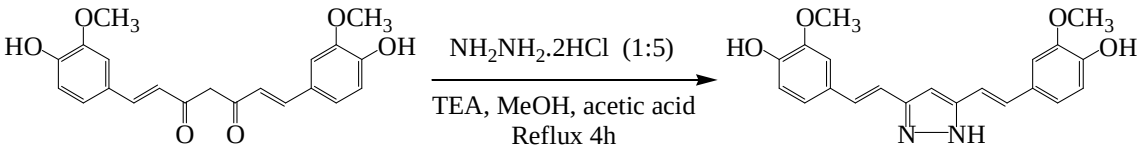

1 **13**

4,4'-(*1E,1'E*)-2,2'-(*1H*-pyrazole-3,5-diyl)-bis-(ethane-2,1-diyl)-bis--[2-(4-chloro-phenyl)]diazenyl-6-methoxy-phenol **(13)** was proved on the basis of both analytical and spectral data. The H^1-NMR spectrum revealed the olefinic protons of a trans-double bond at δ 6.9 and 7.4 ppm, and contained signal at δ 6.6 of methane proton. Since the intensity of the proton signal was almost half of others, this methane must be corresponded to the C-10 symmetric center of the molecule.

In addition, the H^1-NMR showed singlet signal at δ 9.6 attributable to NH proton. The IR spectrum showed the bands of the two carbonyl groups and instead showed bands at 1620 and 3230 cm^{-1} due to the (C=N) and (NH) groups of the pyrazole ring. The mass spectrum gives a more evidence for the proposed structure. **(Fig 18)**

In continuation of our study on the chemistry of heterocyclic and the synthesis of new ring system of curcumin with the hope to have a pharmacological importance, we report herein on the use of compound **(13)** as a key intermediate for the synthesis of new series of curcumin derivatives, which have not been investigated so far. Selective *N*-bromination of **(13)** using *N*-bromosuccinimide in chloroform gave a gummy bromopyrazoline derivative **(14)** which was converted directly into the corresponding 4,4'-(*1E,1'E*)-2,2'-(1-hydrazinyl-*1H*-pyrazole-3,5-diyl)-bis-(ethane-2,1-diyl)-bis-(2-methoxy-phenol) **(15)**

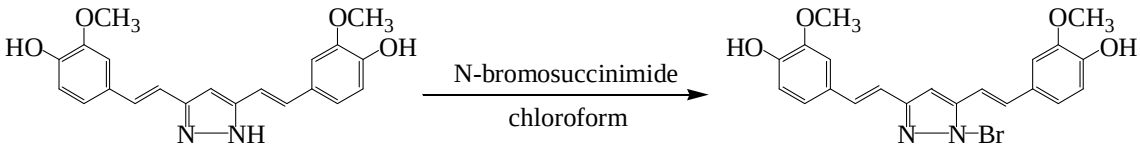

13 **14**

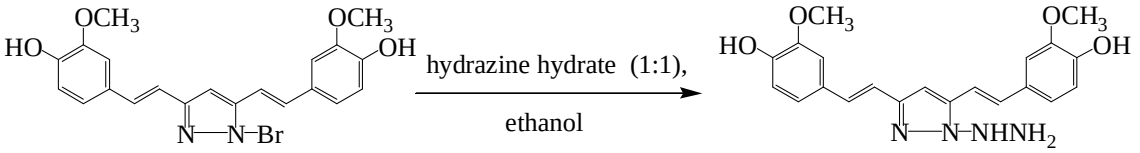

14 **15**

structure of compound **(14)** was elucidated by the formation of compound **(15)**. structure **(15)** were established on the basis of both analytical and spectral data. The IR spectrum of compound **(14)** showed the

absence of band at 3230 cm^{-1} due to the absorption frequency of (NH) and instead appeared new band at 720 cm^{-1} due to (C-Br) absorption. Also, the H^1-NMR showed the absence of the singlet signal at δ 9.6 due to (NH) proton. While the IR spectrum of **(15)** showed the absence of absorption band at 720 cm^{-1} and appear new bands 3450 cm^{-1} (NH_2) and 3200 cm^{-1} (NH). The H^1-NMR spectrum of **(15)** revealed signals at δ 6.2 and δ 4.6 due to (NH) and (NH_2) protons, respectively.

The mass spectrum of compound **(15)** gave a confirmation for the proposed correct structure. Which showed the molecular ion peak at m/e 395 (M^++1). **(Fig 19)**

N-Nitrosopyrazoline derivative **(16)** was also obtained on treating **(13)** with sodium nitrite and hydrochloric acid, the structure which was confirmed from IR, H^1-NMR and mass spectra. The absence of absorption due to (NH) group and the appearance of new absorption band at ύ (1580 cm^{-1}) in the IR spectrum of **(16)** substantiate the assigned structure of this product. Further support was gathered from H^1-NMR spectrum which displayed no signal at δ 9.6 for (NH) proton, on the other hand, the mass spectrum showed the molecular ion peak at m/e 393 (M^+). **(Fig 20)**

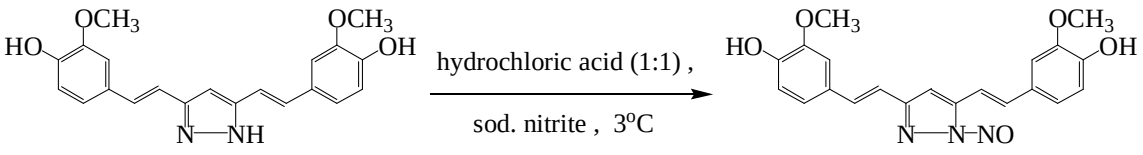

13 **16**

Moreover, it has been found that, fusion of **(13)** with chloroacetyl chloride at 95°C for 2 hours afforded the corresponding chloroacetyl derivative **(17)**.

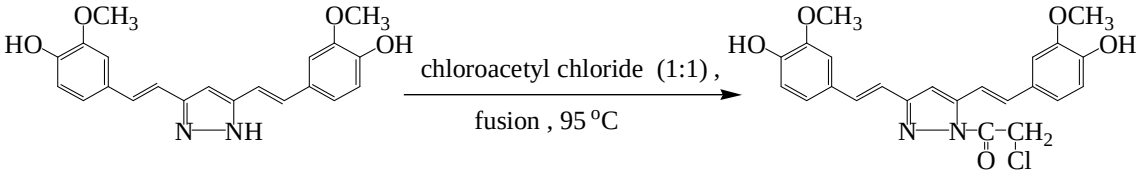

13 **17**

The structure of compound **(17)** was proved by both analytical and spectral analyses. The IR spectrum showed absorption at 2900, 1685 and 760 cm^{-1} due to (CH_2), (CO) and (C-Cl) functions. Further confirmation was obtained from its H^1-NMR and mass spectra. The H^1-NMR showed singlet signal at δ 3.5 ppm of (CH_2) protons, in addition to the other expected signals (cf. experimental part), while its mass spectrum showed the molecular ion peak at m/e 440 (M^+).

It is well known that pyrazole moiety possesses pronounced biological properties. On the other hand, many substituted arylazo compounds show antibacterial and antifungal activities. From these facts we though to extend this synthetic approach by preparing compounds having a combination of such pyrazole and arylazo moieties might afford less toxic and more potent drugs in the field of medicinal chemistry of curcumin and curcuminoids compounds.

Thus, it was found that, the pyrazole derivative **(13)** was subjected to coupling reaction with *p*-chlorophenyl diazonium chloride in (1:2) molar ratio afforded the corresponding 3,5-bis-[*β*-(5-{4-chloro-phenylazo}-4-hydroxy-3-methoxy-phenyl)-ethynyl]-*1H*-pyrazole **(18)**.

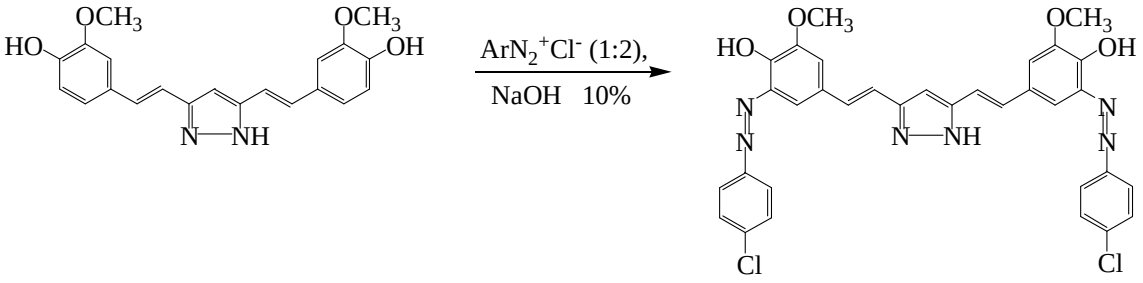

13 **18**

Structure of compound **(18)** was established on the basis of both elemental and spectral analysis. So, the IR of this compound indicates the azo-hydrazo tautomerism of such compound and showed characteristic absorption bands at 3423, 3230, 1598, and 1585 cm^{-1}corresponding to the stretching frequencies to (OH), (NH), (C=C) and (N=N) groups, respectively. More over, the structure of compound **(18)** was more confirmed by the mass spectrophotometric measurement which showed the molecular ion peak at m/e 641 (M^+). **(Fig 21)**

Reaction of 3,5-bis-[*β*-(5-{4-Chloro-phenylazo}-4-hydroxy-3-methoxy-phenyl)-ethynyl]-*1H*-pyrazole **(18)** with formamide in methanol gave 3,5-bis-{*β*-[3-(4-chloro-phenylazo)-4-hydroxy-5-methoxy-phenyl]-ethynyl}-pyrazole-1-formyl **(19)**.

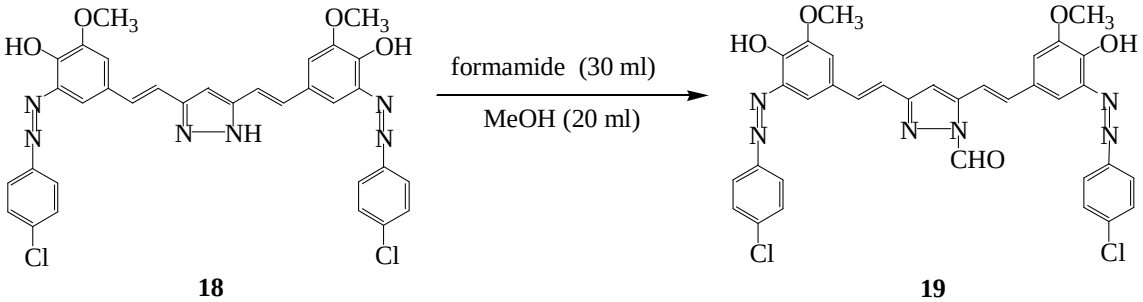

18 **19**

The structure of compound **(19)** was established on the basis of both elemental analyses and spectral data. The IR spectra in general showed

absorption frequencies at 3423, 1690, 1595 and 1580 cm^{-1} due to (OH), (C=O), (C=C) and (N=N) groups, respectively. The H^1-NMR spectrum showed singlet signal at δ 8.8 ppm due to the (CHO) proton (cf. experimental part). In addition the mass spectroscopic measurement showed the molecular ion peak at m/e 670 (M^++2). **(Fig 22)**

Treatment of 3,5-bis-[*β*-{5-(4-Chloro-phenylazo)-4-hydroxy-3-methoxy-phenyl}-ethynyl]-*1H*-pyrazole with formaldehyde in methanol afforded 3,5-bis-[*β*-(5-{4-Chloro-phenylazo}-4-hydroxy-3-methoxy-phenyl)-ethynyl]-2-hydroxy-methyl-pyrazole **(20)**. The spectral data of the compound **(20)** was consistent with its structure. The IR spectrum of compound **(20)** showed absorption bands at 3425, 1600 and 1582 cm^{-1} due to (OH), (C=N), and (N=N) groups, respectively.

The mass spectrum measurement gave an evidence for the proposed structure, which showed the molecular ion peak at m/e 671 (M^+). **(Fig. 23)**

The H^1-NMR spectrum revealed the signals at δ 2.0 (s, OH), 3.83 (s, 2×OCH_3), 5.97 (s, CH_2), 6.2 (s, CH), 6.9 (s, 2×CH=CH), 7.5 (s, 2×CH=CH), 7.06-7.94 (m, Ar-H), 9.8 (s, 2×OH).

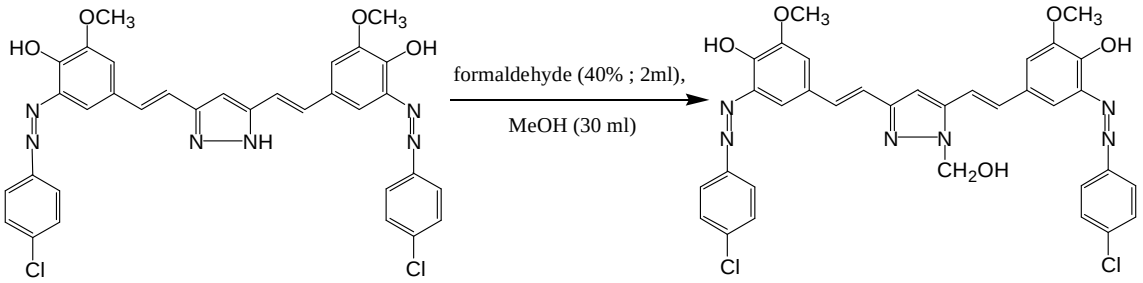

18 **20**

Conclusion

The pharmaceutical importance and phytosanitary uses of curcumin and its curcuminoid derivatives are well documented.

The biological importance of curcumin derivatives has resulted in much interest in their synthesis and chemistry.[10-12] For the past decade the authors have been exploring the synthetic potential, scope, and limitations of activated nitriles in heterocyclic synthesis.[144-147] Several new approaches for the synthesis of five membered, six membered rings and their fused heterocyclic derivatives have been developed during this work.

As an extension of this work, and in continuation of our interest in the synthesis of new heterocycles incorporating a curcumin nucleus, we reported here the behaviour of **(1)** towards some active reagents as a facile and convenient route to some heterocyclic derivatives containing a curcumin moiety.

The resulting curcumin derivatives have latent functional substituents, which have potential for further chemical transformation, and new route for the preparation of substituted curcumin derivatives in excellent yields with possible biological activity.

Curcumin is a non-toxic, highly promising natural antioxidant compound having a wide spectrum of biological functions. It is expected that the newly synthesized curcumin derivative involved in this work may find applications as a novel drug in the near future to control various diseases, including inflammatory disorders, carcinogenesis and oxidative stress-induced pathogenesis.

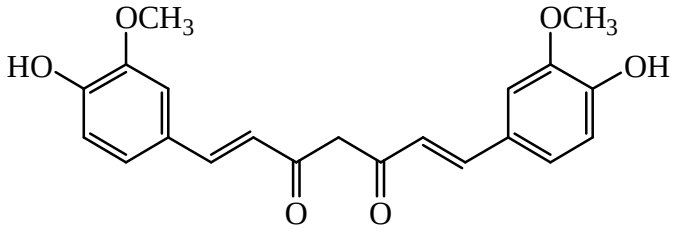

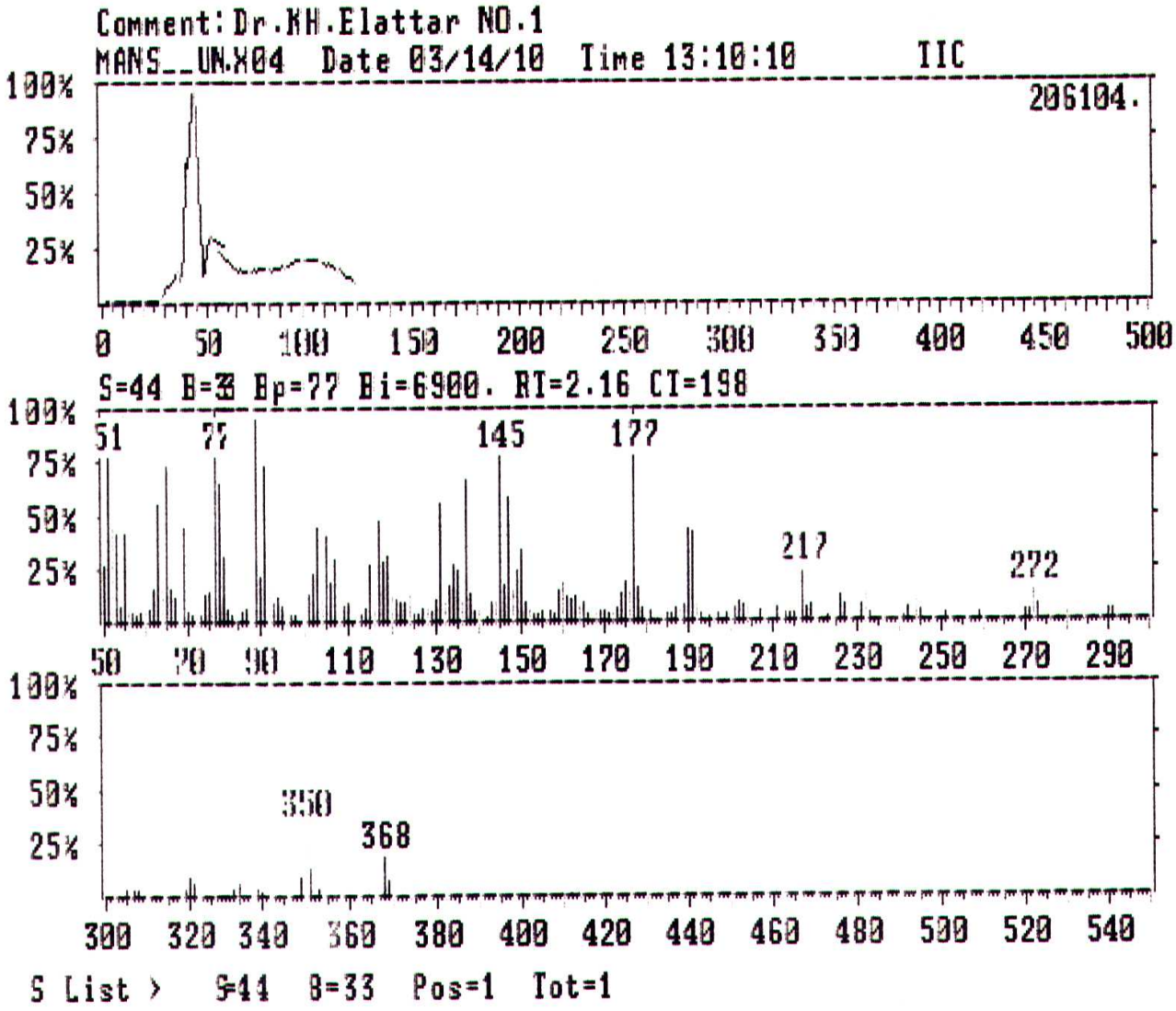

Fig.1 Mass Spectrum Of Compound **(1)**

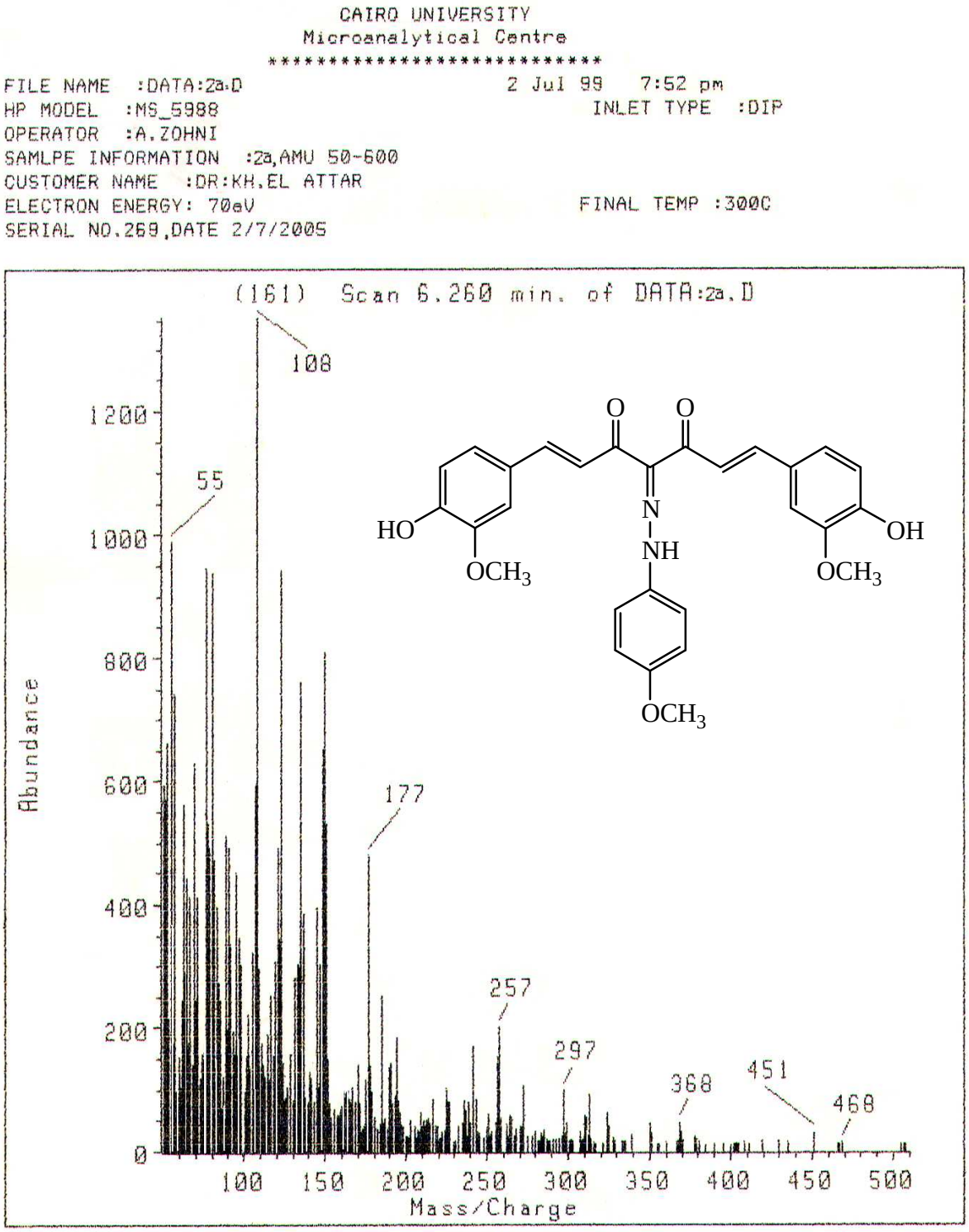

Fig.2 Mass Spectrum Of Compound **(2a)**

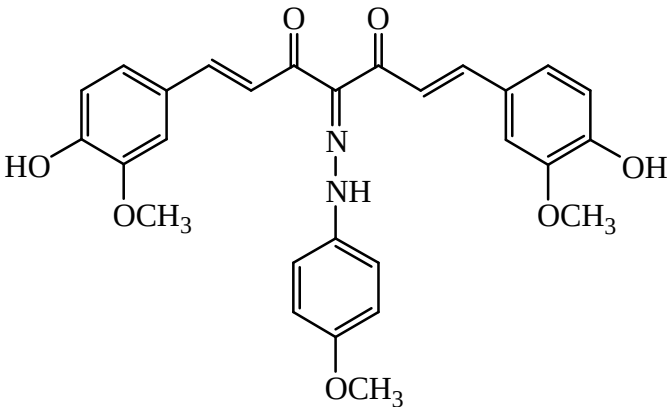

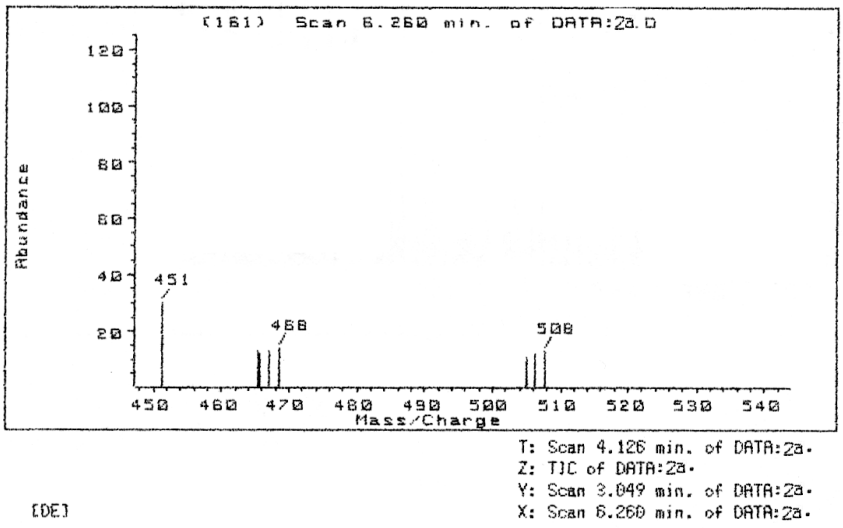

Fig.2 Mass Spectrum Of Compound **(2a)**

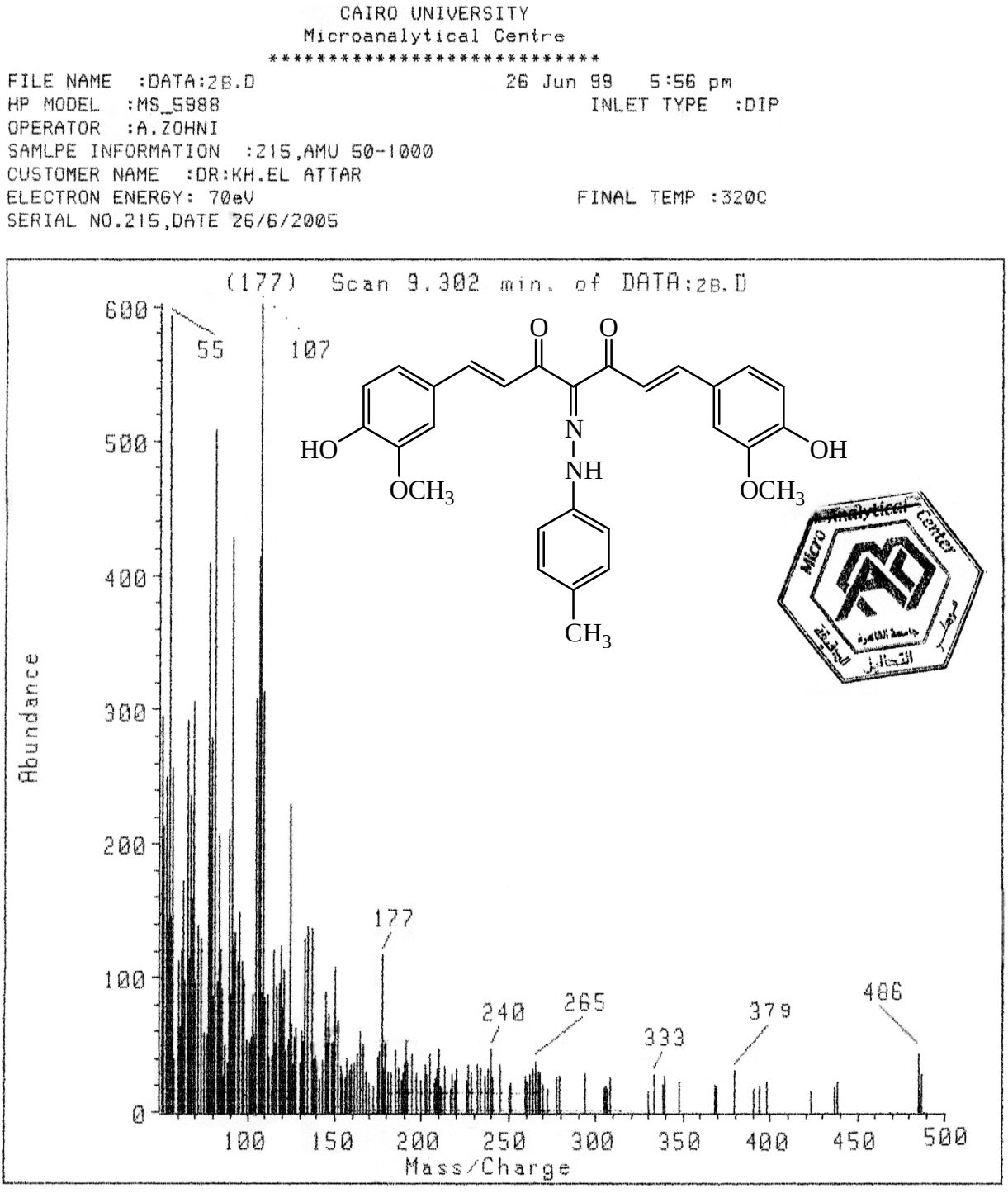

Fig.3 Mass Spectrum Of Compound **(2b)**

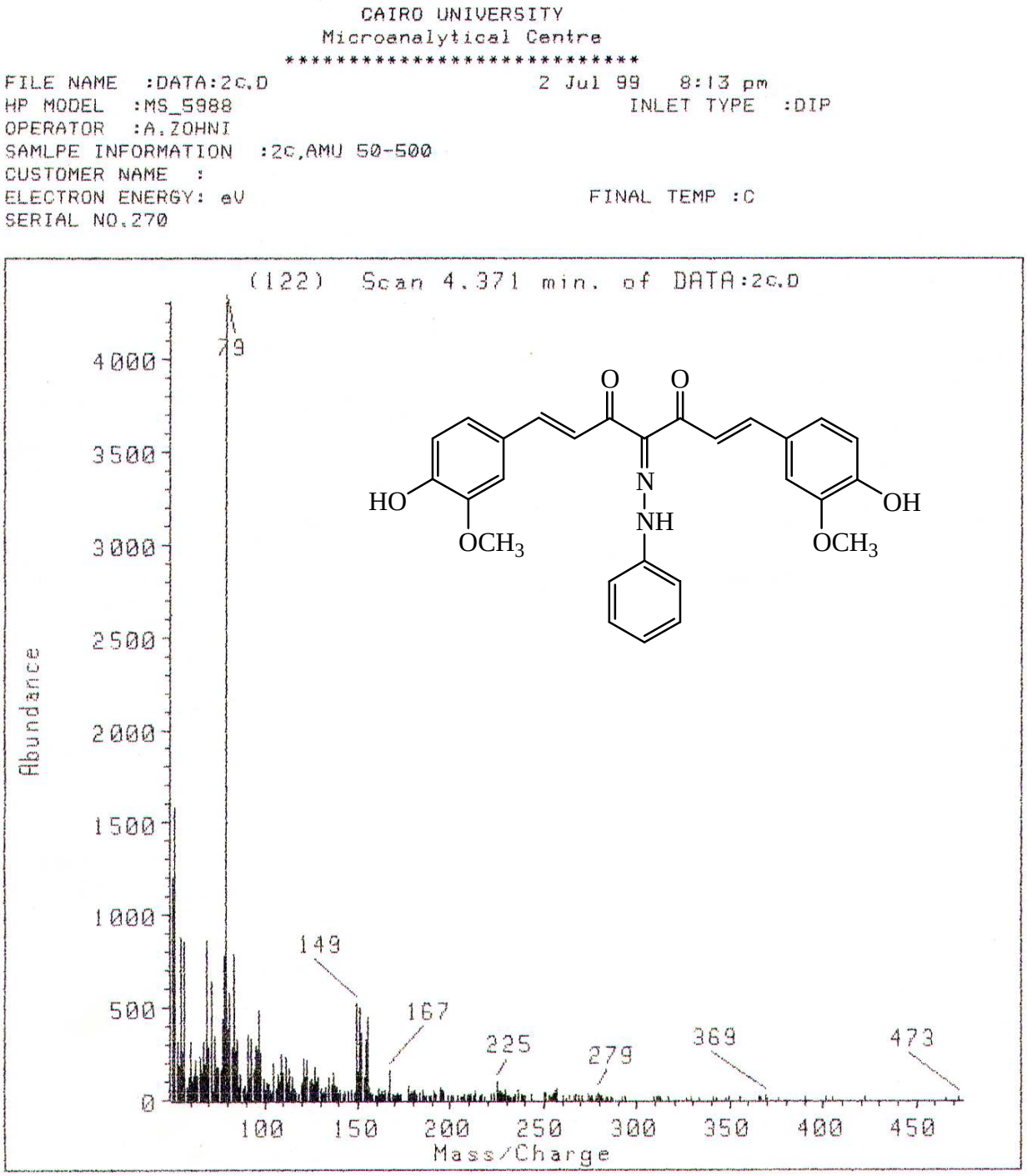

Fig.4 Mass Spectrum Of Compound **(2c)**

CAIRO UNIVERSITY
Microanalytical Centre
****

FILE NAME :DATA:2D.D 20 Nov 99 2:48 pm
HP MODEL :MS_5988 INLET TYPE :DIP
OPERATOR :A.ZOHNI
SAMLPE INFORMATION :2D,AMU 50-600
CUSTOMER NAME :
ELECTRON ENERGY: eV FINAL TEMP :C
SERIAL NO.99

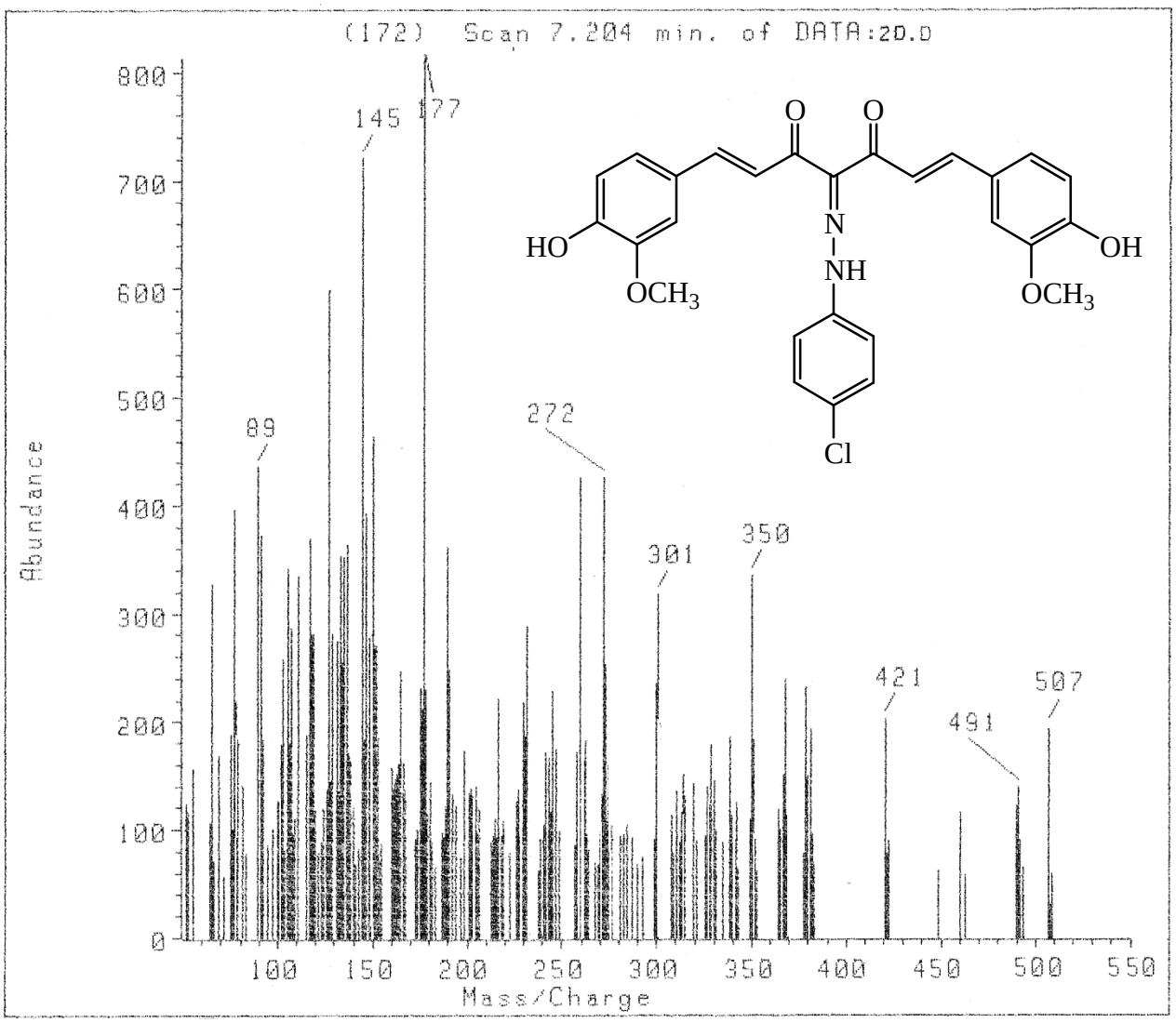

Fig.5 Mass Spectrum Of Compound **(2d)**

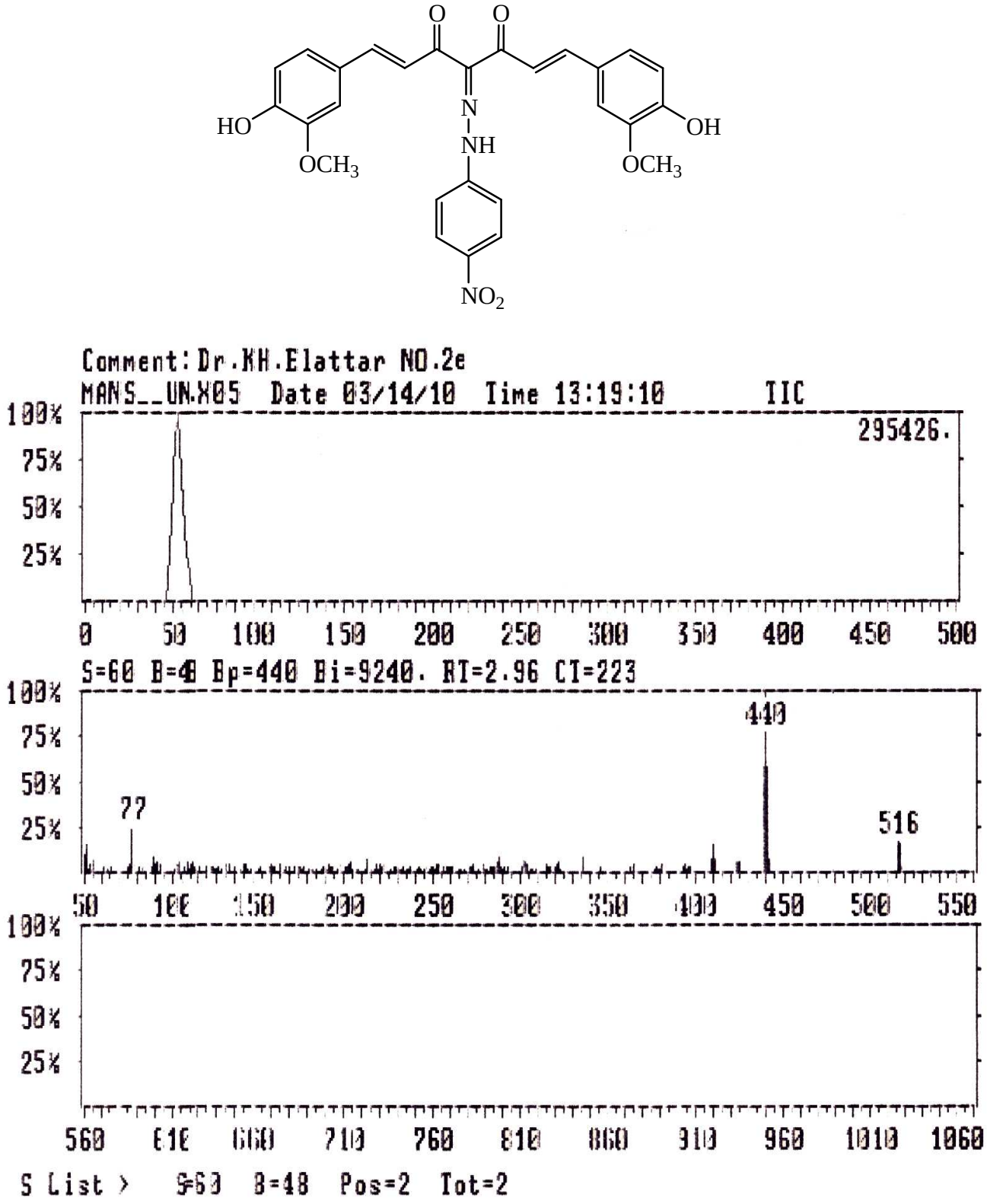

Fig.6 Mass Spectrum Of Compound **(2e)**

CAIRO UNIVERSITY
Microanalytical Centre
****

FILE NAME :DATA:2F.D 20 Nov 99 2:32 pm
HP MODEL :MS_5988 INLET TYPE :DIP
OPERATOR :A.ZOHNI
SAMLPE INFORMATION :2F,AMU 50-600
CUSTOMER NAME :
ELECTRON ENERGY: eV FINAL TEMP :C
SERIAL NO.98

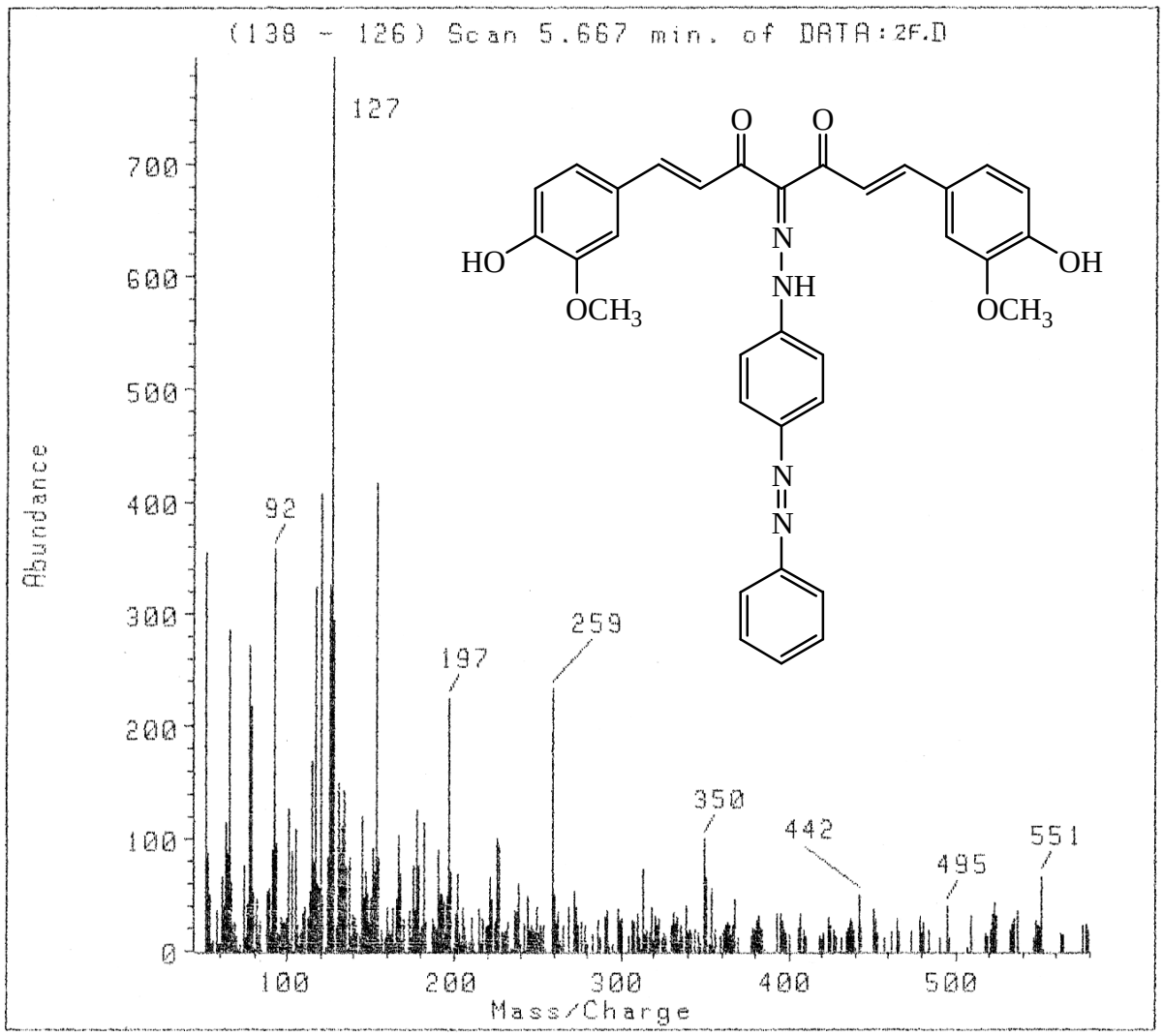

Fig.7 Mass Spectrum Of Compound **(2f)**

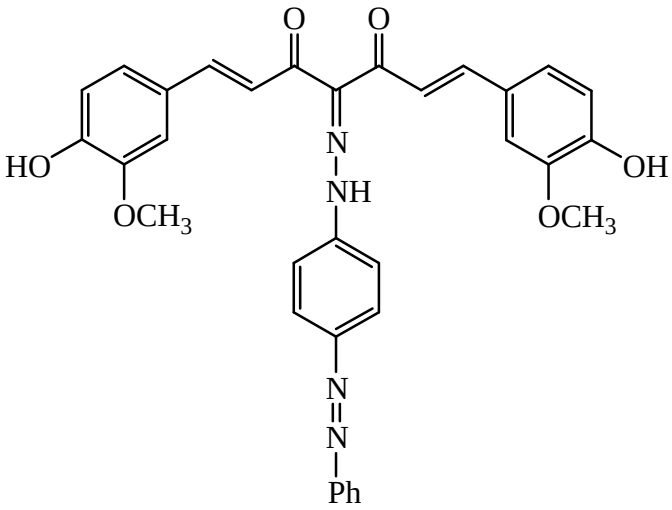

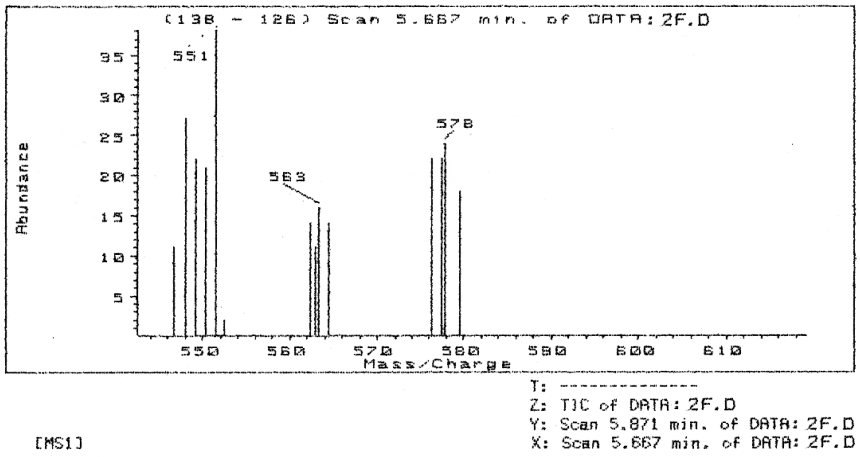

Fig.7 Mass Spectrum Of Compound **(2f)**

CAIRO UNIVERSITY
Microanalytical Centre
****

FILE NAME :DATA:3.D 20 Nov 99 2:06 pm
HP MODEL :MS_5988 INLET TYPE :DIP
OPERATOR :A.ZOHNI
SAMLPE INFORMATION :3,AMU 50-700
CUSTOMER NAME :
ELECTRON ENERGY: eV FINAL TEMP :C
SERIAL NO.97

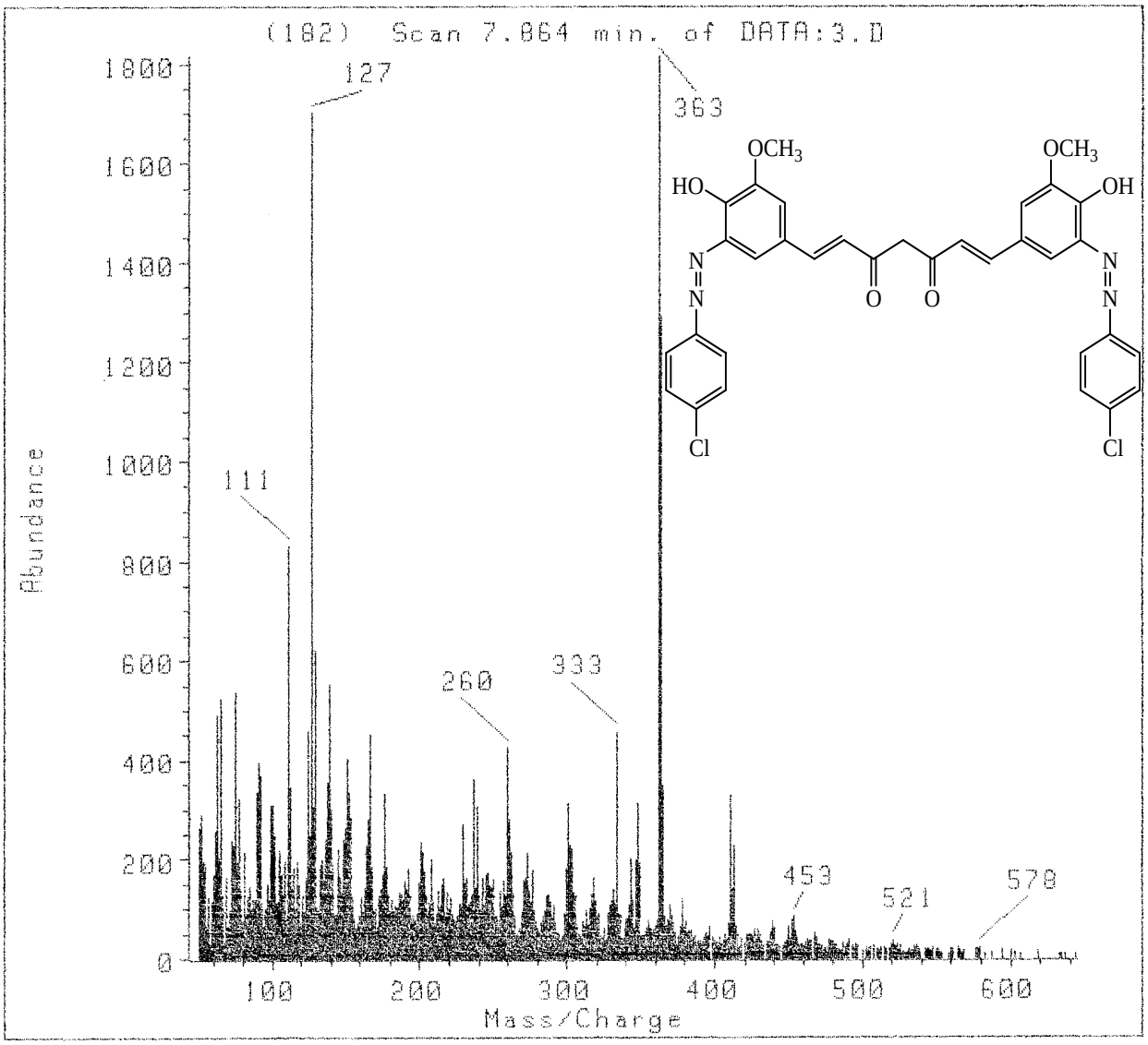

Fig.8 Mass Spectrum Of Compound **(3)**

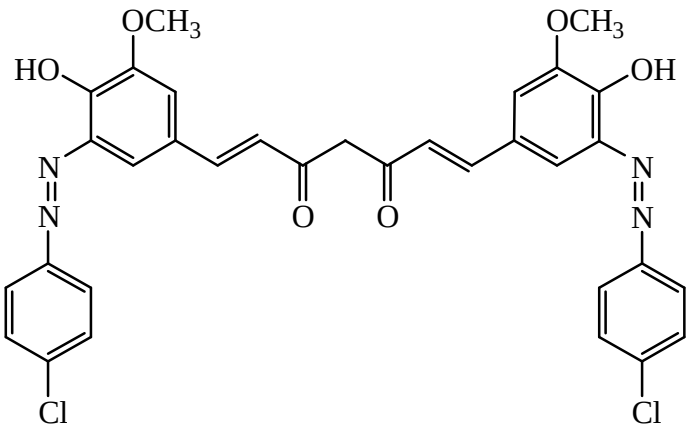

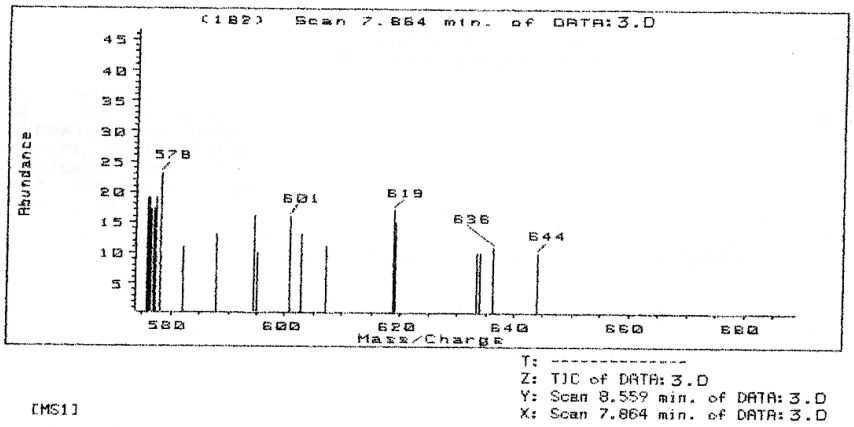

Fig.8 Mass Spectrum Of Compound **(3)**

CAIRO UNIVERSITY
Microanalytical Centre
****

FILE NAME :DATA: 4 .D 6 Sep 99 4:30 pm
HP MODEL :MS_5988 INLET TYPE :DIP
OPERATOR :A.ZOHNI
SAMLPE INFORMATION :AMU 50-750
CUSTOMER NAME :DR.KH.EL-ATTAR
ELECTRON ENERGY: 70eV FINAL TEMP :300C
SERIAL NO.18-DATE:6/9/2005

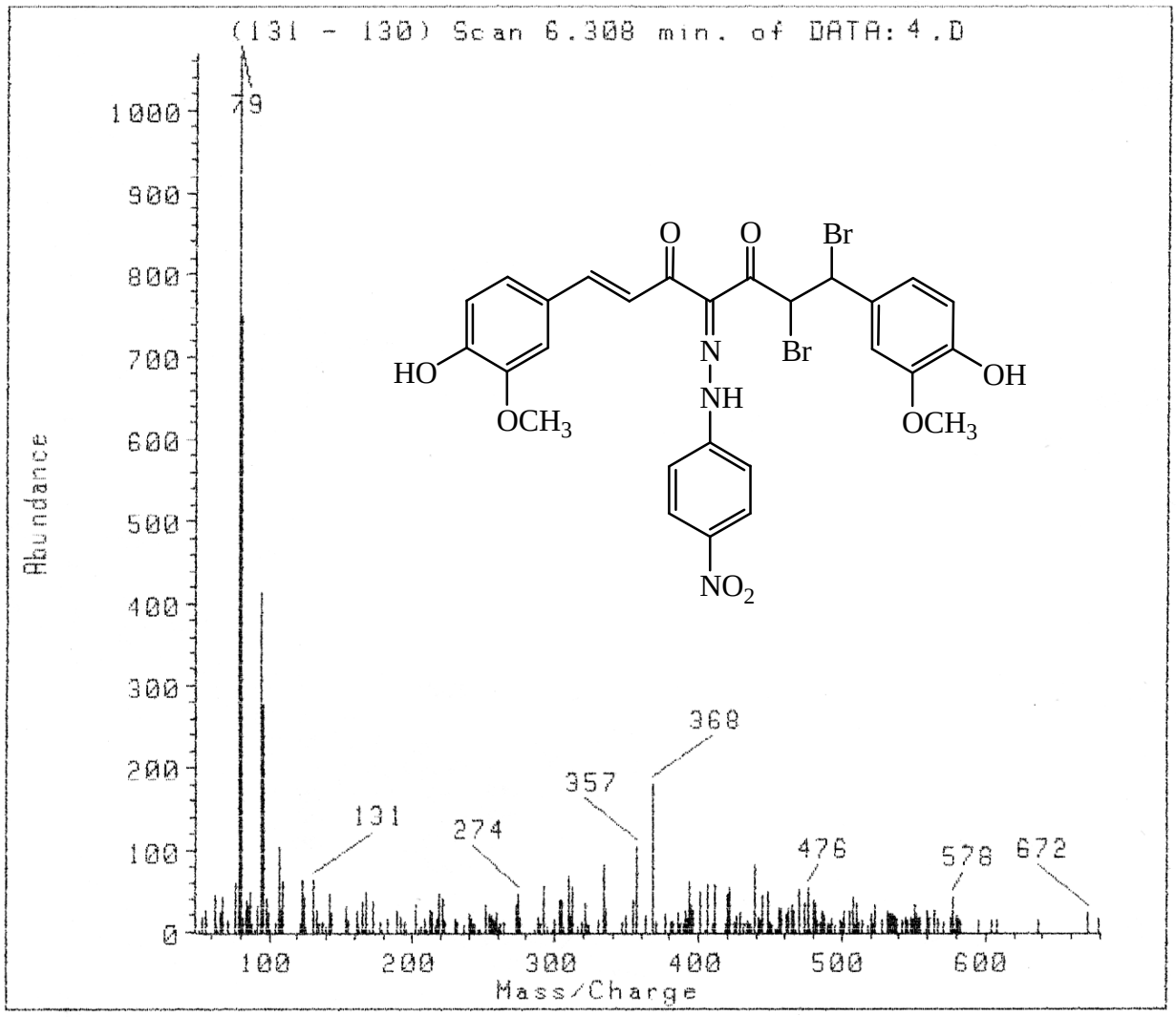

Fig.9 Mass Spectrum Of Compound **(4)**

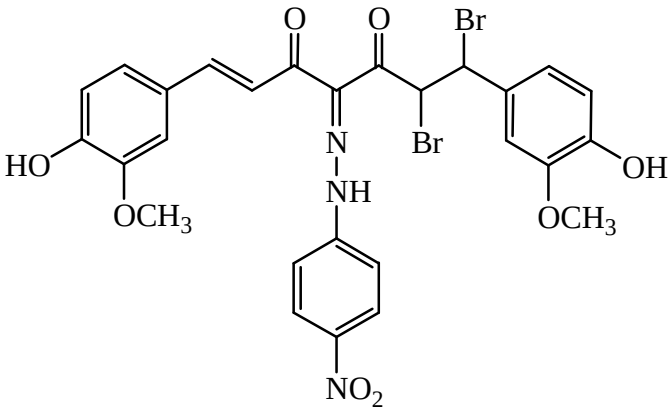

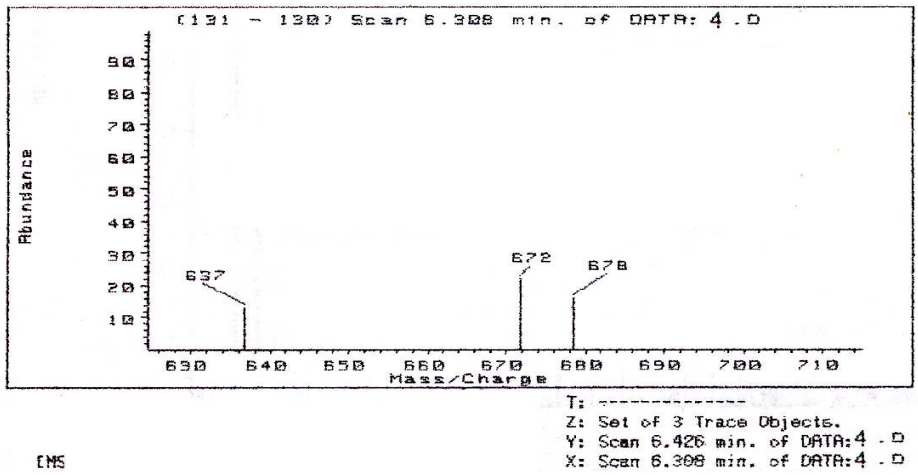

Fig.9 Mass Spectrum Of Compound **(4)**

CAIRO UNIVERSITY
Microanalytical Centre
****

FILE NAME :DATA:S.D 12 Sep 99 1:22 pm
HP MODEL :MS_5988 INLET TYPE :DIP
OPERATOR :A.ZOHNI
SAMLPE INFORMATION :S,AMU 50-700
CUSTOMER NAME :DR:KH.EL ATTAR
ELECTRON ENERGY: 70eV FINAL TEMP :300C
SERIAL NO.103,DATE 12/9/2005

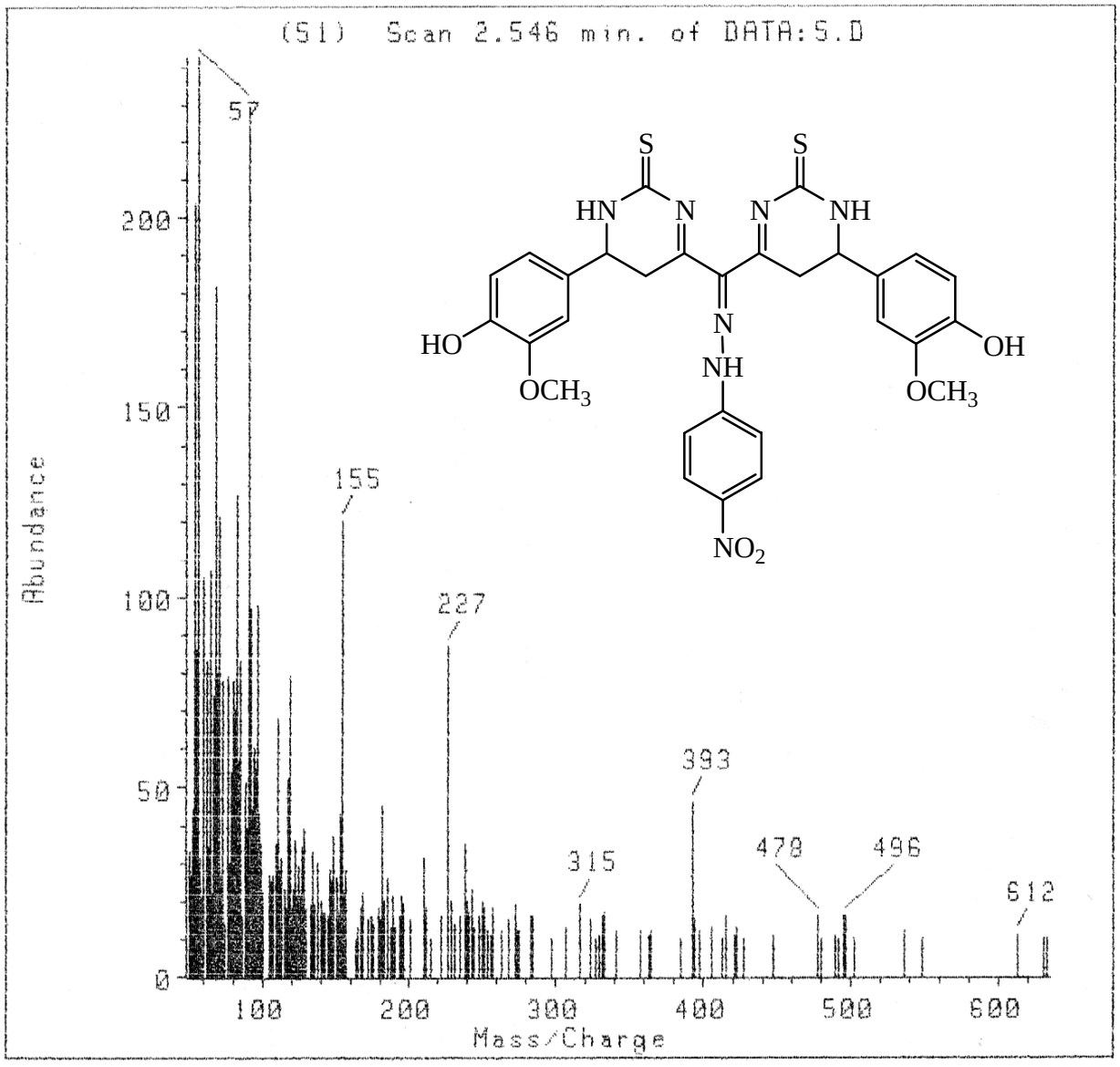

Fig.10 Mass Spectrum Of Compound **(5)**

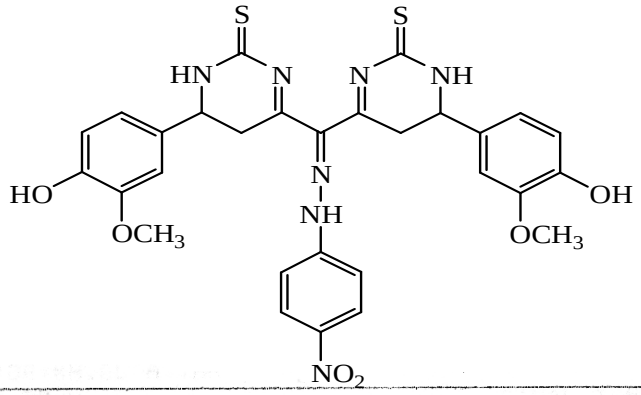

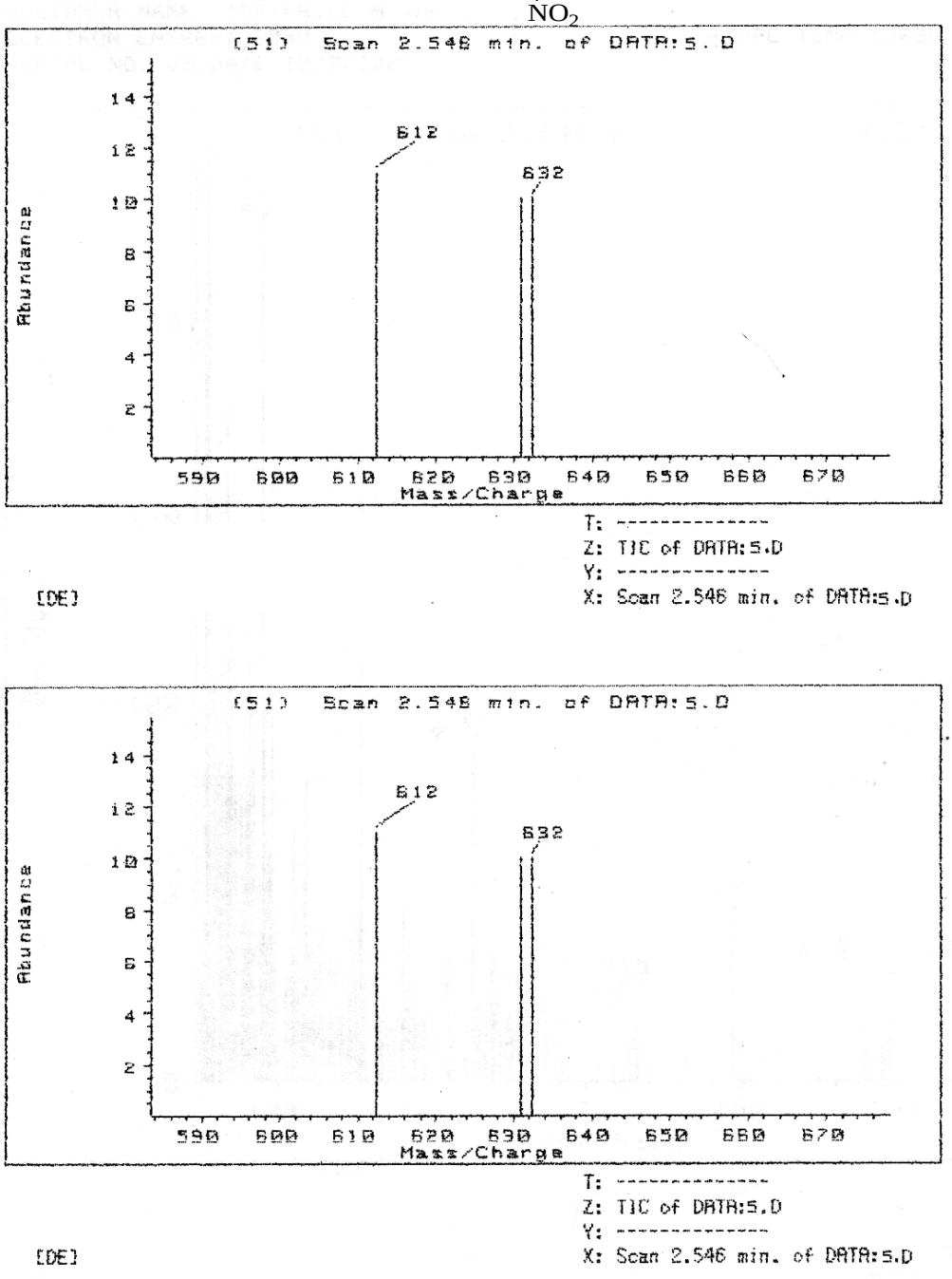

Fig.10 Mass Spectrum Of Compound **(5)**

CAIRO UNIVERSITY
Microanalytical Centre
****

FILE NAME :DATA:6.D 9 Aug 99 11:42 am
HP MODEL :MS_5988 INLET TYPE :DIP
OPERATOR :A.ZOHNI
SAMLPE INFORMATION :KH,AMU 50-700
CUSTOMER NAME :DR:KH.EL ATTAR
ELECTRON ENERGY: 70eV FINAL TEMP :250C
SERIAL NO.32,DATE 9/8/2005

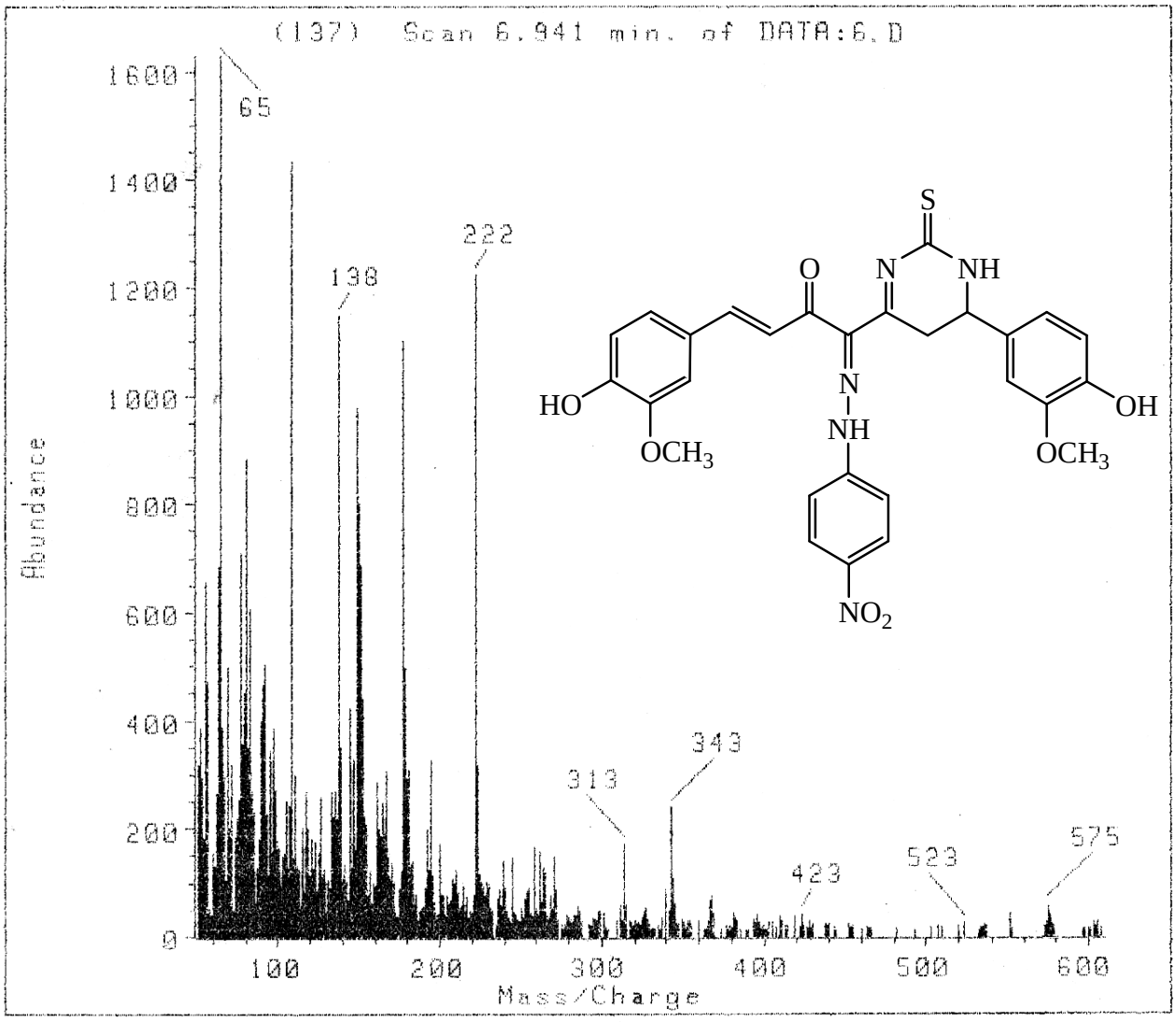

Fig.11 Mass Spectrum Of Compound **(6)**

CAIRO UNIVERSITY
Microanalytical Centre
****

FILE NAME :DATA:7.D 12 Sep 99 1:37 pm
HP MODEL :MS_5988 INLET TYPE :DIP
OPERATOR :A.ZOHNI
SAMLPE INFORMATION :7,AMU 50-600
CUSTOMER NAME :
ELECTRON ENERGY: eV FINAL TEMP :C
SERIAL NO.104

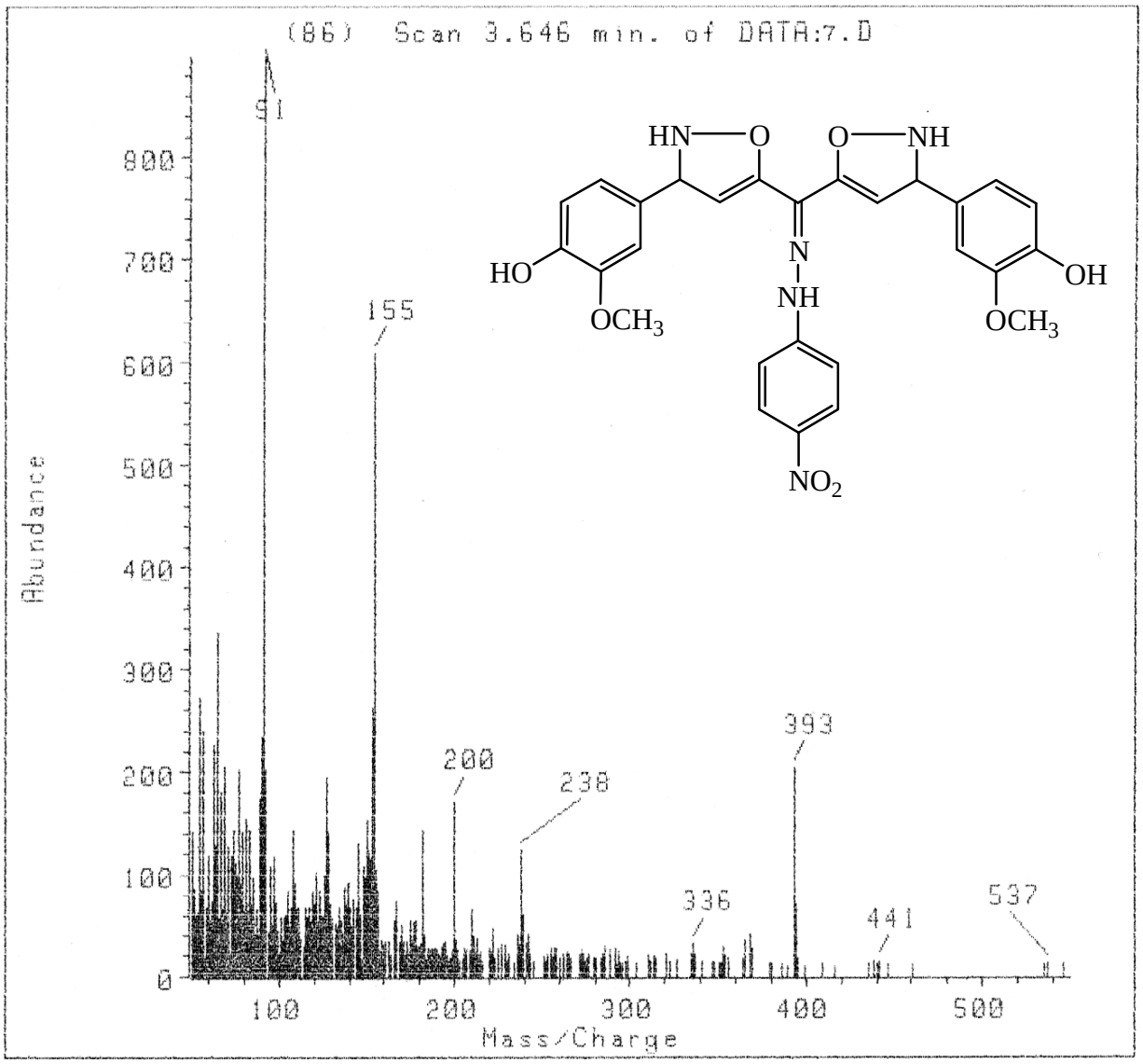

Fig.12 Mass Spectrum Of Compound **(7)**

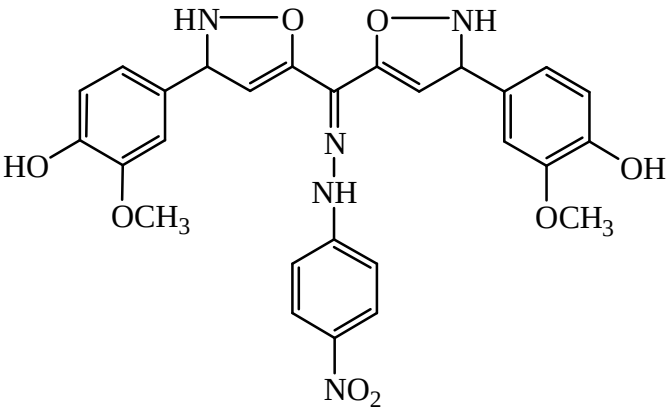

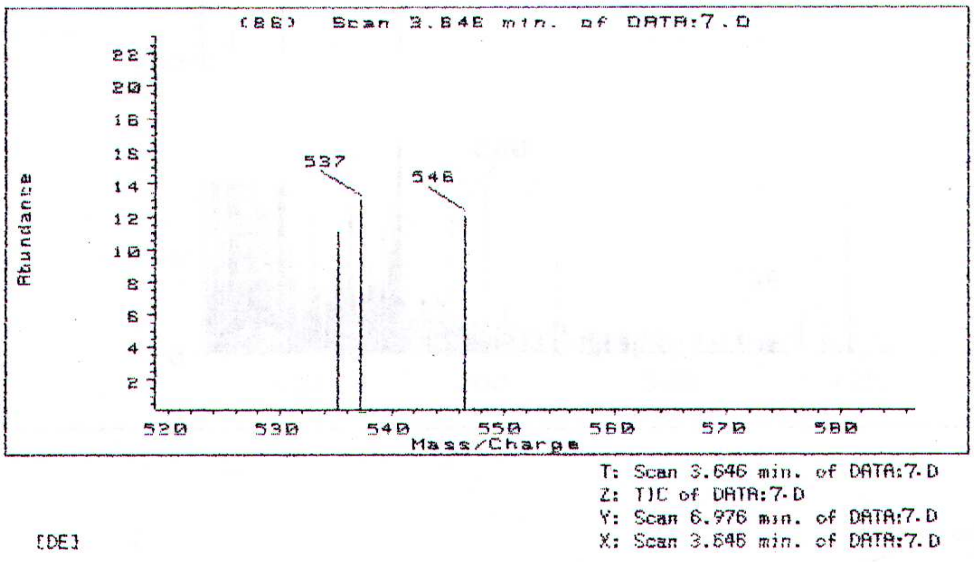

Fig.12 Mass Spectrum Of Compound **(7)**

CAIRO UNIVERSITY
Microanalytical Centre
****

FILE NAME :DATA:8.D 12 Sep 99 1:56 pm
HP MODEL :MS_5988 INLET TYPE :DIP
OPERATOR :A.ZOHNI
SAMLPE INFORMATION :8,AMU 50-600
CUSTOMER NAME :
ELECTRON ENERGY: eV FINAL TEMP :C
SERIAL NO.105

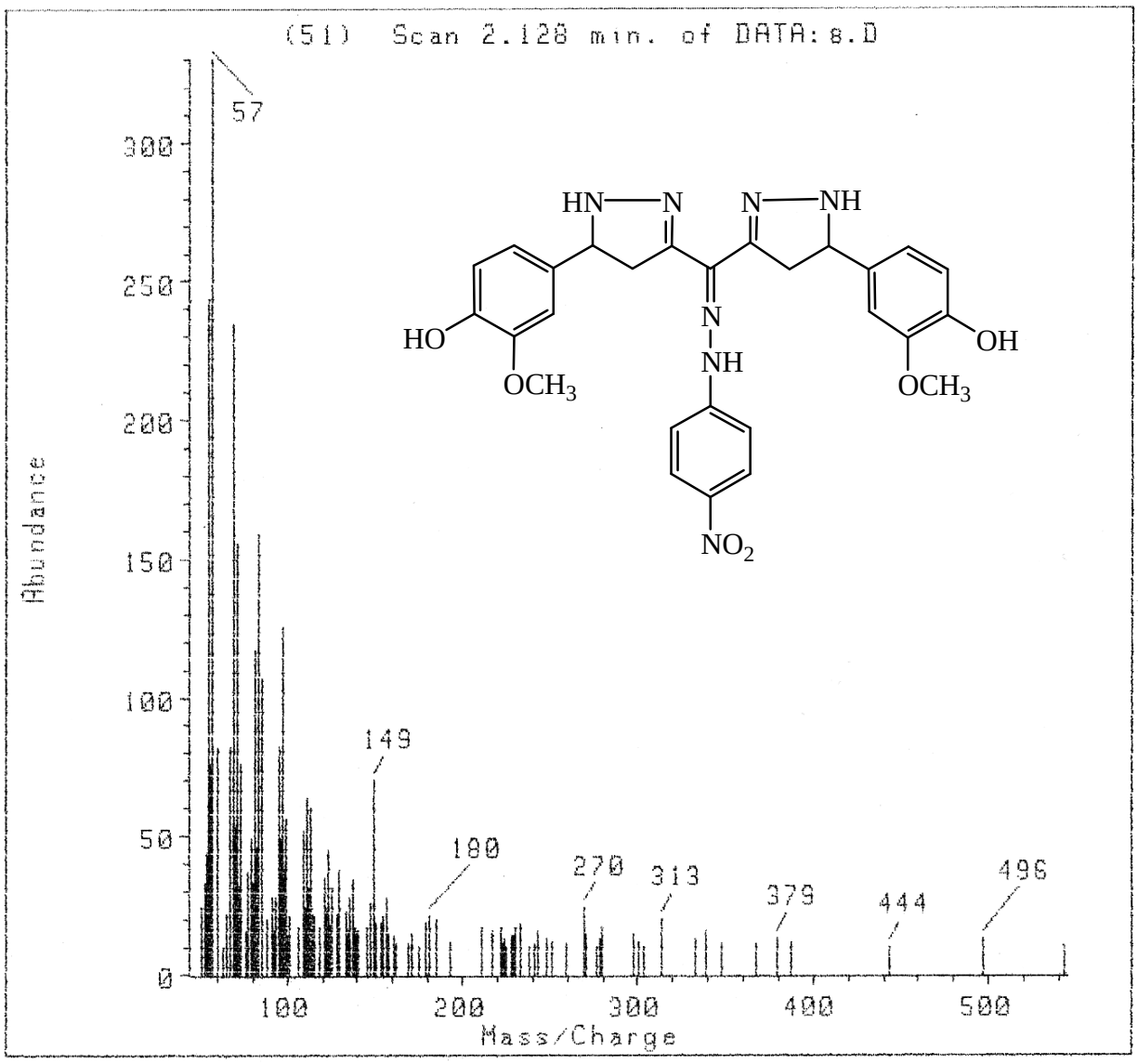

Fig.13 Mass Spectrum Of Compound **(8)**

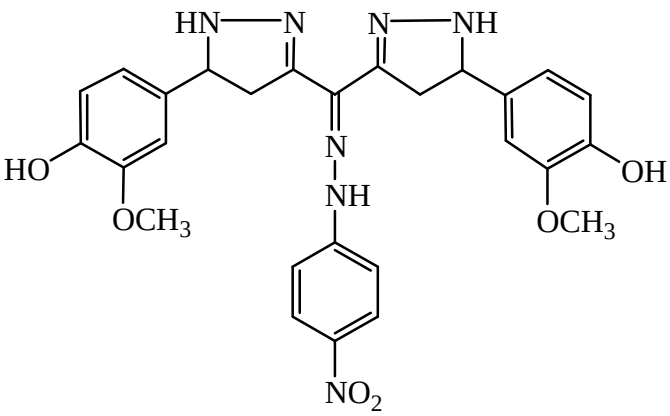

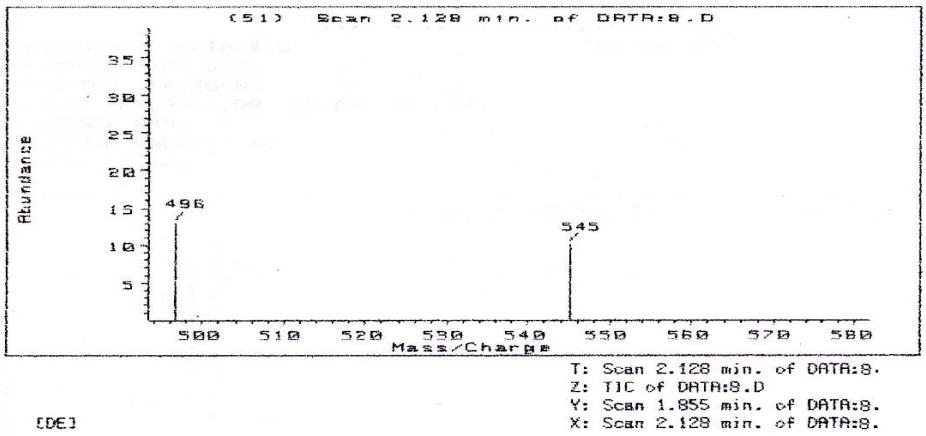

Fig.13 Mass Spectrum Of Compound **(8)**

CAIRO UNIVERSITY
Microanalytical Centre
****

FILE NAME :DATA:9.D 15 Aug 99 3:52 am
HP MODEL :MS_5988 INLET TYPE :DIP
OPERATOR :A.ZOHNI
SAMLPE INFORMATION :M.S,AMU 50-600
CUSTOMER NAME :DR:KH.EL ATTAR
ELECTRON ENERGY: 70eV FINAL TEMP :250C
SERIAL NO.67,DATE 15/8/2005

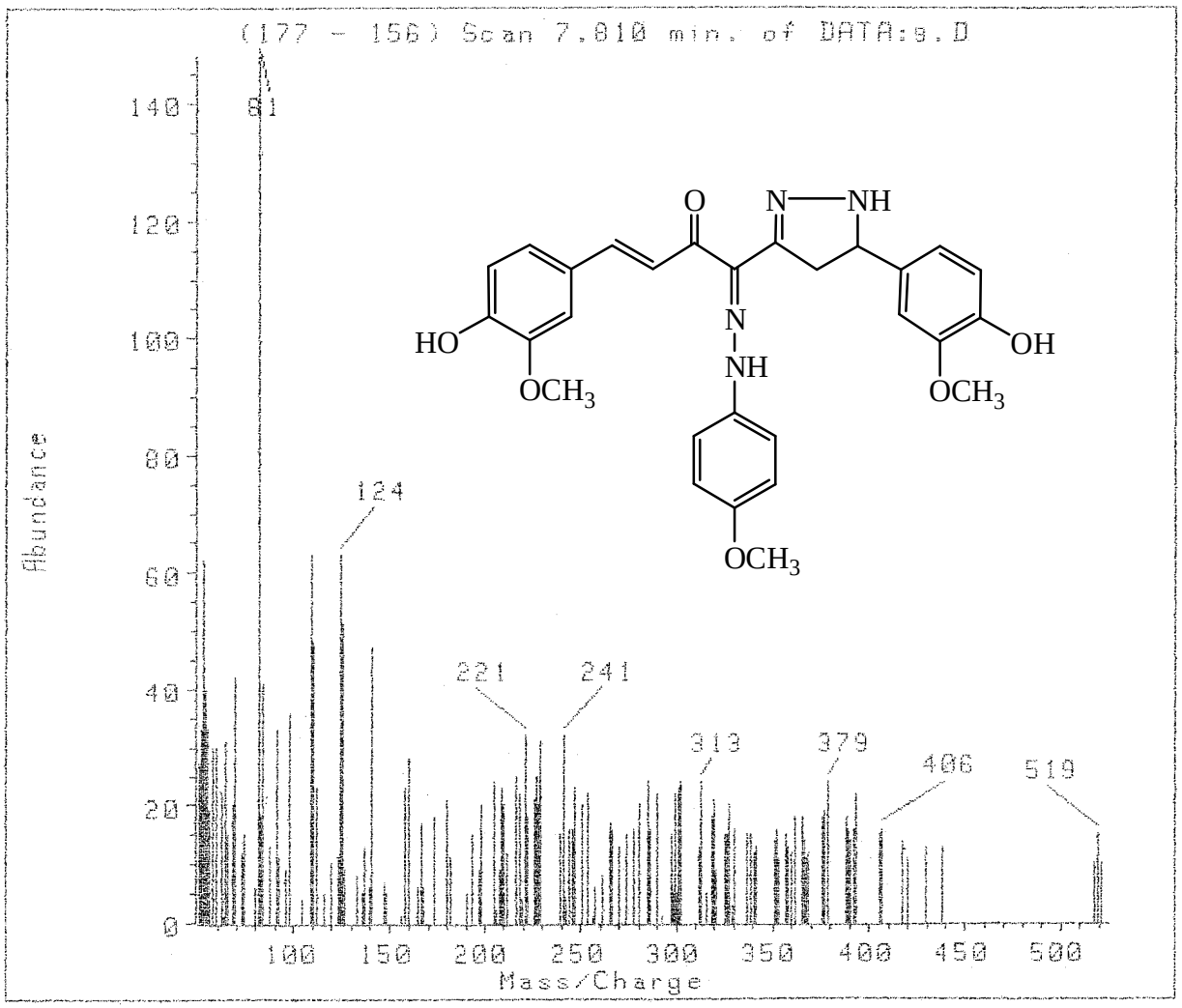

Fig.14 Mass Spectrum Of Compound **(9)**

CAIRO UNIVERSITY
Microanalytical Centre
****

FILE NAME :DATA:10.D 12 Sep 99 2:13 pm
HP MODEL :MS_5988 INLET TYPE :DIP
OPERATOR :A.ZOHNI
SAMLPE INFORMATION :10,AMU 50-800
CUSTOMER NAME :
ELECTRON ENERGY: eV FINAL TEMP :C
SERIAL NO.106

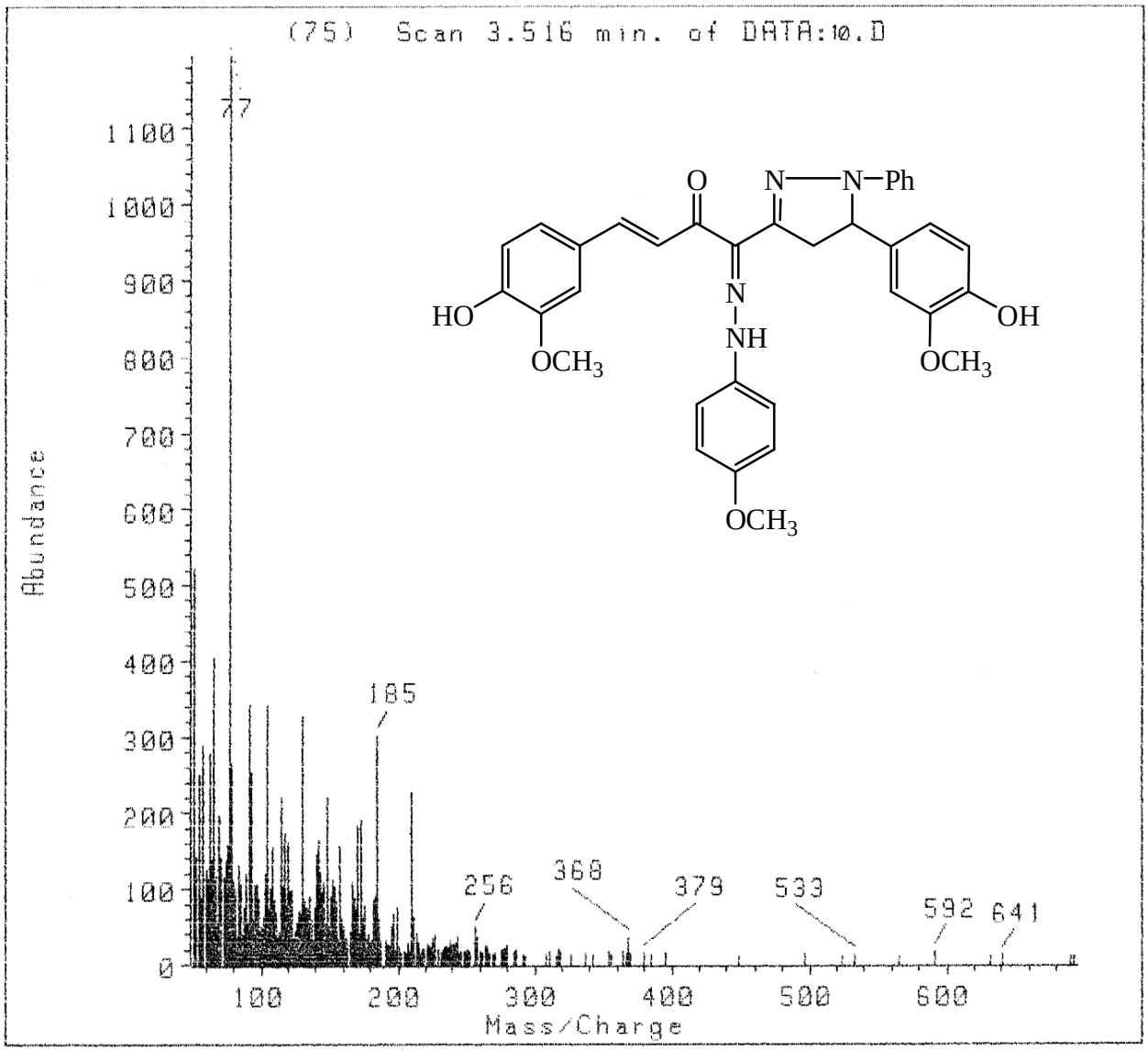

Fig.15 Mass Spectrum Of Compound **(10)**

CAIRO UNIVERSITY
Microanalytical Centre
****

FILE NAME :DATA:11.D 12 Sep 99 2:25 pm
HP MODEL :MS_5988 INLET TYPE :DIP
OPERATOR :A.ZOHNI
SAMLPE INFORMATION :11,AMU 50,800
CUSTOMER NAME :
ELECTRON ENERGY: eV FINAL TEMP :300C
SERIAL NO.107,

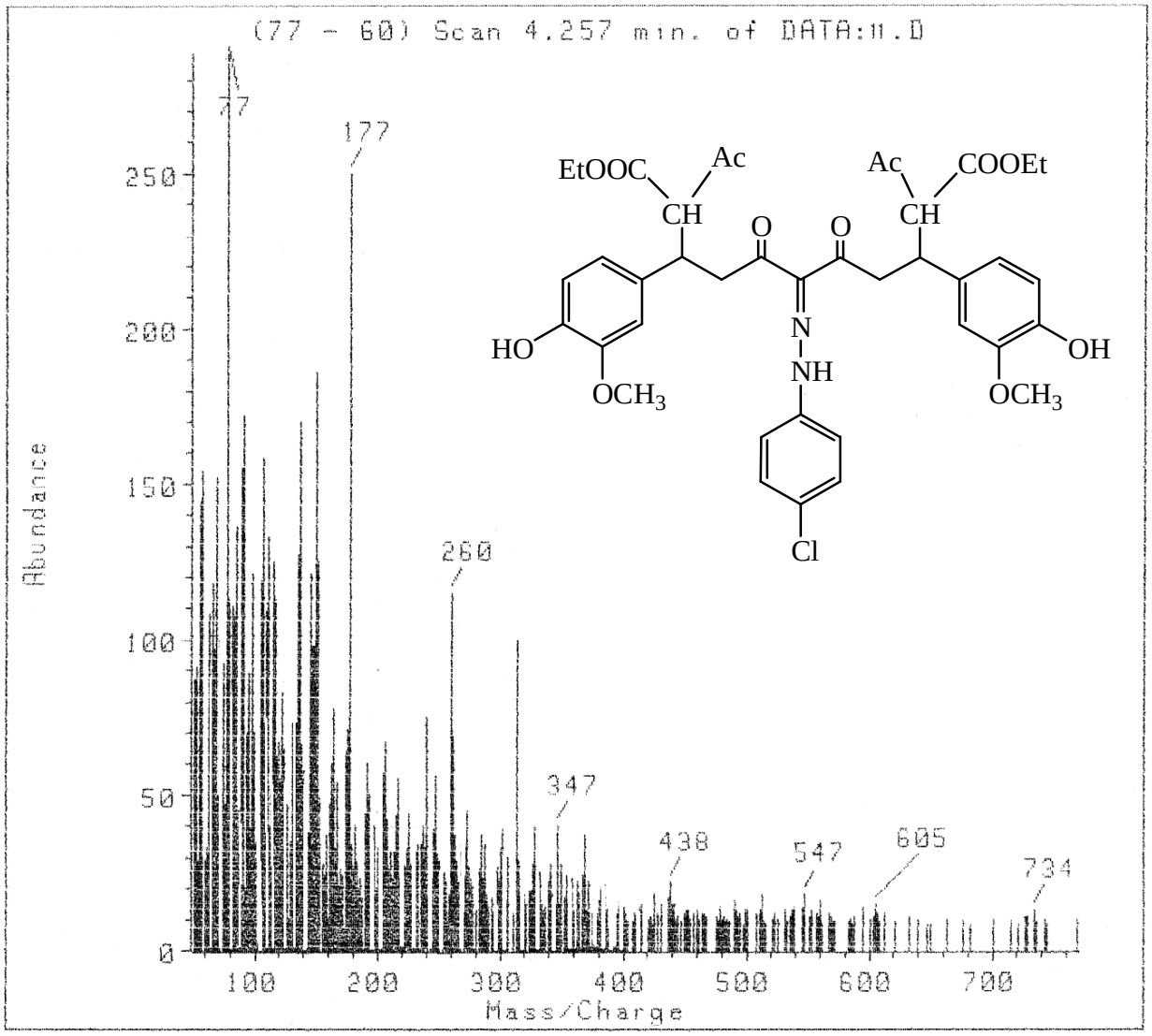

Fig.16 Mass Spectrum Of Compound **(11)**

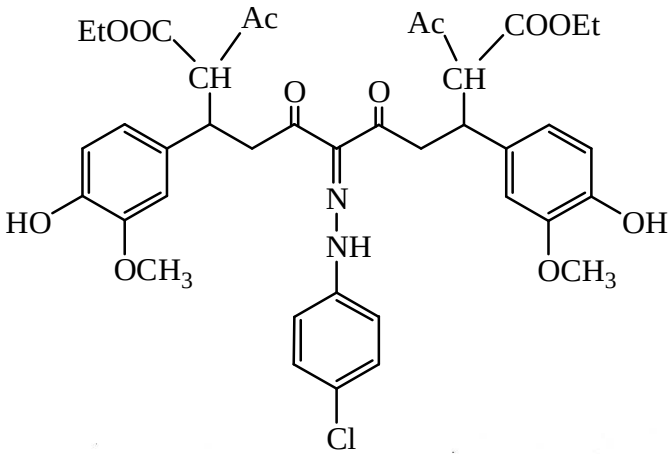

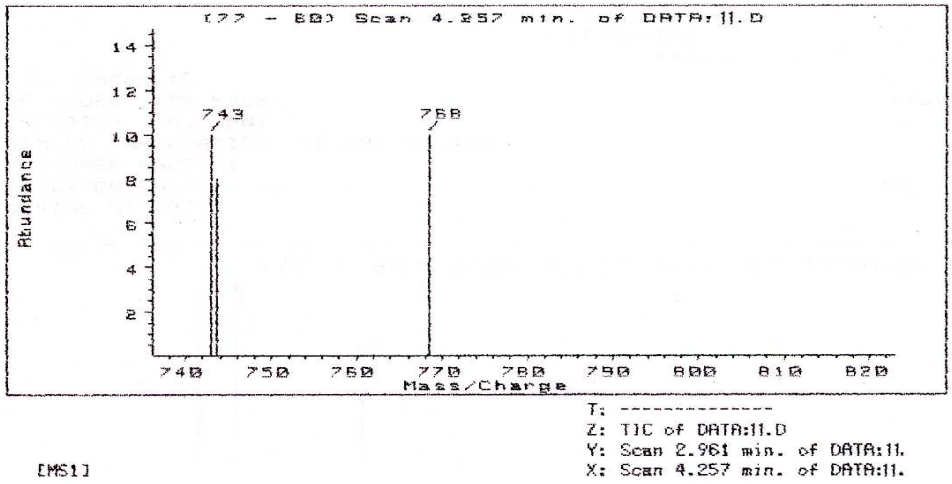

Fig. 16 Mass Spectrum Of Compound **(11)**

CAIRO UNIVERSITY
Microanalytical Centre
****

FILE NAME :DATA:12.D 20 Nov 99 12:11 pm
HP MODEL :MS_5988 INLET TYPE :DIP
OPERATOR :A.ZOHNI
SAMLPE INFORMATION :12,AMU 50-800
CUSTOMER NAME :DR:KH.EL ATTAR
ELECTRON ENERGY: 70eV FINAL TEMP :300C
SERIAL NO.91,DATE 20/11/2005

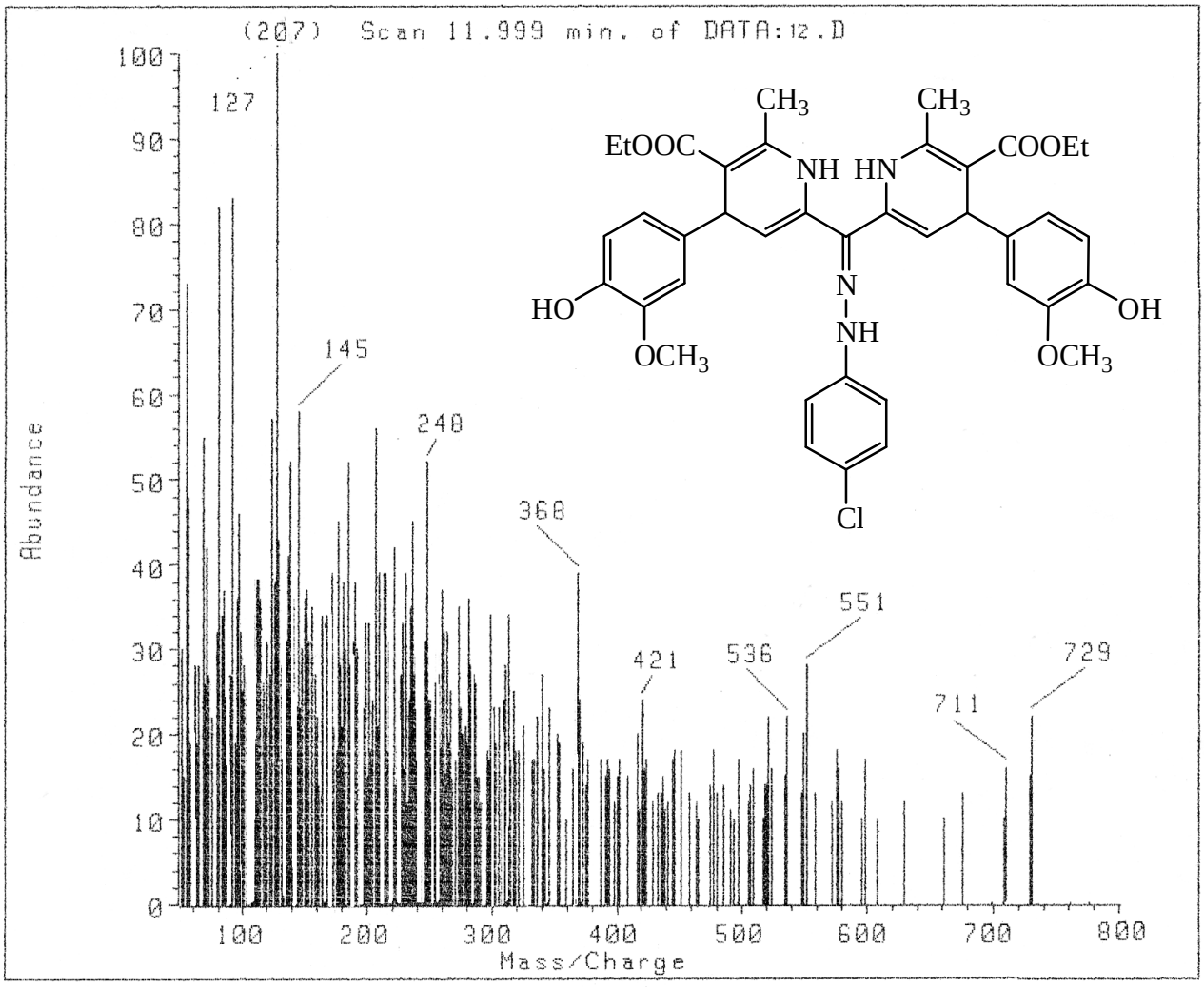

Fig.17 Mass Spectrum Of Compound **(12)**

CAIRO UNIVERSITY
Microanalytical Centre
****

FILE NAME :DATA:13.D 20 Nov 99 1:34 pm
HP MODEL :MS_5988 INLET TYPE :DIP
OPERATOR :A.ZOHNI
SAMLPE INFORMATION :13,AMU 50-500
CUSTOMER NAME :
ELECTRON ENERGY: eV FINAL TEMP :C
SERIAL NO.95

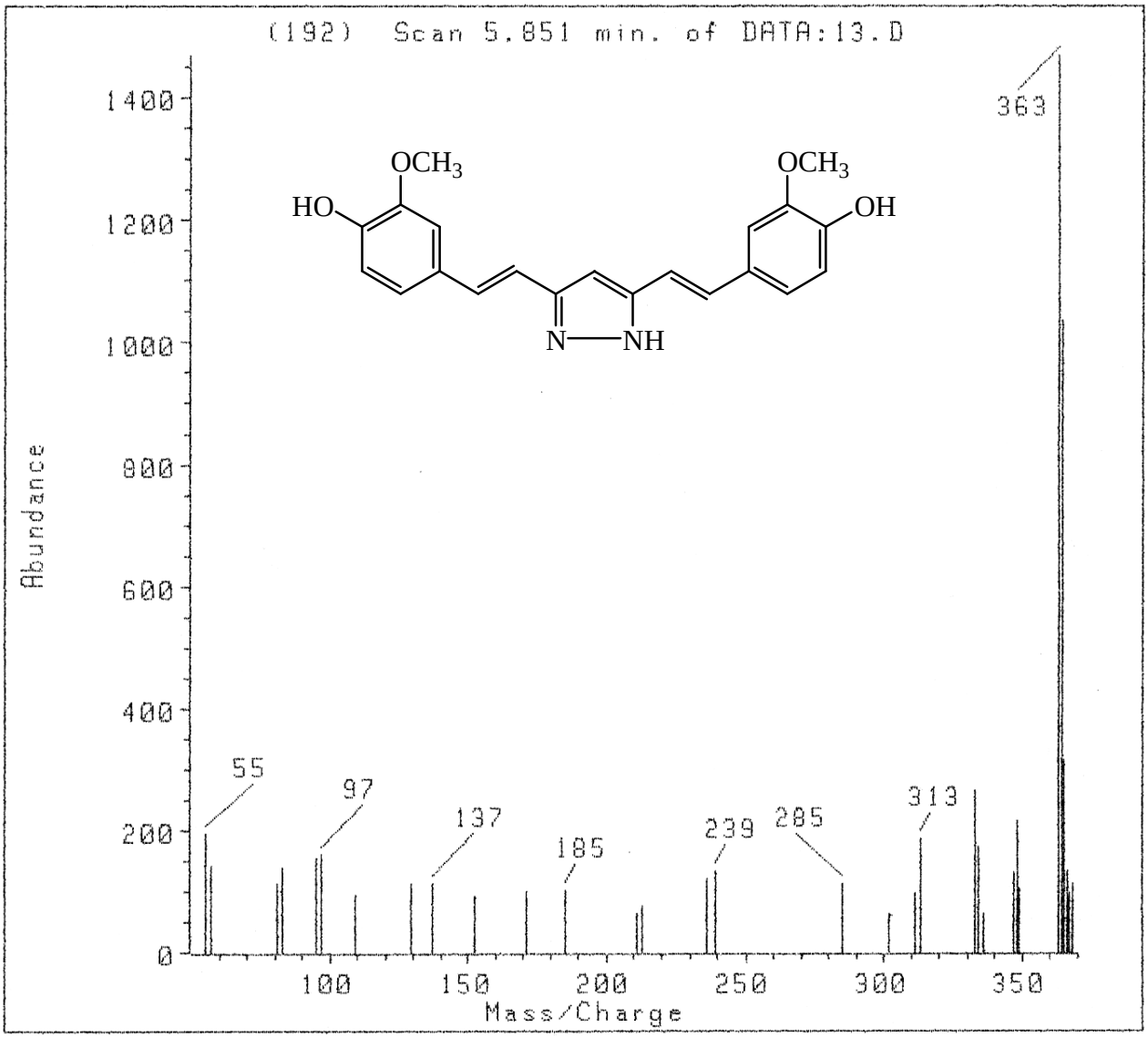

Fig.18 Mass Spectrum Of Compound **(13)**

CAIRO UNIVERSITY
Microanalytical Centre
****

FILE NAME :DATA:13a.D 20 Nov 99 12:57 pm
HP MODEL :MS_5988 INLET TYPE :DIP
OPERATOR :A.ZOHNI
SAMLPE INFORMATION :13a,AMU 50-500
CUSTOMER NAME :
ELECTRON ENERGY: eV FINAL TEMP :C
SERIAL NO.93

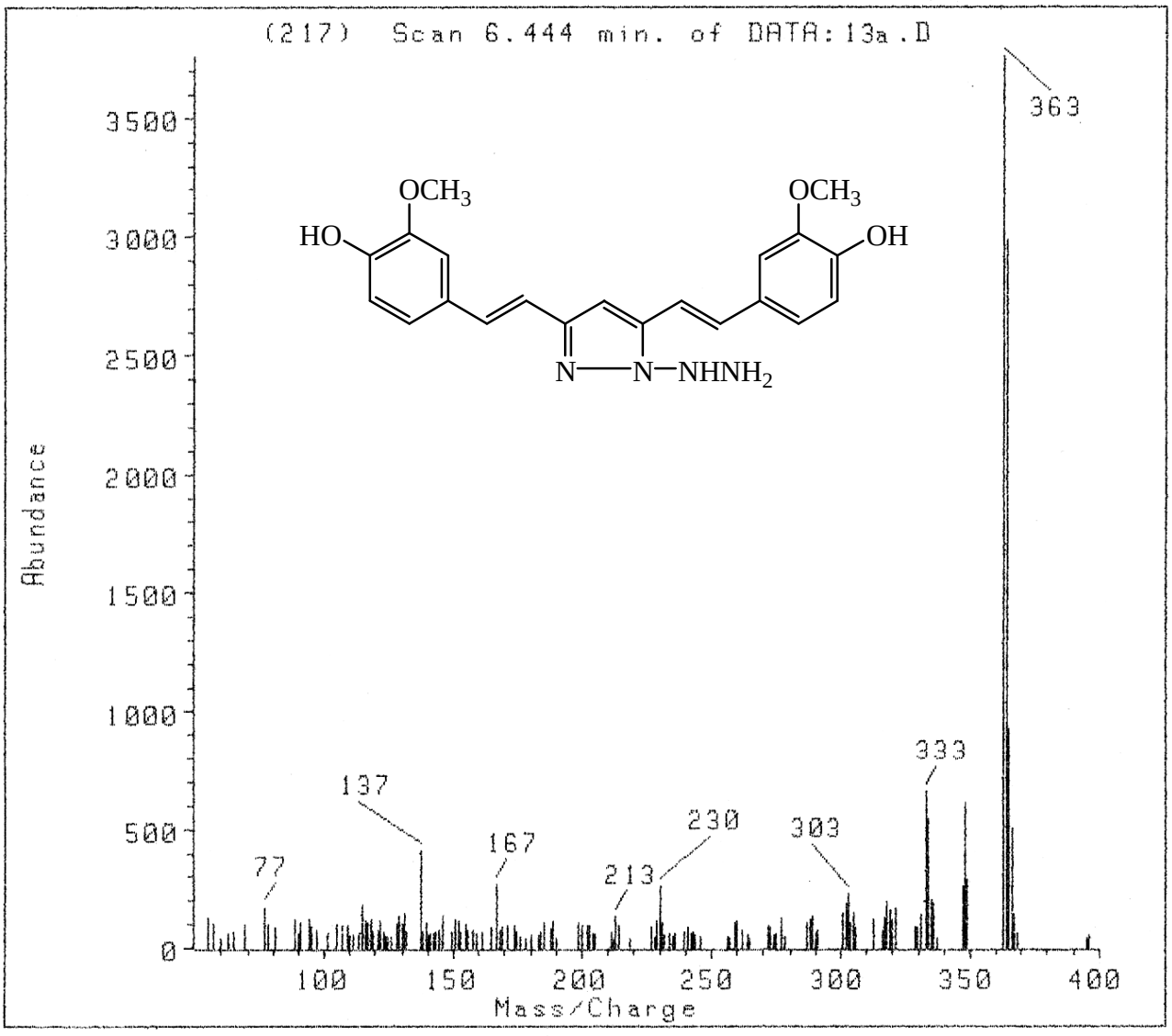

Fig.19 Mass Spectrum Of Compound **(15)**

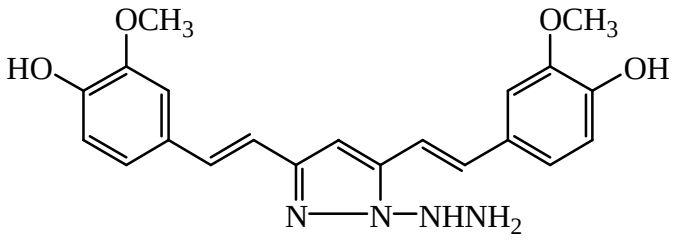

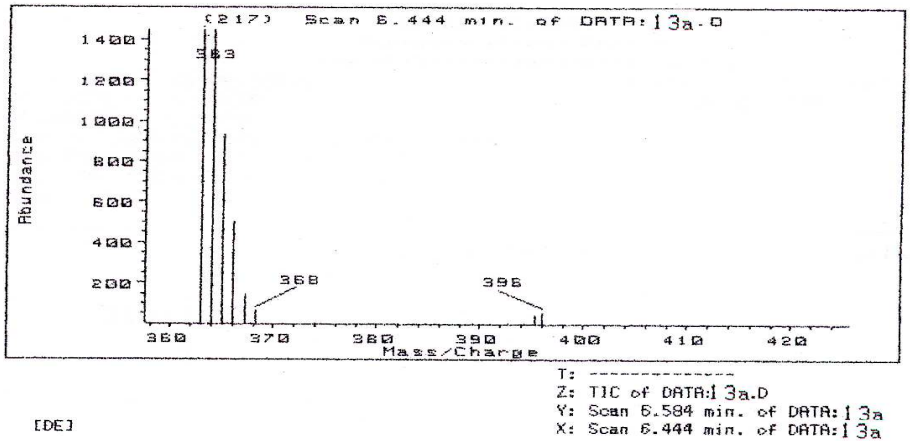

Fig.19 Mass Spectrum Of Compound **(15)**

CAIRO UNIVERSITY
Microanalytical Centre
****

FILE NAME :DATA:13P.D 24 Jan 99 6:42 pm
HP MODEL :MS_5988 INLET TYPE :DIP
OPERATOR :A.ZOHNI
SAMLPE INFORMATION :13P,AMU 50-500
CUSTOMER NAME :
ELECTRON ENERGY: eV FINAL TEMP :C
SERIAL NO.174

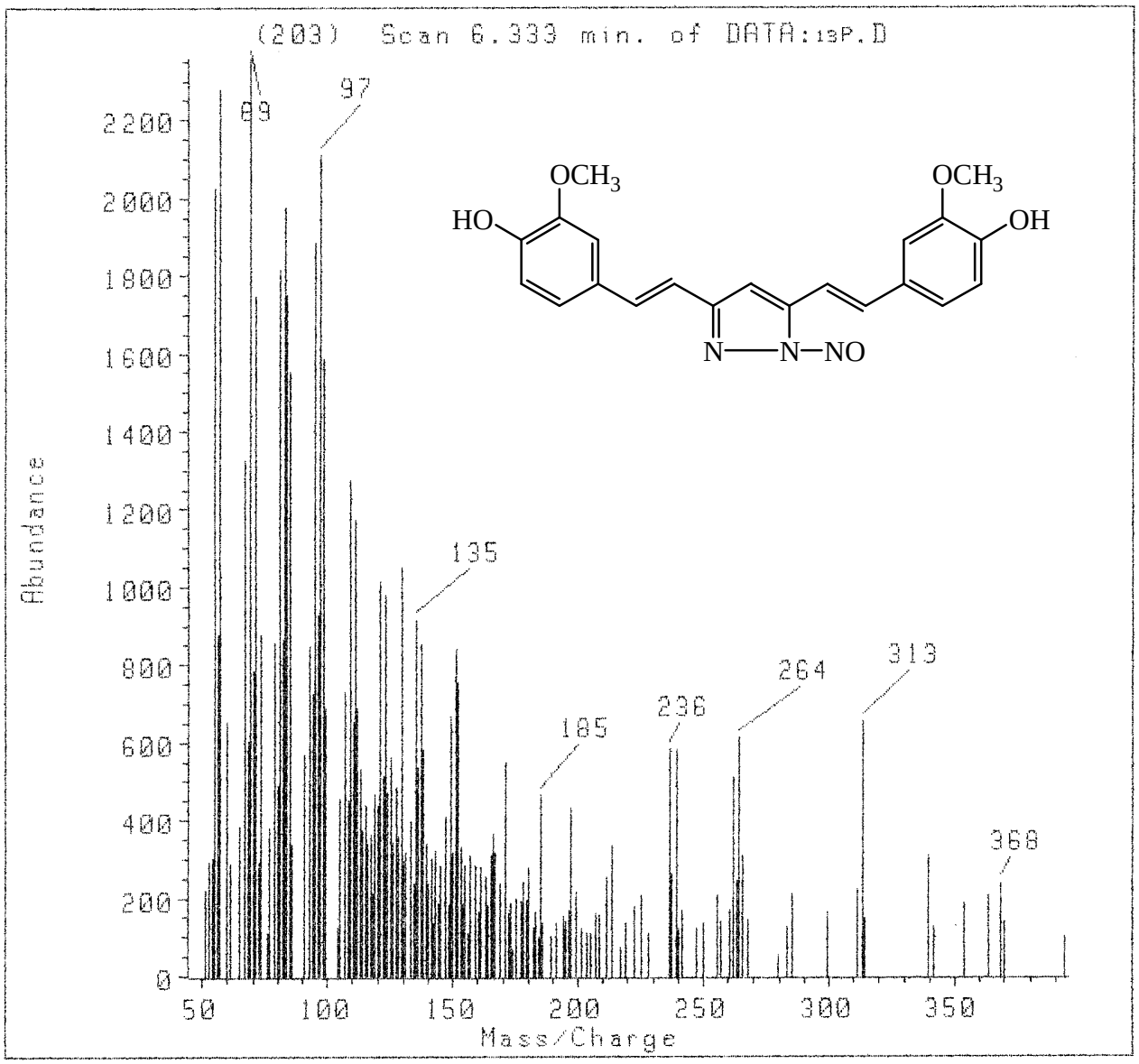

Fig.20 Mass Spectrum Of Compound **(16)**

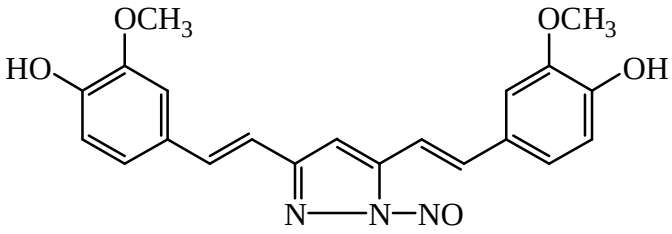

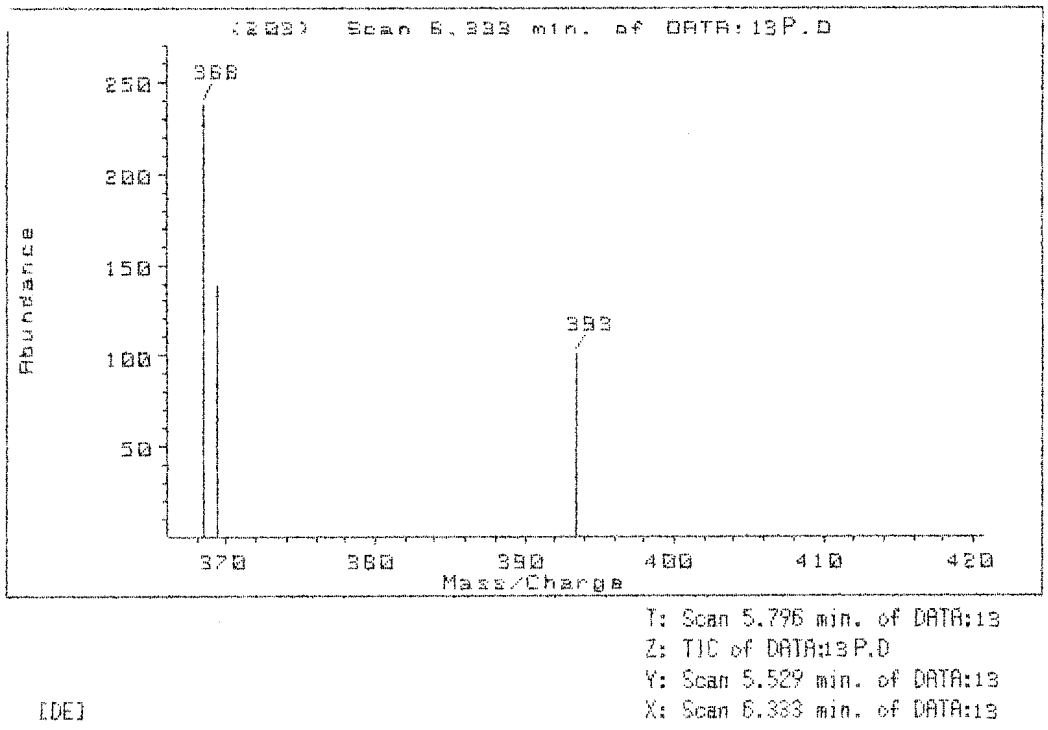

Fig.20 Mass Spectrum Of Compound **(16)**

CAIRO UNIVERSITY
Microanalytical Centre
****

FILE NAME :DATA:14.D 20 Nov 99 1:47 pm
HP MODEL :MS_5988 INLET TYPE :DIP
OPERATOR :A.ZOHNI
SAMLPE INFORMATION :14 ,AMU 50-700
CUSTOMER NAME :
ELECTRON ENERGY: eV FINAL TEMP :C
SERIAL NO.96

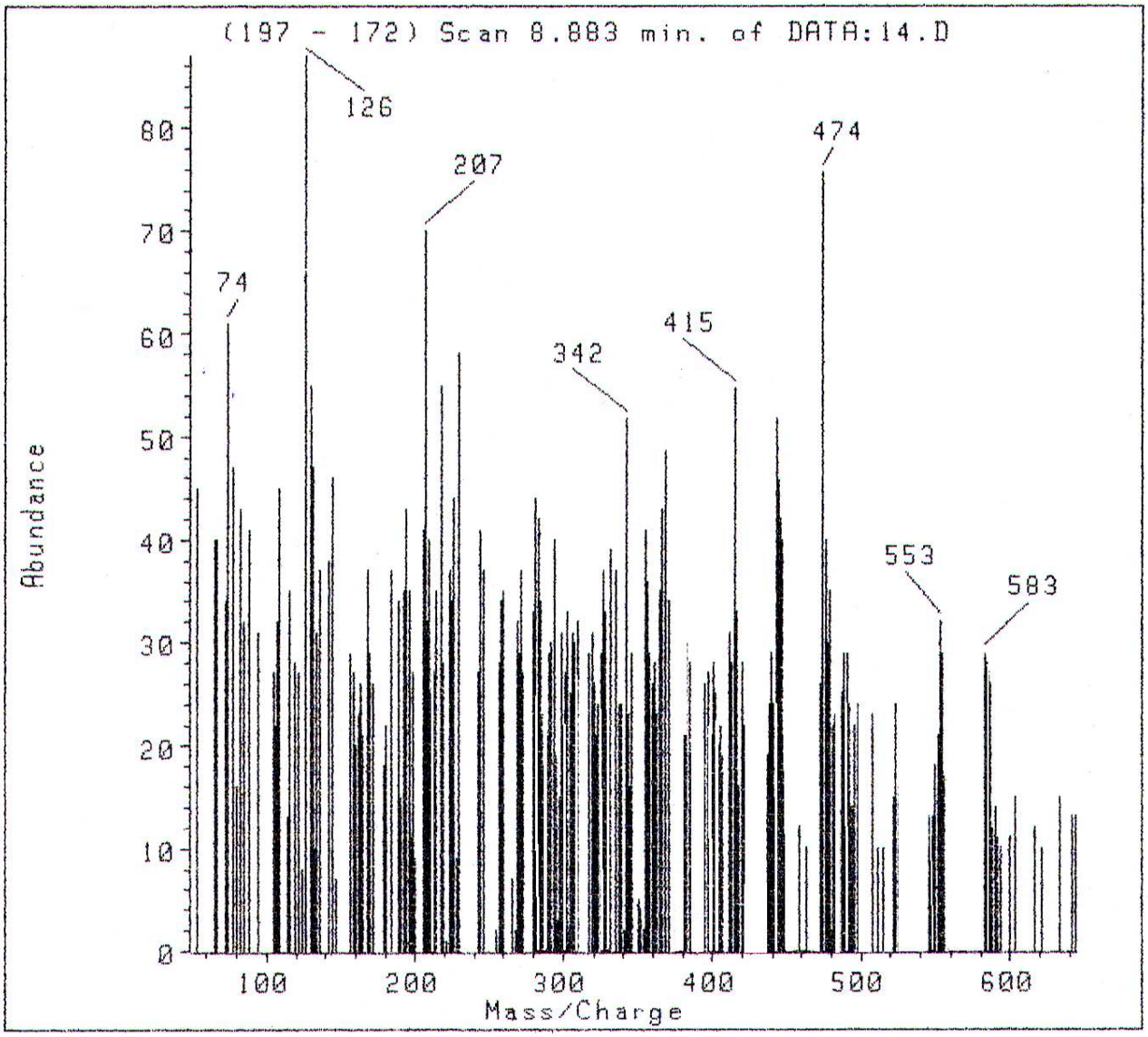

Fig. 21 Mass Spectrum Of Compound **(18)**

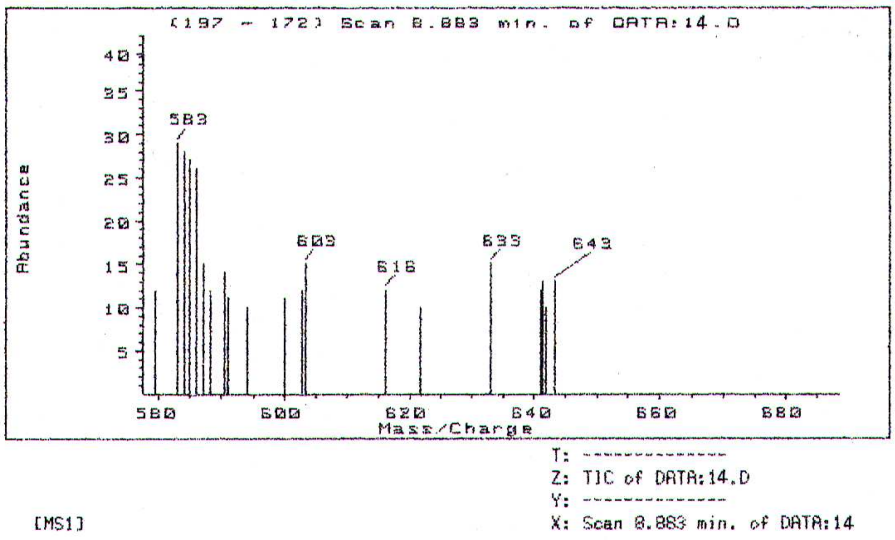

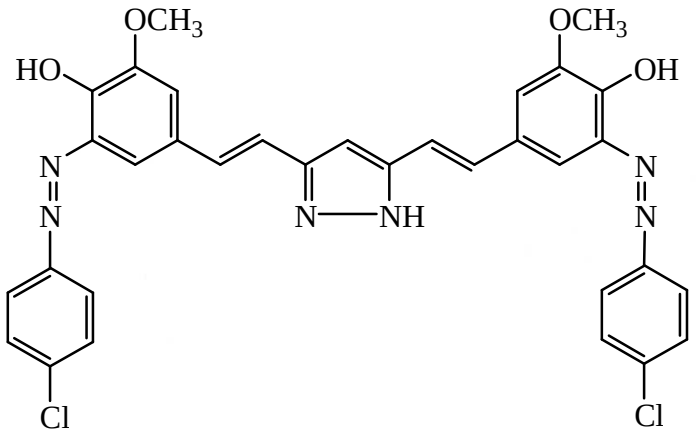

Fig. 21 Mass Spectrum Of Compound **(18)**

CAIRO UNIVERSITY
Microanalytical Centre
****

FILE NAME :DATA:14a.D 20 Nov 99 1:15 pm
HP MODEL :MS_5988 INLET TYPE :DIP
OPERATOR :A.ZOHNI
SAMLPE INFORMATION :14a,AMU 50-700
CUSTOMER NAME :
ELECTRON ENERGY: eV FINAL TEMP :C
SERIAL NO.94

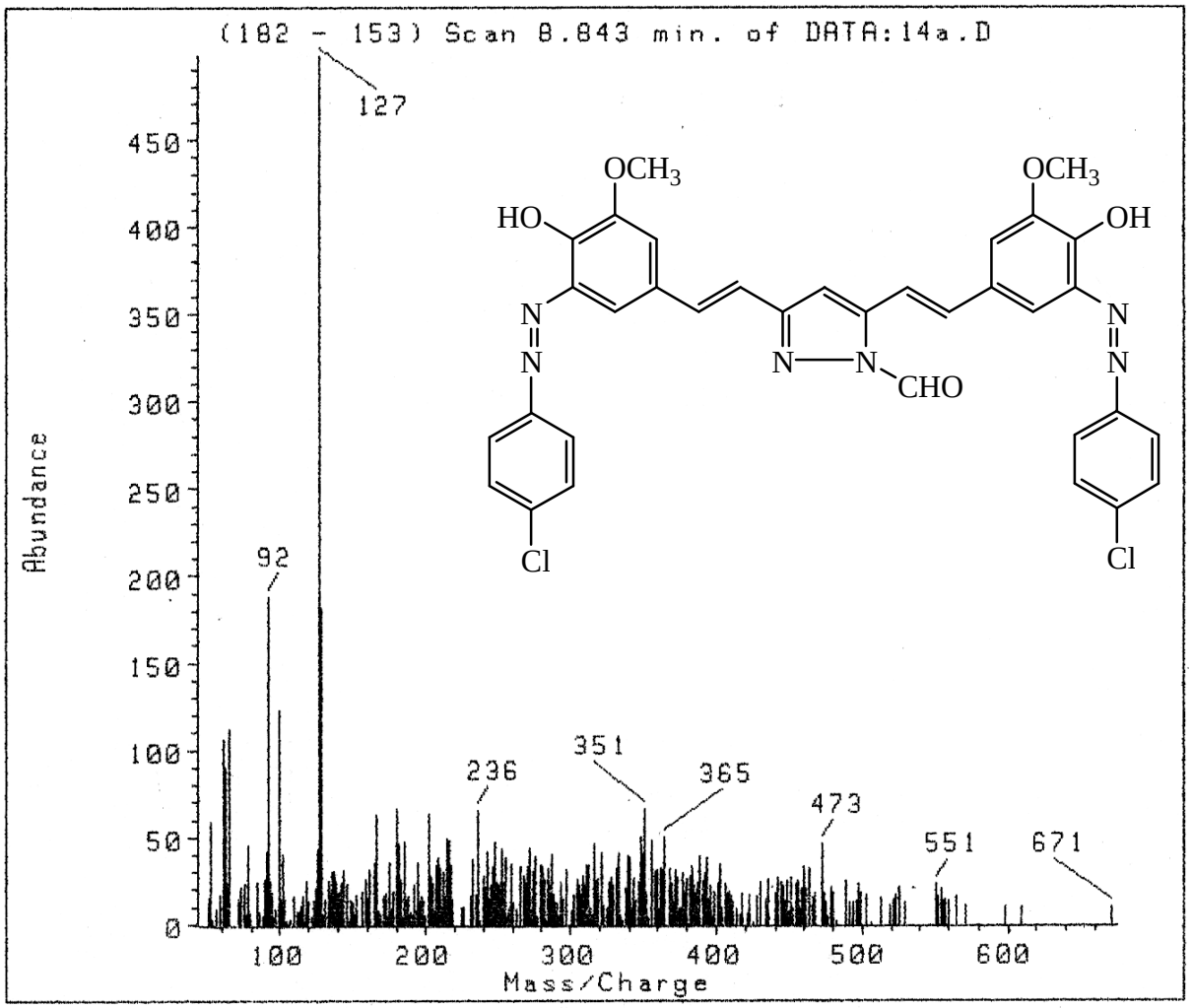

Fig.22 Mass Spectrum Of Compound **(19)**

CAIRO UNIVERSITY
Microanalytical Centre
****

FILE NAME :DATA:14B.D 20 Nov 99 12:35 pm
HP MODEL :MS_5988 INLET TYPE :DIP
OPERATOR :A.ZOHNI
SAMLPE INFORMATION :14B,AMU 50-700
CUSTOMER NAME :
ELECTRON ENERGY: eV FINAL TEMP :C
SERIAL NO.92

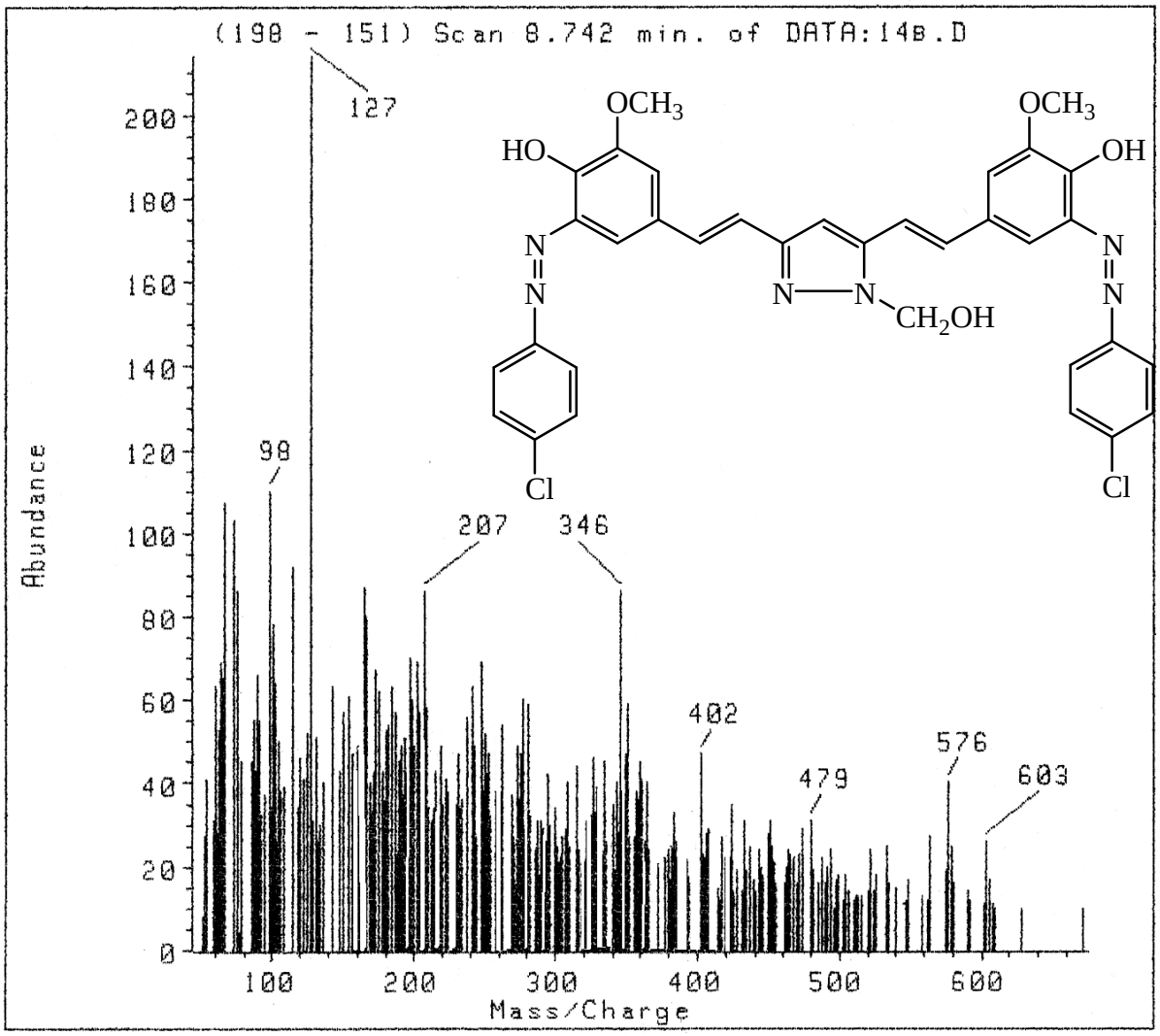

Fig.23 Mass Spectrum Of Compound **(20)**

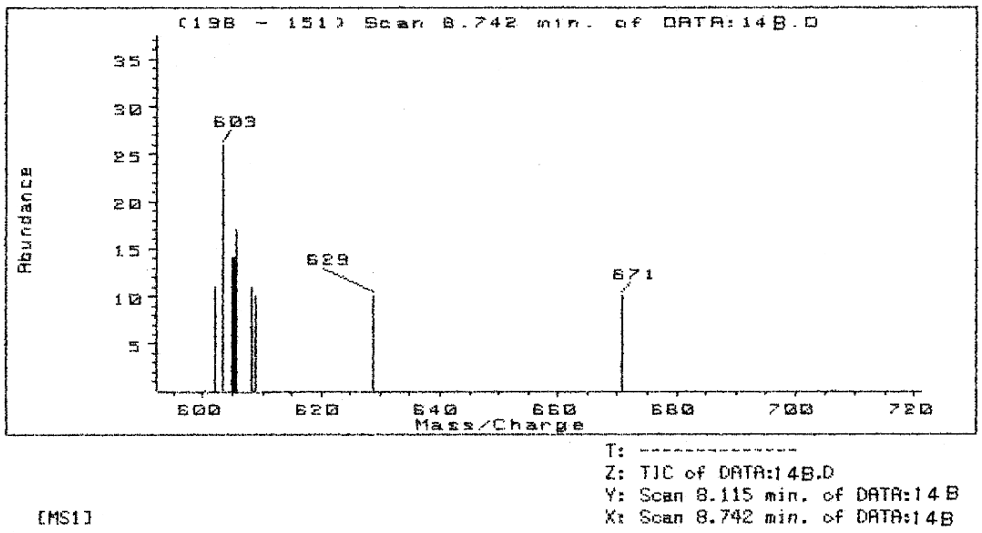

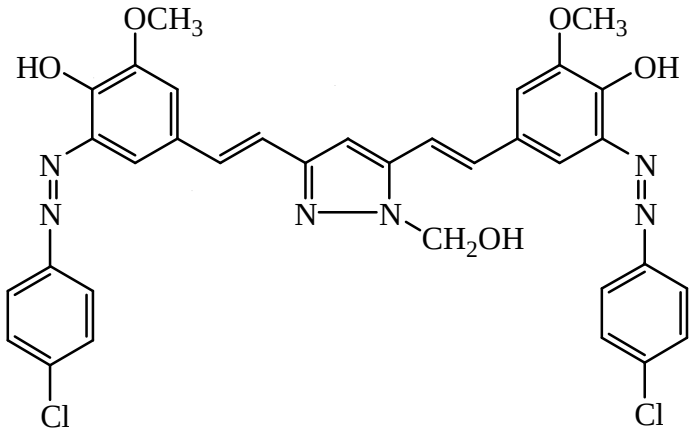

Fig.23 Mass Spectrum Of Compound **(20)**

PART (II)

(A) The inhibitive character of arylazo curcumin derivatives towards the corrosion of a-brass

*Effect of inhibitors (***2a-e***) concentrations on the corrosion of a-brass:*

The effectiveness of the organic compounds **(2a-e)** as inhibitors for the corrosion of α-brass in 2M nitric acid solution has been examined, two independent techniques were used to evaluate the inhibition efficiency of the mentioned compounds in 2M nitric acid these are:

(a) Chemical technique (the weight loss method).

(b) Electrochemical technique (polarization method).

1. Chemical technique (weight loss method):

Weight loss in mg per cm^2 of the surface area was determined in an open system at various time intervals in absence and presence of the additives.

The obtained weight loss-time curves in 2M nitric acid **Figs.(24 – 29)** are characterized by a sharp rise in weight loss from the beginning. Curves for additives containing system fall below that of the free acid. These curves indicated that, the weight loss of α-brass depends on both the type and concentration of these additives. Increase in bulk concentration and consequently increase of surface coverage by the additive increases their inhibition efficiencies towards α-brass dissolution as indicated by the decrease in weight loss per cm^2.

The percentage inhibition of α-brass dissolution was determined after different time intervals from the start of each concentration and for all studied compounds.

Table (2.1) shows the percentage inhibition (In%) which is defind as :

$$\%In = \frac{W_{pure} - W_{inh}}{W_{pure}} x100 \qquad (2.1)$$

where W_{pure} and W_{inh} are weight losses in absence and presence of inhibitors, respectively.

The results of the Table (2.1) show that the inhibition efficiency of all additives increases with the increase of their concentrations in the corrosive medium.It is thus obvious that increase of bulk concentration and consequently, increase of surface area coverage by the additive retards the dissolution of α-brass. The order of the inhibition efficiency of the additive compounds in 2M nitric acid solution over most of the concentration ranges used after 120 minutes is : **2a>2b>2c>2d>2e**

Table (2.1):Variation of the percentage inhibition efficiency of the studied compounds with their molar concentrations after120 min, immersion at 30 ^{o}C.

Concentration (M)	Inhibition efficiency,%				
	2a	2b	2c	2d	2e
$1x10^{-6}$	16.7	13.5	11.4	9.3	7.2
$3x10^{-6}$	19.8	17.2	15.7	13.6	12.3
$5x10^{-6}$	23.7	20.6	18.2	16.2	14.5
$7x10^{-6}$	27.4	23.3	21.6	20.2	17.9
$9x10^{-6}$	32.0	28.5	26.8	24.6	22.8
$11x10^{-6}$	33.9	31.6	28.7	27.4	26.6

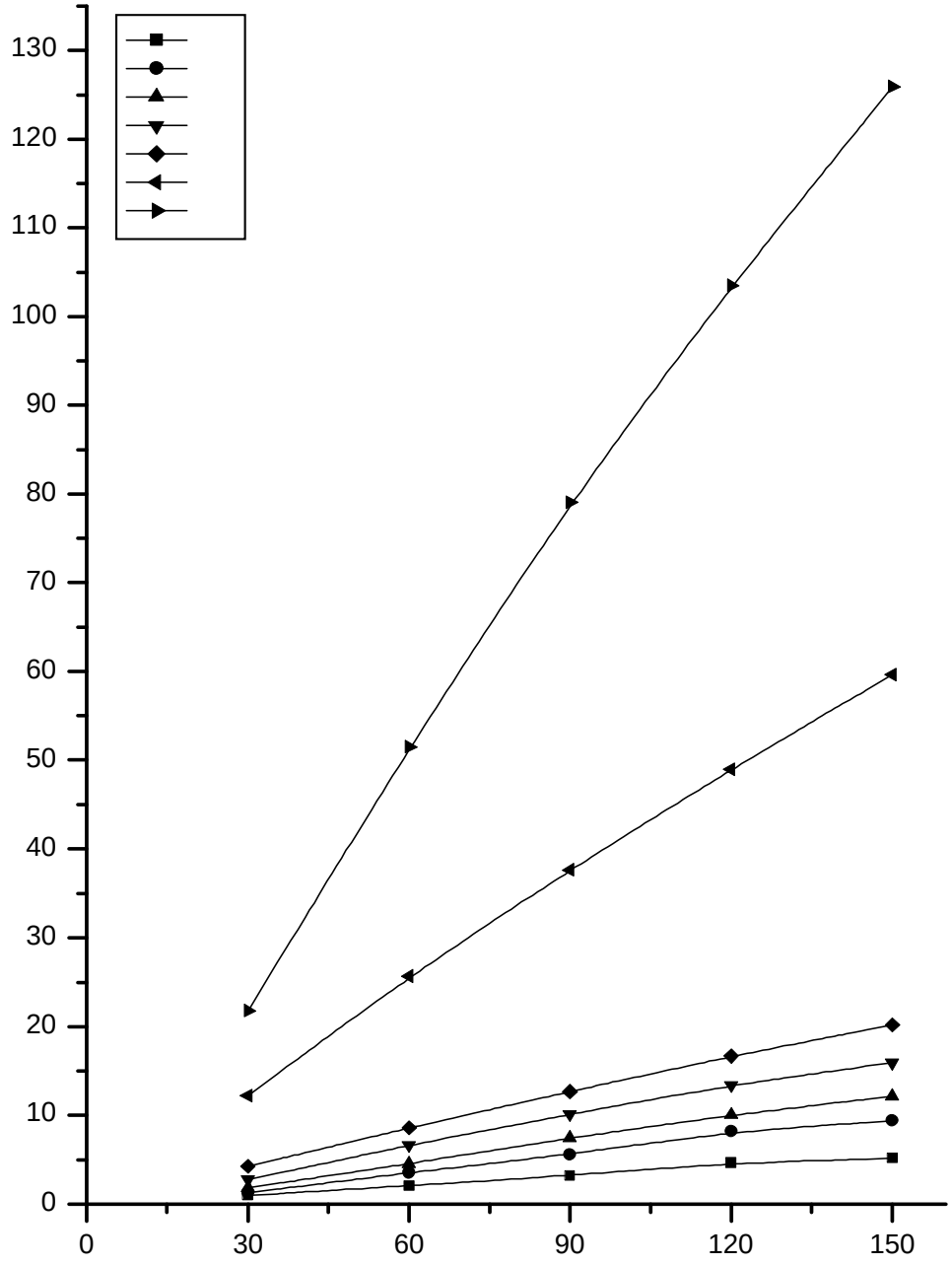
130
120
110
100
90
80
70
60
50
40
30
20
10
0
0
30
60
90
120
150

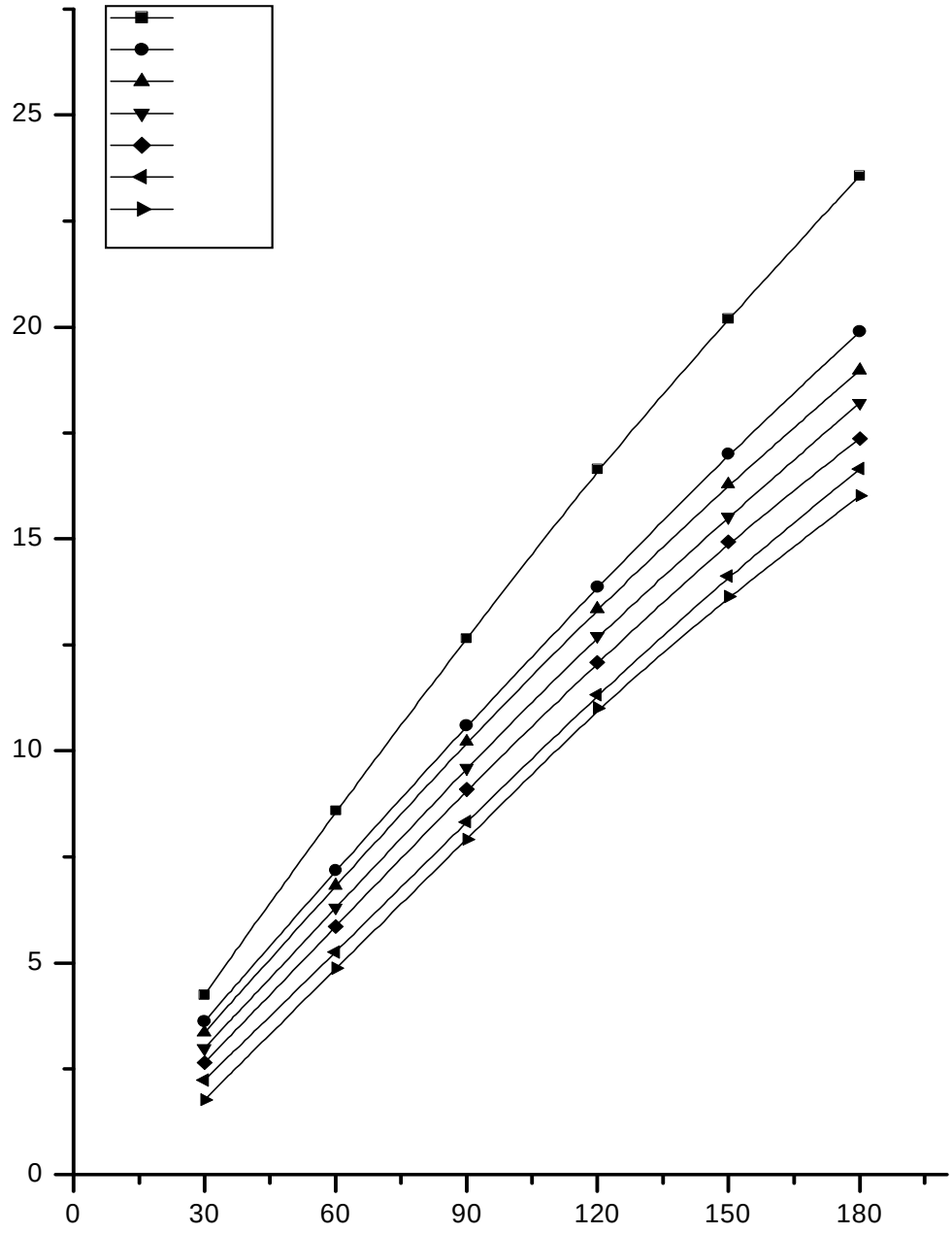
25
20
15
10
5
0
0
30
60
90
120
150
180

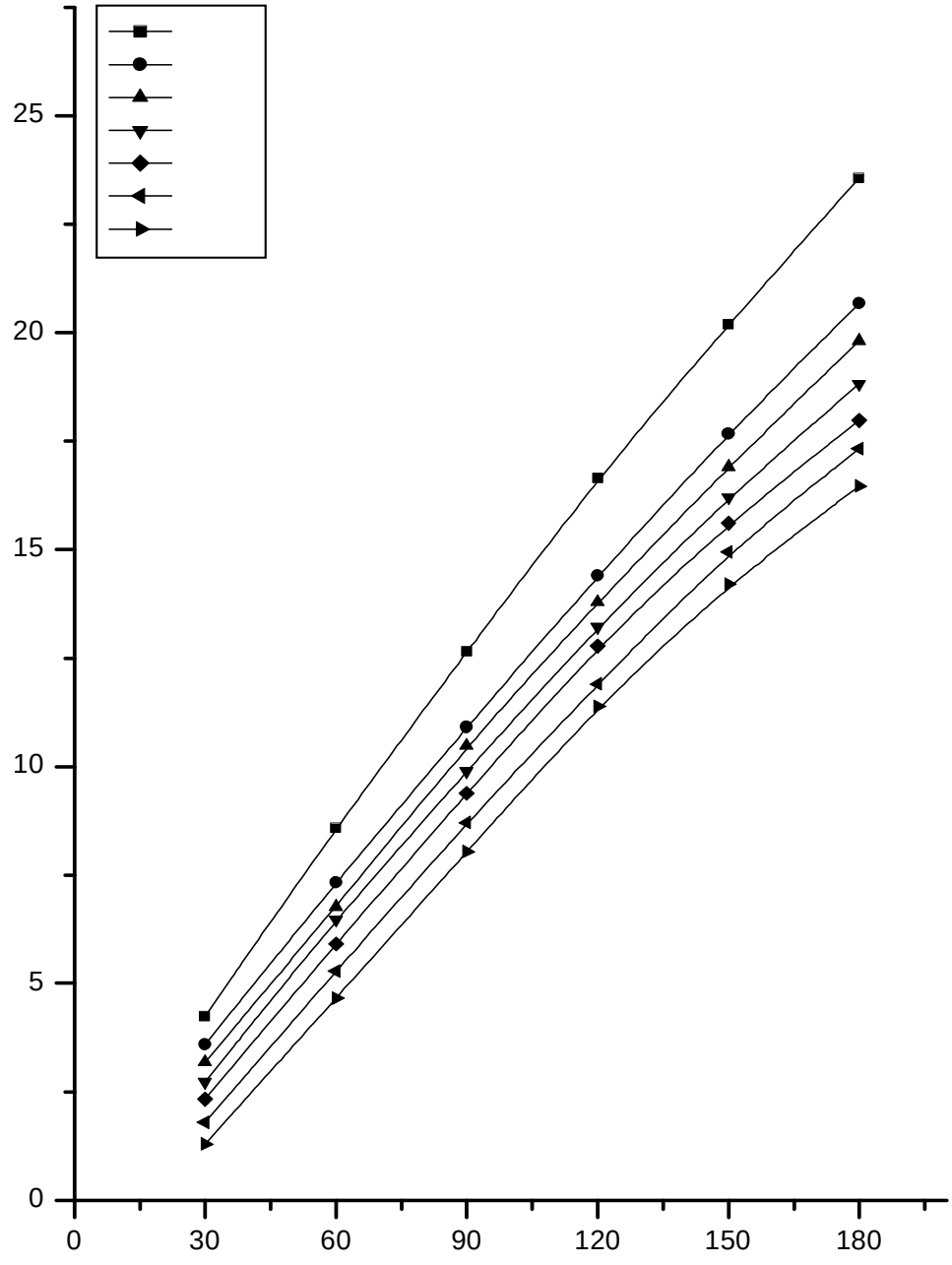
25
20
15
10
5
0
0
30
60
90
120
150
180

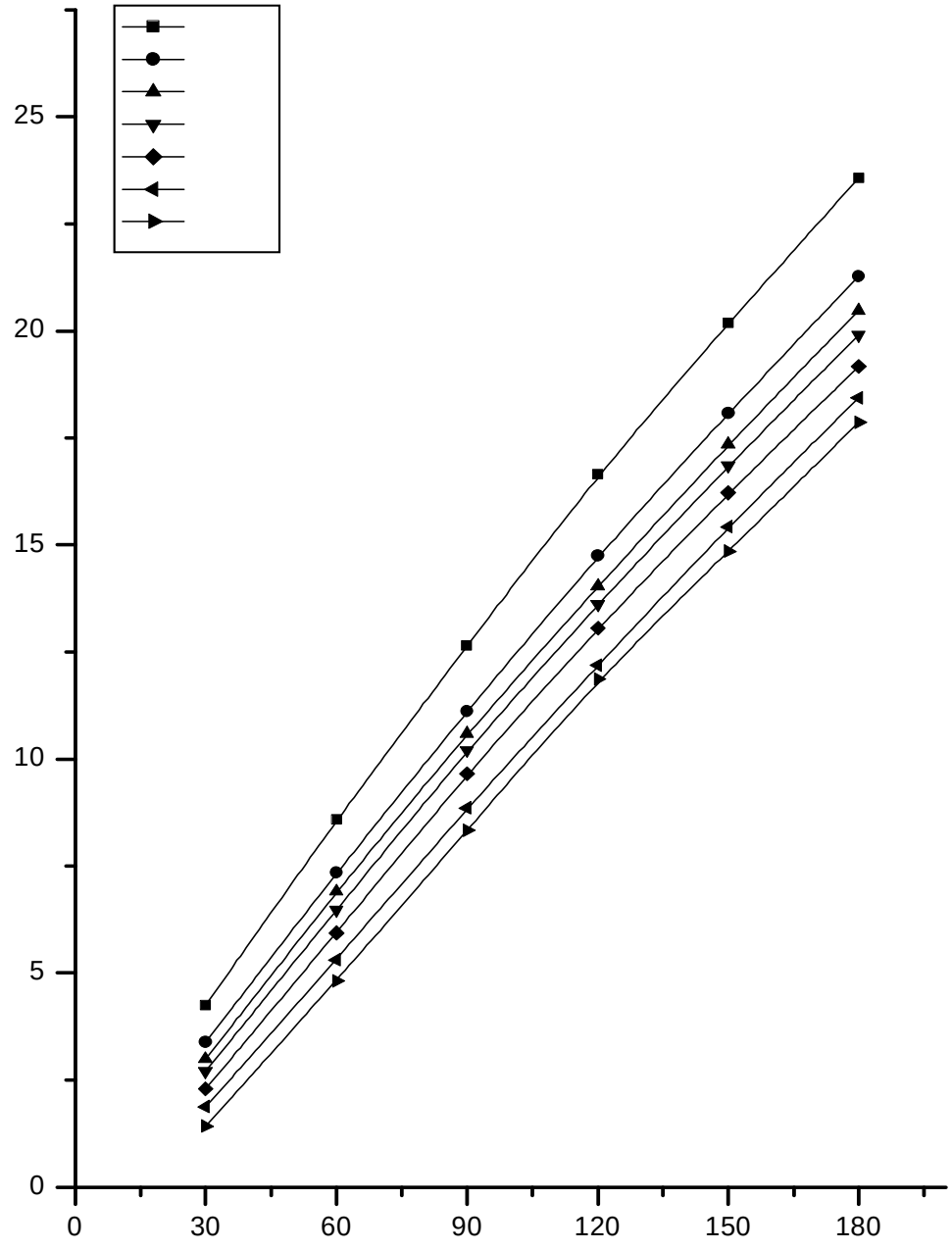
25
20
15
10
5
0
0
30
60
90
120
150
180

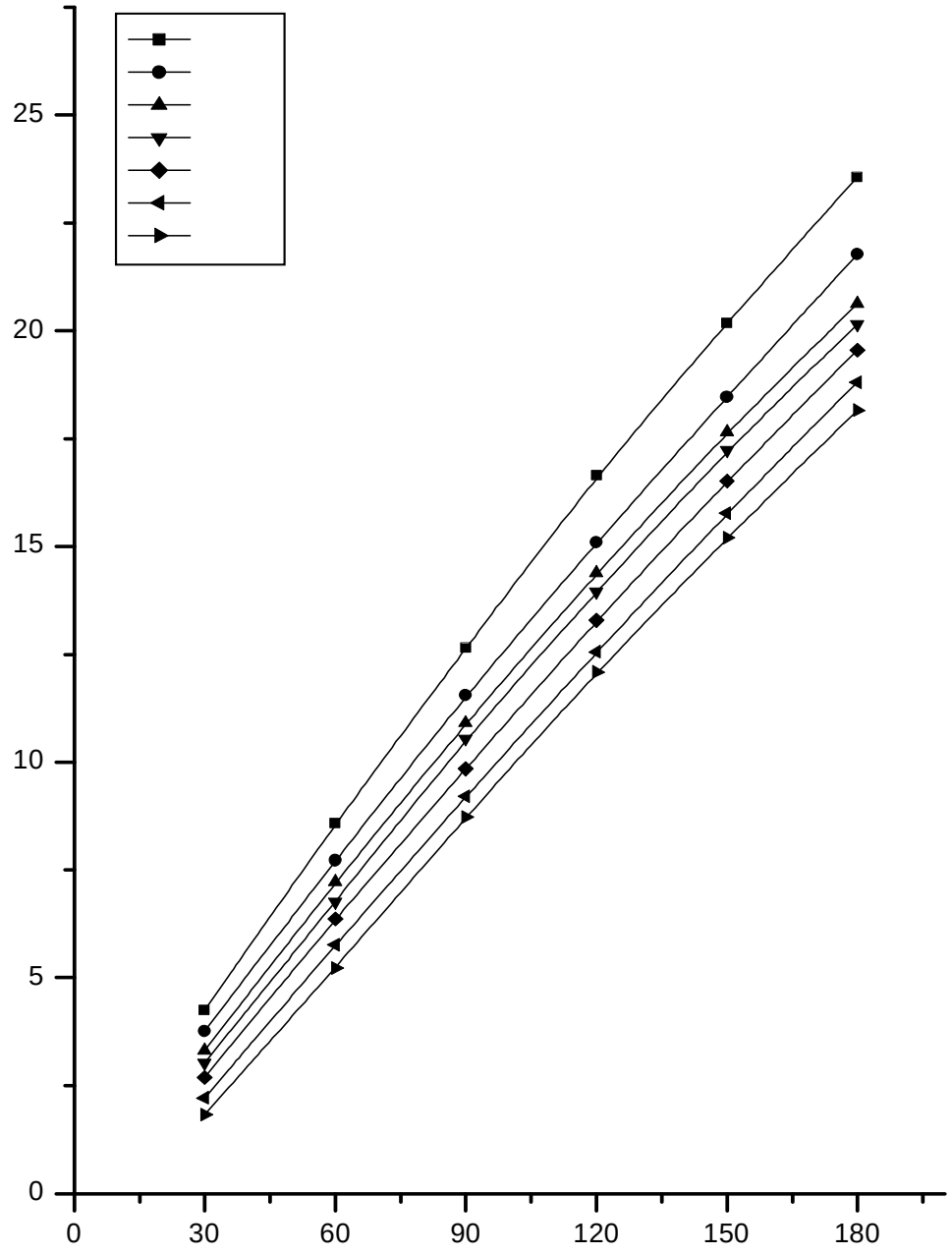
25
20
15
10
5
0
0
30
60
90
120
150
180

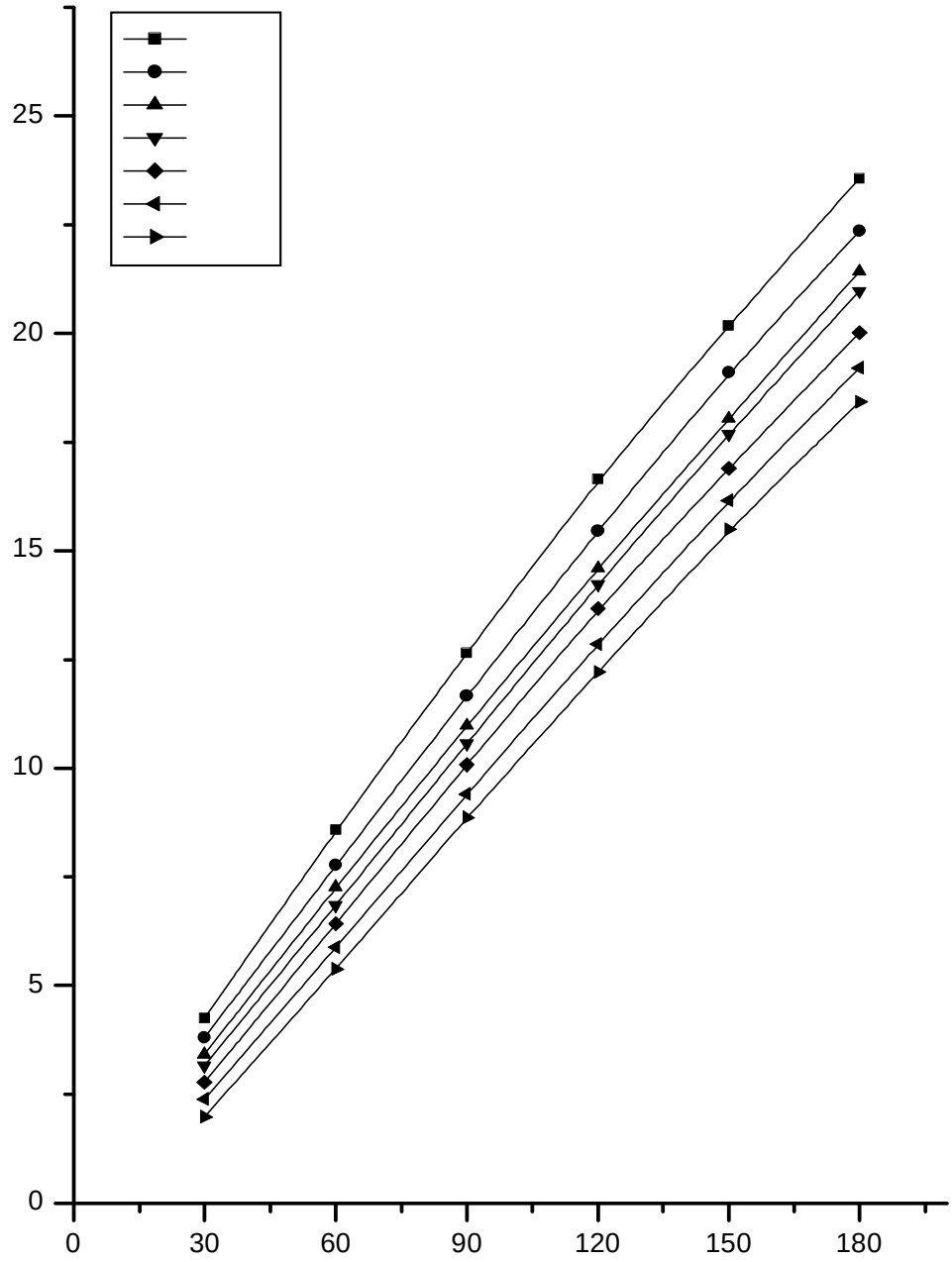
25
20
15
10
5
0
0
30
60
90
120
150
180

2. Adsorption isotherms:

The degree of surface coverage (θ) which represents the part of metal surface covered by inhibitor molecules was calculated using the following equation:

$$\theta = 1 - \frac{W_{pure} - W_{inh}}{W_{pure}} \qquad (2.2)$$

The values of θ have been shown in Table (2.2).

The degree of surface coverage was found to increase with increasing the concentration of the used additives. Attempts were made to fit θ values to various isotherms including Frumkin, Freundlich, Langmuir and Temkin. By far, the best fit was obtained with Frumkin's isotherm which has the following equation:

$$\theta = Const + (2.303 / f) \log C \qquad \textbf{(2.3)}$$

where $f = 1/RT\ [d(\Delta G_a^o / d\theta]$ **(2.4)**

where C = inhibitor concentration

ΔG_a^o = the free energy of adsorption.

Figure (30) represents the relation between θ and log C for the inhibitors **(2a-e)**. The Frumkin's adsorption isotherm is obeyed. From these results it could be concluded that there is a kind of interaction between the molecules adsorbed at the metal surface.

Table (2.2): Variation of degree of surface coverage (θ) of different compounds **(2a-e)** with their molar concentrations at 30 ^{o}C from weight loss meaasurements at 120 min. Immersion

Concentration (M)	Surface coverage (θ)				
	2a	2b	2c	2d	2e
$1x10^{-6}$	0.167	0.135	0.114	0.093	0.072
$3x10^{-6}$	0.198	0.172	0.157	0.136	0.123
$5x10^{-6}$	0.237	0.206	0.182	0.162	0.145
$7x10^{-6}$	0.274	0.233	0.216	0.202	0.179
$9x10^{-6}$	0.320	0.285	0.268	0.246	0.228
$11x10^{-6}$	0.339	0.316	0.287	0.274	0.266

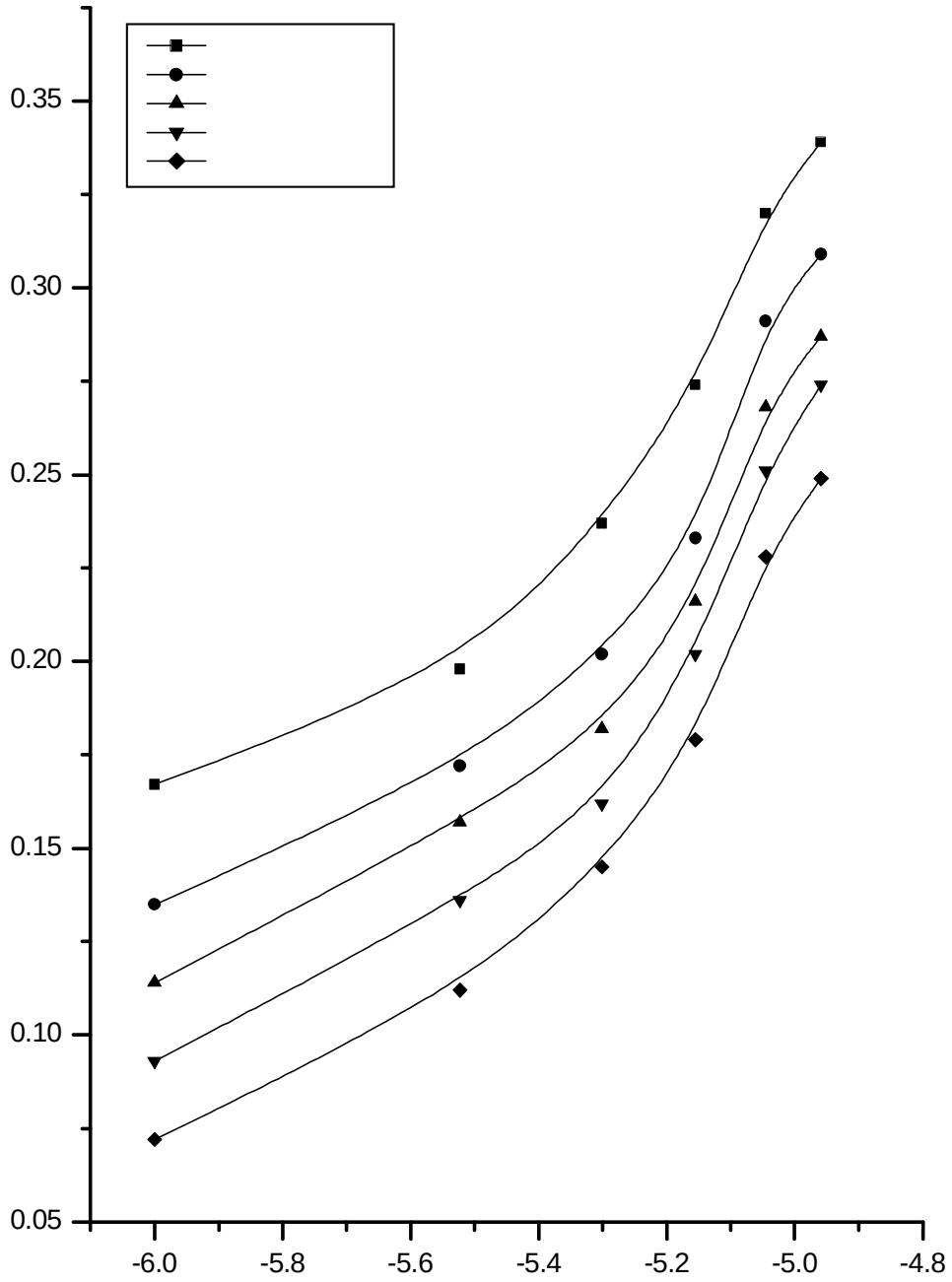
0.35
0.30
0.25
0.20
0.15
0.10
0.05
-6.0
-5.8
-5.6
-5.4
-5.2
-5.0
-4.8

3. ***Effect of temperature on the corrosion inhibition of a-brass:***

The dissolution of α-brass in 2M nitric acid increases by increasing temperatures **Fig. (31)**.The dissolution of α-brass in 2M nitric acid in presence of different inhibitors at $11x10^{-6}$ M was studied by weight loss method over a temperature range 30-50^{o}C. The weight loss-time curves obtained **[Fig. (32-36)]** in presence of additives indicate that the rate of α-brass dissolution increases as the temperature increases, but at lower rate than in uninhibited solutions. The protection efficiency of the additives decreases (rate constant of α-brass dissolution increases) with rise in temperature which proves that the adsorption of these compounds on the surface of α-brass occurs through physical adsorption of the additives on the metal surface. Desorption is aided by increasing the reaction temperature.

The apparent activation energy E_a^*, the enthalpy of activation ΔH^* and the entropy of activation ΔS^* for the corrosion of α-brass in 2M nitric acid solutions in the absence and presence of different concentrations of arylazo curcumin compounds were calculated from Arrhenius-type equation:

$$\text{Rate} = A \exp(-E_a^*/RT) \qquad (2.5)$$

and transition-state equation:

$$\text{Rate} = RT/Nh \exp(\Delta S^*/R) \exp(-\Delta H^*/RT) \qquad (2.6)$$

where A is the frequency factor, h is the Planck's constant, N is Avogadro's number and R is the universal gas constant. A plot of log Rate vs. 1/T and log (Rate/T) vs. 1/T give straight lines with slope of $-E_a^*/2.303R$, and $-\Delta H^*/2.303R$, respectively. The intercepts will be A and

log R/Nh+ΔS^*/2.303R for Arrhenius and transition state equations, respectively.

Figures (37,38) represent plots of the log rate vs. 1/T and log (rate/T) vs. 1/T data. The calculated values of the apparent activation energy, E_a^*, activation entropies, ΔS^*,and activation enthalpies, ΔH^*, are given in Table (2.3).

The almost similar values of E_a^* suggested that the inhibitors are similar in the mechanism of action and the order of efficiency may be related to the preexponential factor A in equation (2.5). This is further related to concentration, steric effects and metal surface characters.

Generally one can say that the nature and concentration of electrolyte affect greatly the activation energy for the corrosion process.

The order of the inhibition efficiencies of arylazo curcumin compounds as gathered from the increase in E_a^* and ΔH^* values and decrease in ΔS^* values is as follow:

2a > 2b>2c > 2d>2e

Table (2.3): Activation energy (E_a^*), enthalpy change (ΔH_a^*) and entropy change (ΔS_a^*)for the α-brass in 2M nitric acid in absence and presence of different inhibitors.

Compound	$-E_a^*$(K J mol^{-1})	ΔH_a^*(K J mol^{-1})	$-\Delta S_a^*$(J mol^{-1} K^{-1})
Blank	32.739	30.18	161.88
2a	34.020	31.46	158.92
2b	34.210	31.65	158.45
2c	34.322	31.76	158.27
2d	34.435	31.88	158.13
2e	34.816	32.26	157.18

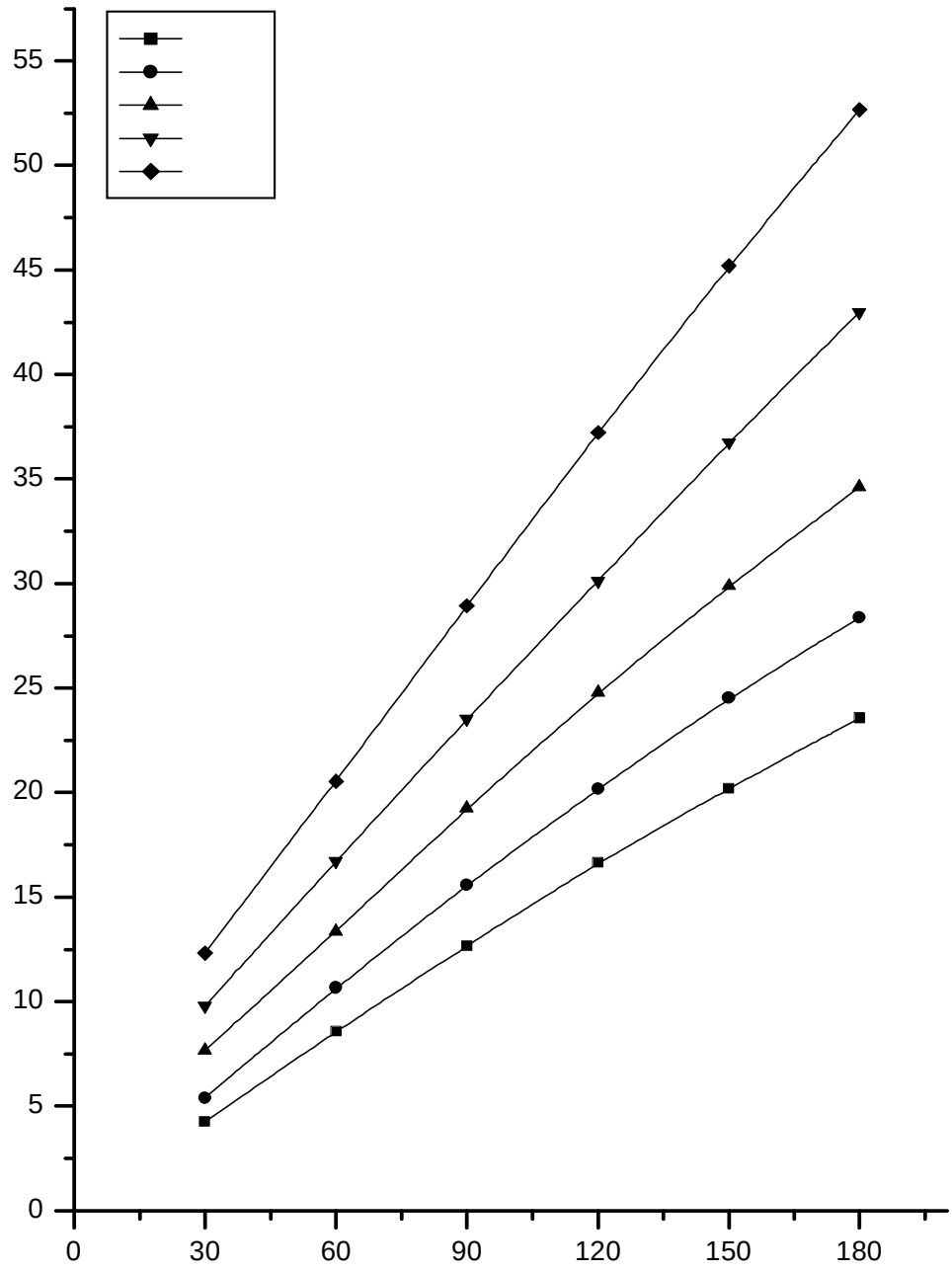
55
50
45
40
35
30
25
20
15
10
5
0
0
30
60
90
120
150
180

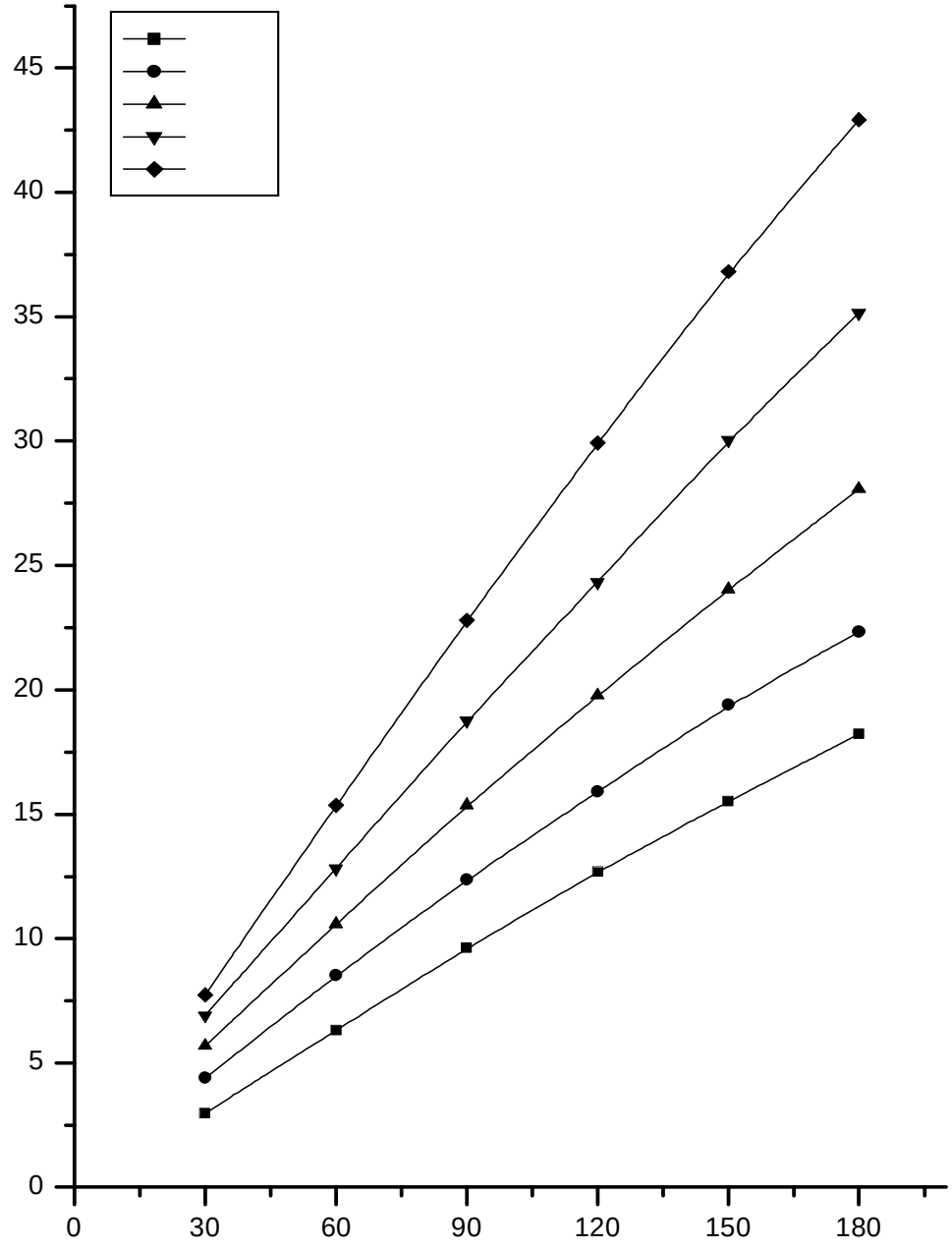
45
40
35
30
25
20
15
10
5
0
0
30
60
90
120
150
180

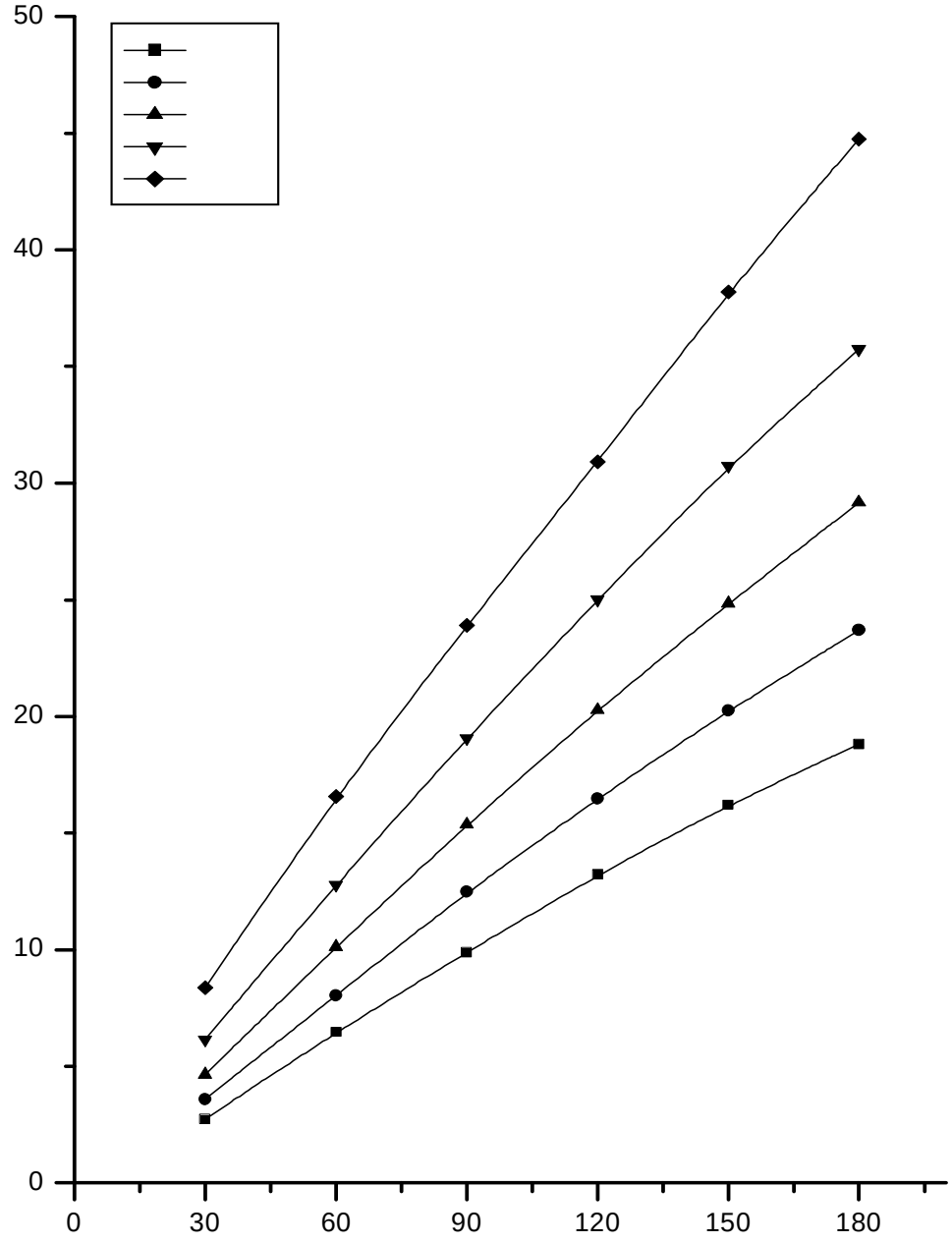
50
40
30
20
10
0
0
30
60
90
120
150
180

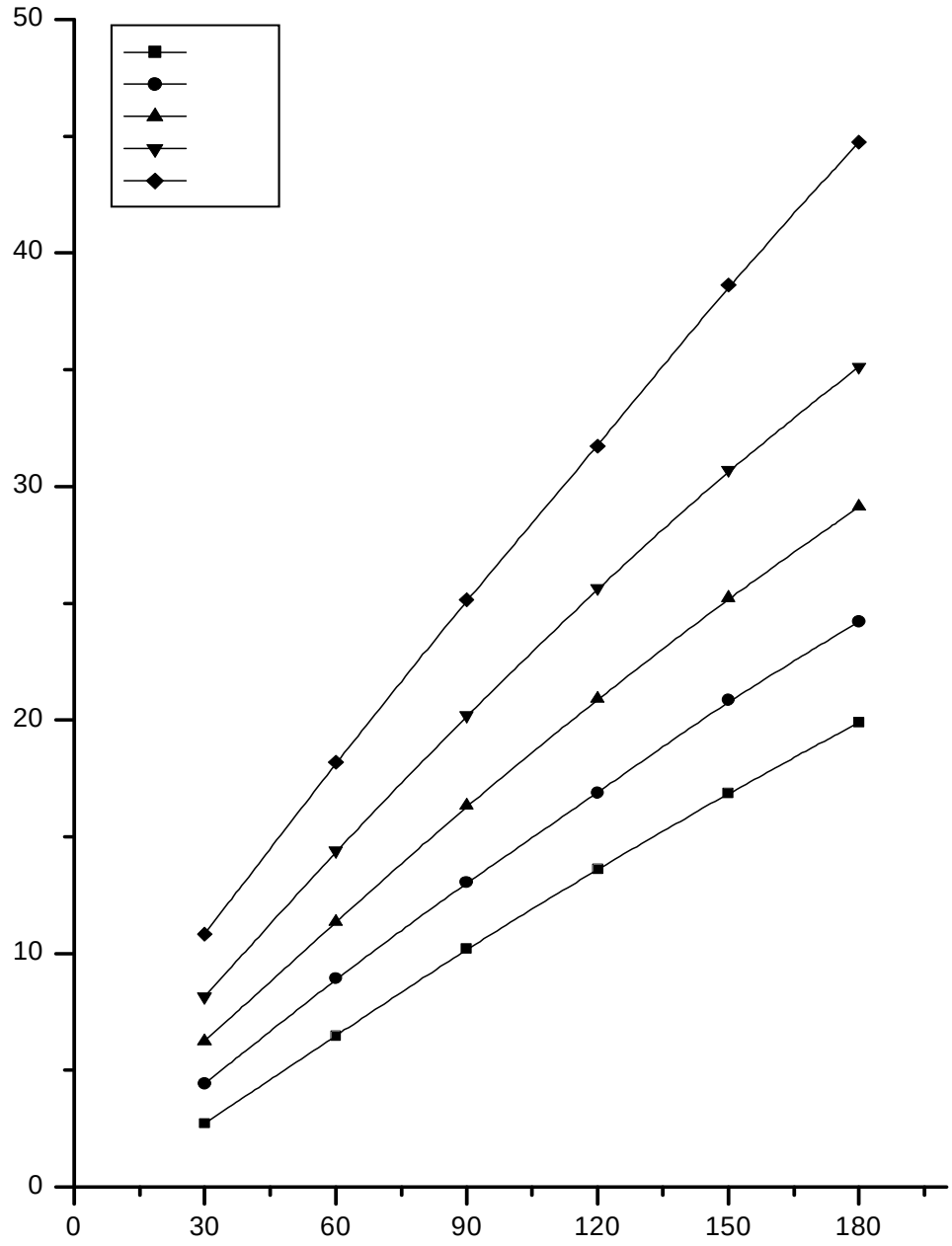
50
40
30
20
10
0
0
30
60
90
120
150
180

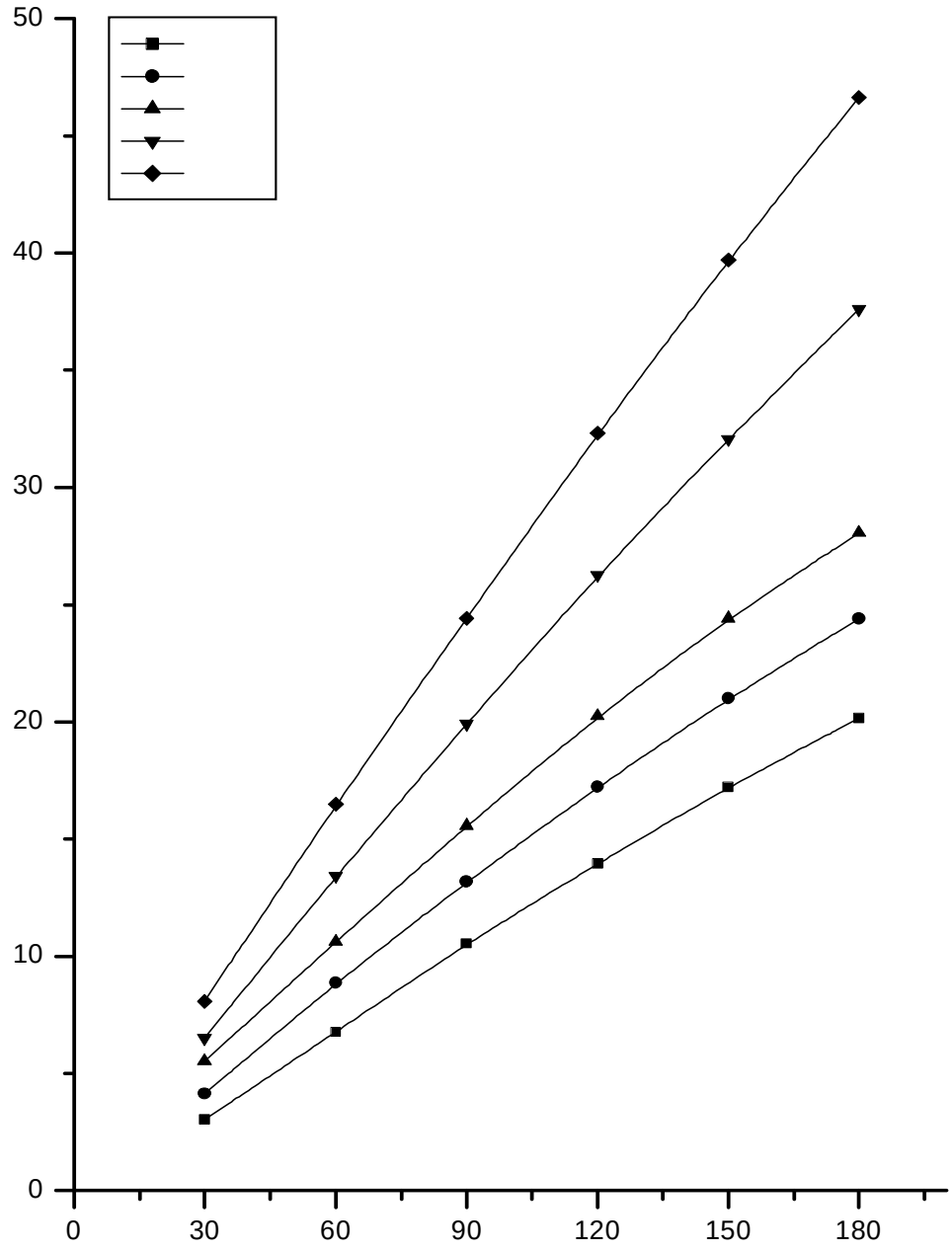
50
40
30
20
10
0
0
30
60
90
120
150
180

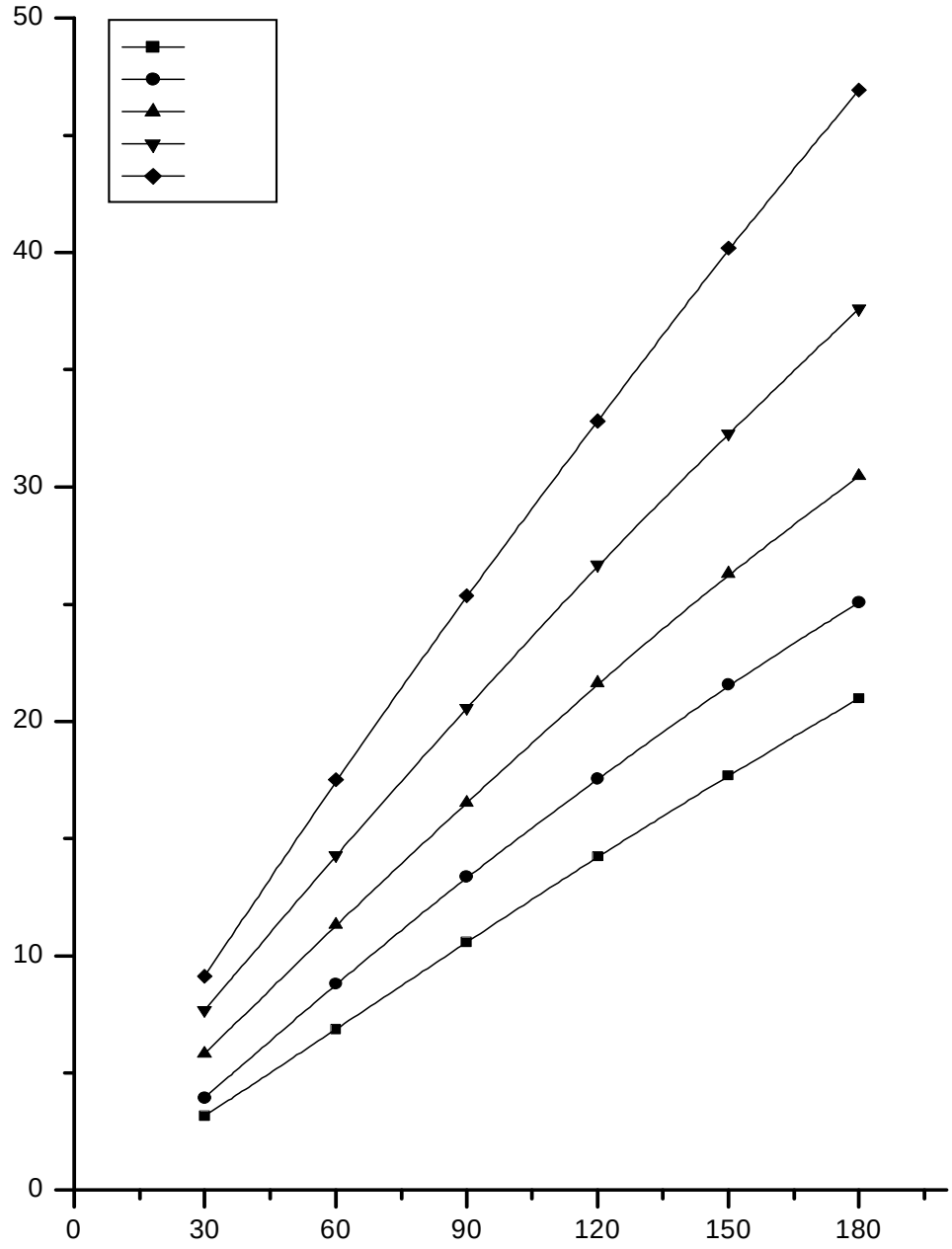
50
40
30
20
10
0
0
30
60
90
120
150
180

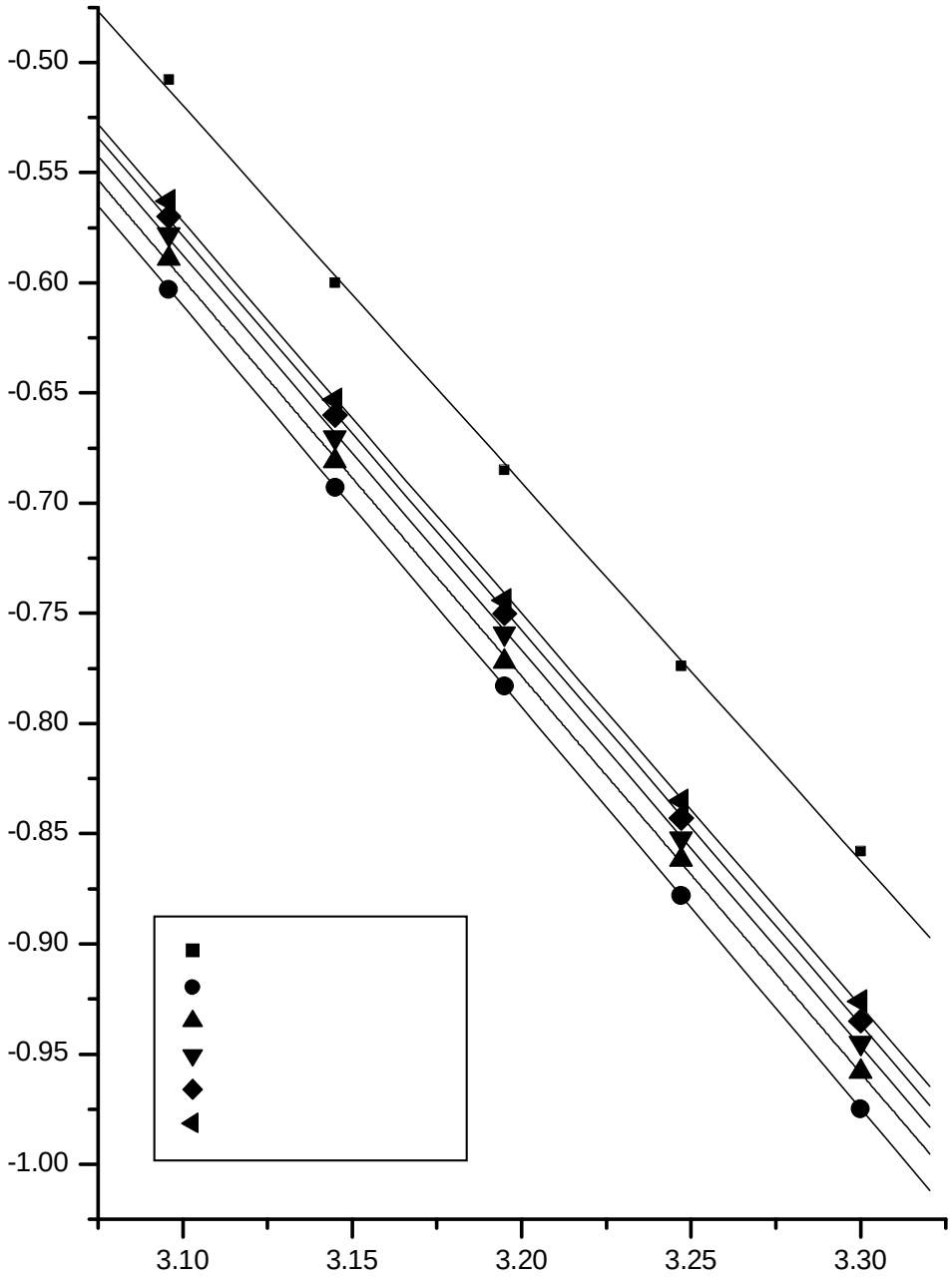
-0.50
-0.55
-0.60
-0.65
-0.70
-0.75
-0.80
-0.85
-0.90
-0.95
-1.00
3.10
3.15
3.20
3.25
3.30

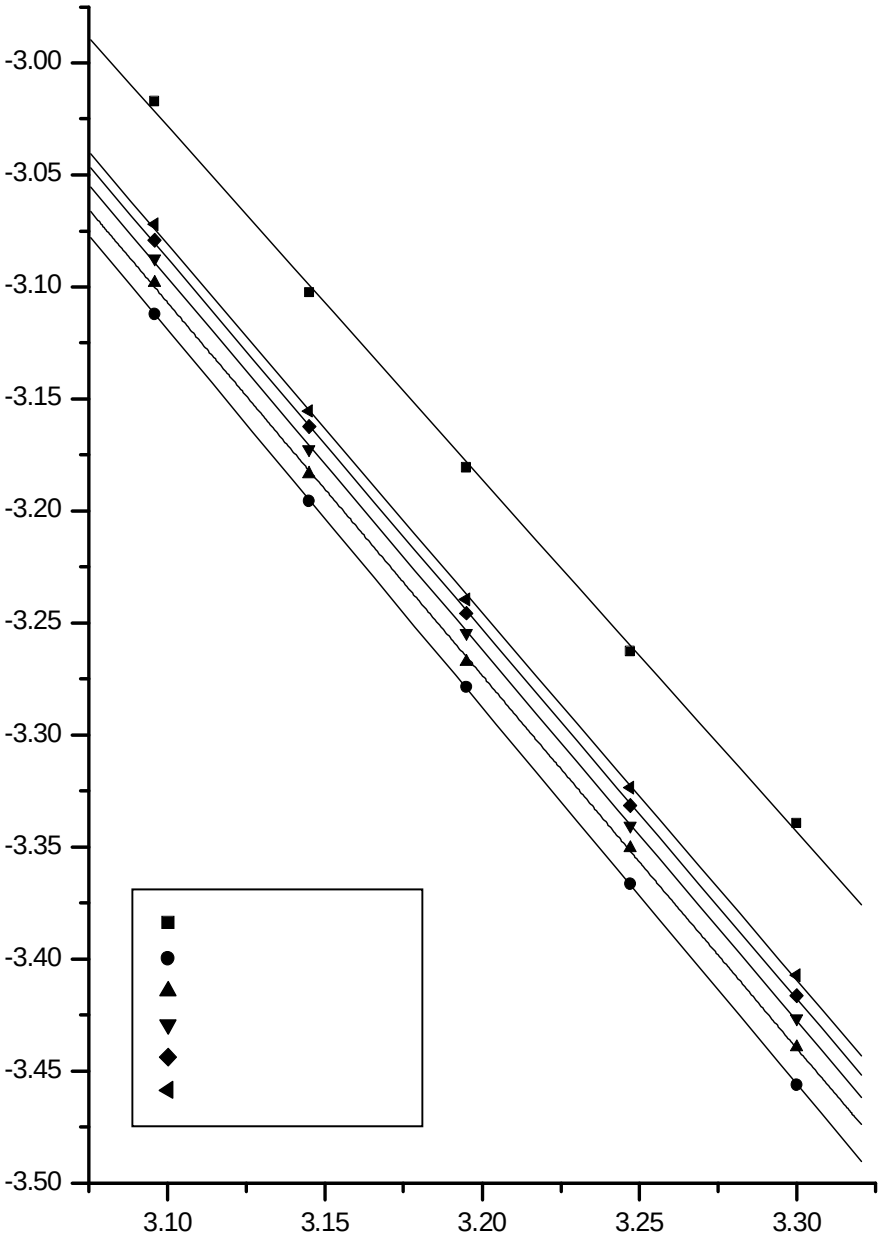
-3.00
-3.05
-3.10
-3.15
-3.20
-3.25
-3.30
-3.35
-3.40
-3.45
-3.50
3.10
3.15
3.20
3.25
3.30

4. Synergistic effect:

Some anions are found to enhance the inhibitive effect of several nitrogen containing organic compounds in acid solutions.[158-161] In the present study the influence of thiocyanide ions on the inhibitive performance of arylazo curcumin compounds has been studied using weight loss technique.

Figures (39-43) represent the weight loss-time curves for α-brass dissolution in 2M nitric acid for various concentrations of arylazo curcumin compounds and at specific concentration ($1X\ 10^{-2}$ M) of this salt. The values of inhibition efficiency (%In) for various concentrations of inhibitors in the presence of specific concentration of potassium thio cyanide are given in Table (2.4).

The synergistic inhibition effect was evaluated using a parameter, S_θ, obtained from the surface coverage values (θ) of the anion, cation and both. Aramaki and Hackerman,[162] calculated the synergism parameter S_θ using the following equation:

$$S_\theta = 1-\theta_{1+2} / 1-\theta'_{1+2} \qquad (2.7)$$

where: $\theta_{1+2} = (\theta_1 + \theta_2) - (\theta_1\theta_2)$;

θ_1 = surface coverage by anion;

θ_2 = surface coverage by cation;

θ'_{1+2} = measured surface coverage by both the anion and cation.

We calculate synergism parameters from the above equation. The plot of the synergism parameter (S_θ) against various concentrations of arylazo curcumin compounds is given in **Fig.(44)** and the corresponding values are shown in Table (2.5). As can be seen from this Table, values nearly equal to unity were obtained, which suggests that the enhanced

inhibition efficiencies caused by the addition of thiocyanide to arylazo curcumin compounds is due mainly to the synergistic effect.

Table (2.5) shows the synergism parameter for constant potassium thiocyanide concentration added to different concentrations of arylazo curcumin compounds.

Finally; It is observed that %In of the inhibitors increases in the presence of thiocyanide ions due to synergistic effects.[163] The synergistic effect of this anion (SCN^-) have been observed.[164] Adsorption of arylazo curcumin compounds at the α-brass /solution interface occurs through physical adsorption via electron rich centers,i.e. benzene ring through its π-electrons and nitrogen atom through their lone pairs of electrons by donation of electrons to the empty d-orbital of the metal.[165] It is known that (SCN^-) anions have strong interactions with α-brass surfaces owing to chemisorption.[166,167] The strong chemisorption of (SCN^-) anions on the metal surface is responsible for the synergistic effect of thiocyanide anions in combination with cation of the inhibitor. The cation is then adsorbed by coulombic attraction on the metal surface where thiocyanide anions are already adsorbed by chemisorption. Stabilization of adsorbed thiocyanide anions with cations leads to greater surface coverage and therefore greater inhibition.

Table (2.4):Values of inhibition efficiencies (%In) of different arylazo curcumin compounds in the presence of $1X10^{-2}$ M KSCN for the corrosion of α-brass in 2M HNO_3 at 30^oC. Duration of the experiment:120 min. immersion.

Concentration (M)	Inhibition efficiency (%In)				
	2a	2b	2c	2d	2e
$1x10^{-6}$	77.72	76.73	75.89	74.97	74.08
$3x10^{-6}$	80.09	78.44	77.29	76.52	75.65
$5x10^{-6}$	82.35	80.42	79.17	78.78	77.08
$7x10^{-6}$	84.39	82.86	80.87	80.42	78.37
$9x10^{-6}$	86.34	85.16	82.72	82.02	80.04
$11x10^{-6}$	88.29	86.73	84.32	83.49	81.57

Table (2.5): Synergism parameter (S_θ) for various concentrations of different arylazo curcumin compounds in the presence of $1X10^{-2}$ M KSCN. Duration of the experiment: 120 min. immersion.

Concentration (M)	Synergism parameter (S_θ)				
	2a	2b	2c	2d	2e
$1x10^{-6}$	0.832	1.031	1.008	0.998	0.986
$3x10^{-6}$	1.117	1.046	1.009	0.995	0.973
$5x10^{-6}$	1.169	1.090	1.058	1.021	1.006
$7x10^{-6}$	1.245	1.138	1.103	1.063	1.014
$9x10^{-6}$	1.310	1.128	1.129	1.095	1.018
$11x10^{-6}$	1.463	1.182	1.224	1.146	1.033

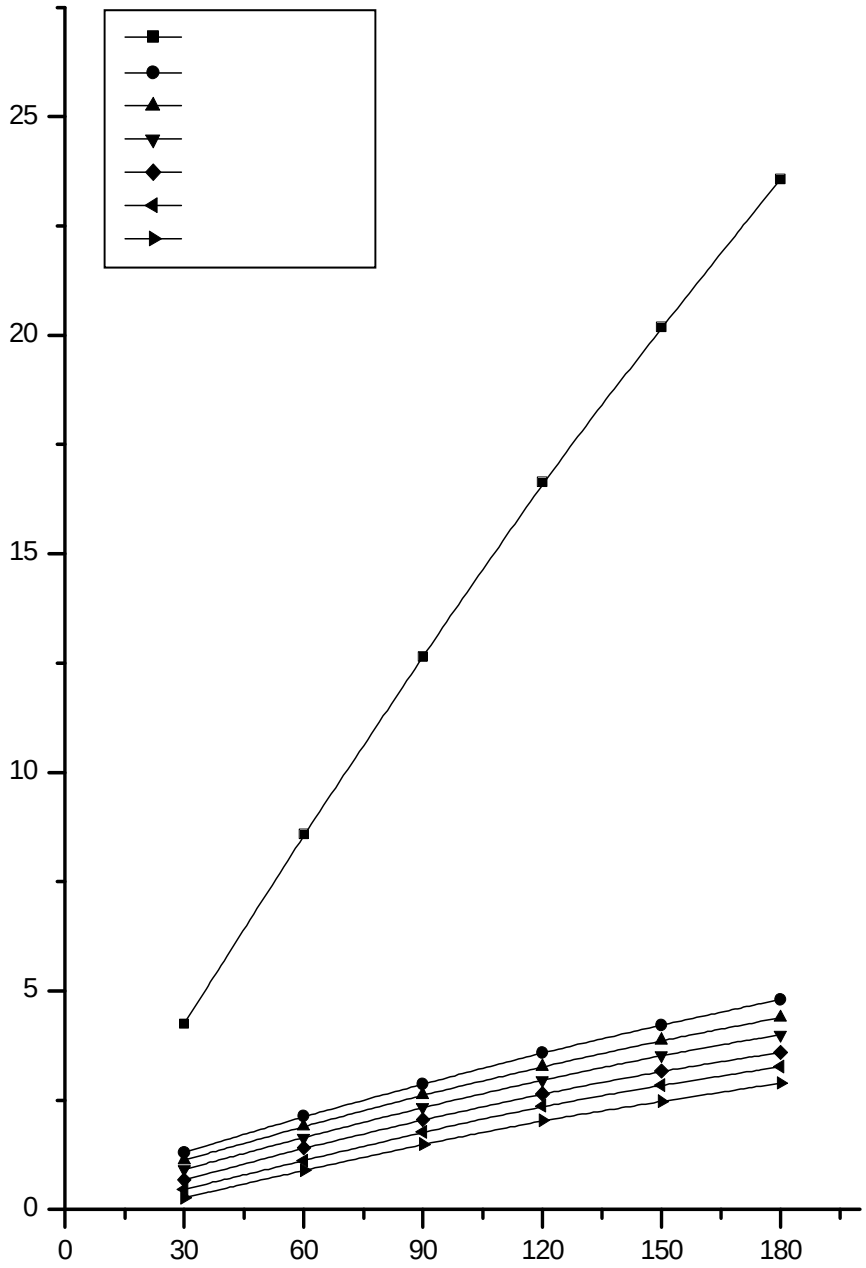
25
20
15
10
5
0
0
30
60
90
120
150
180

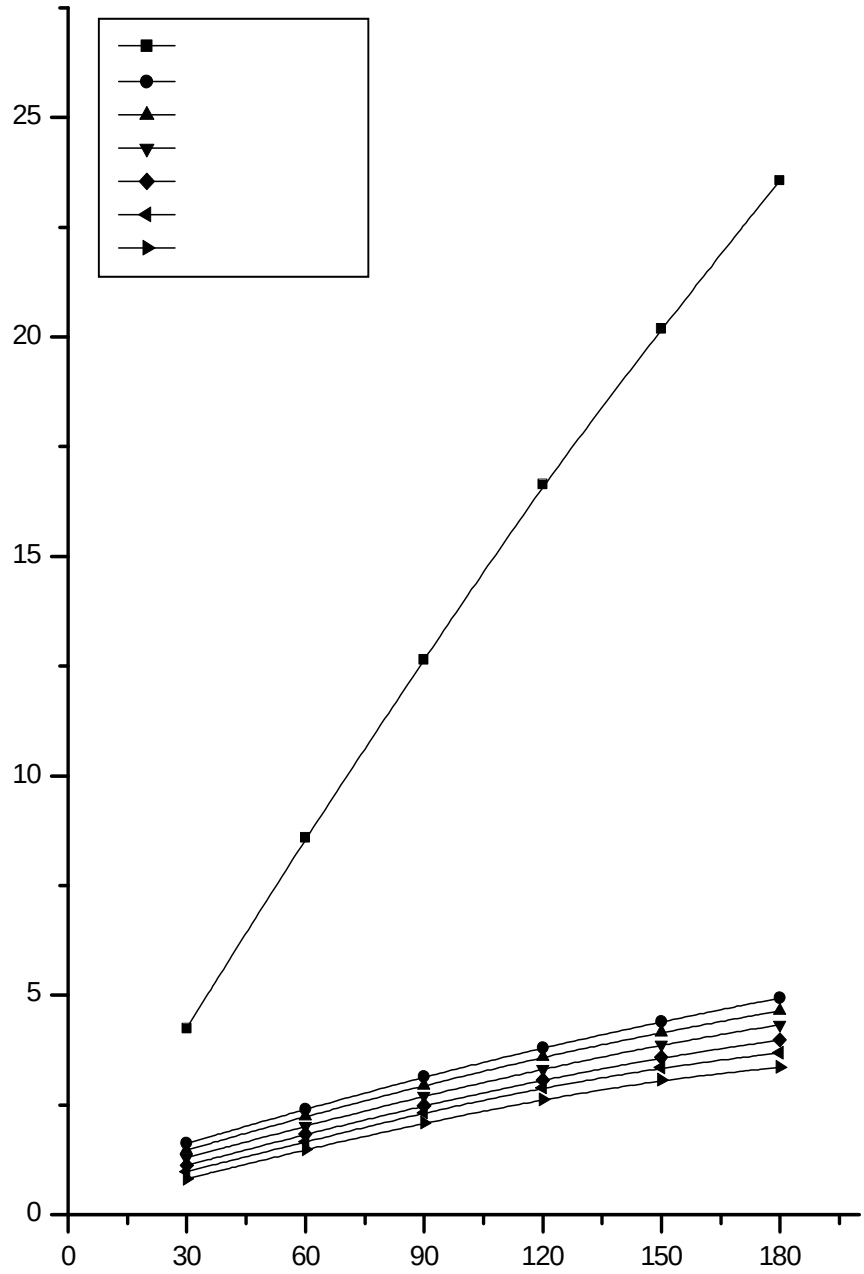
25
20
15
10
5
0
0
30
60
90
120
150
180

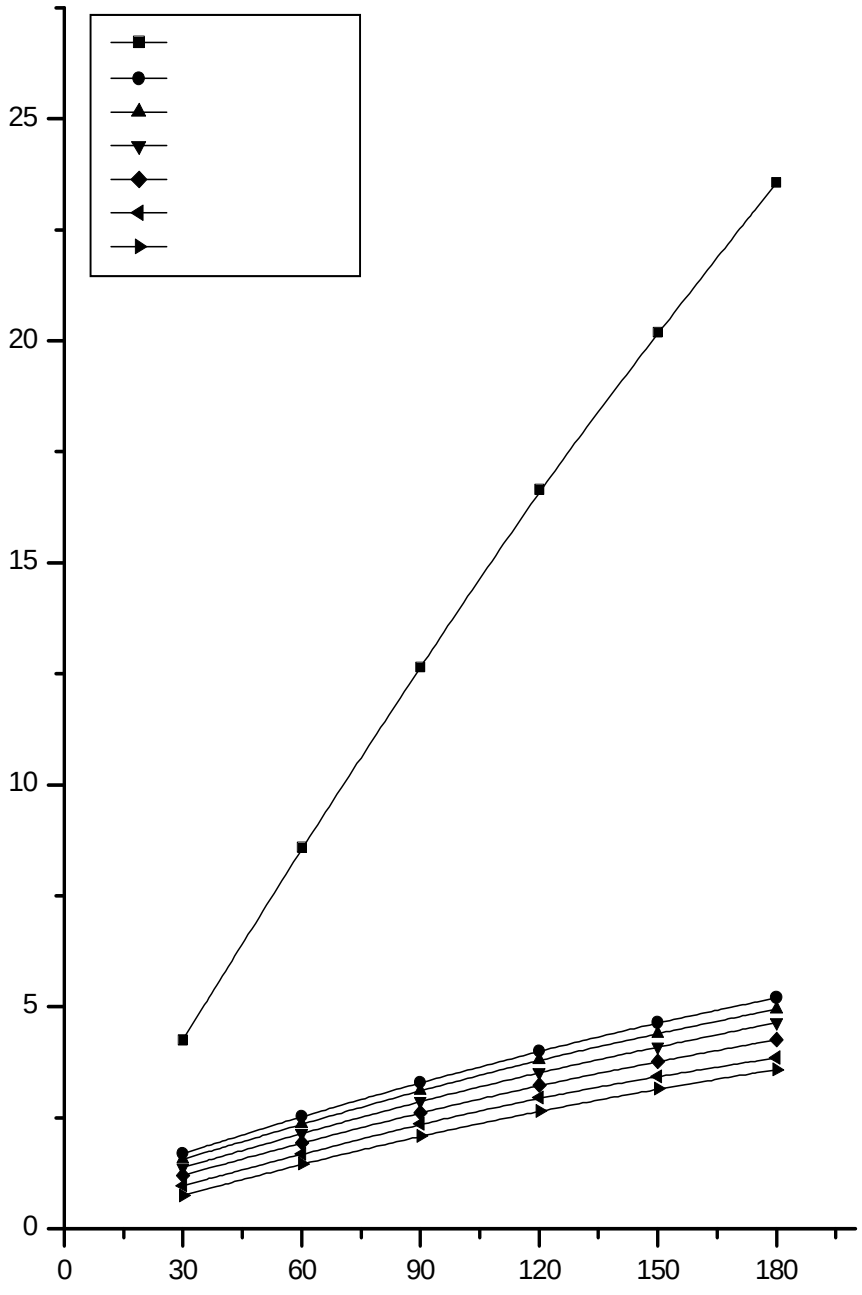
25
20
15
10
5
0
0
30
60
90
120
150
180

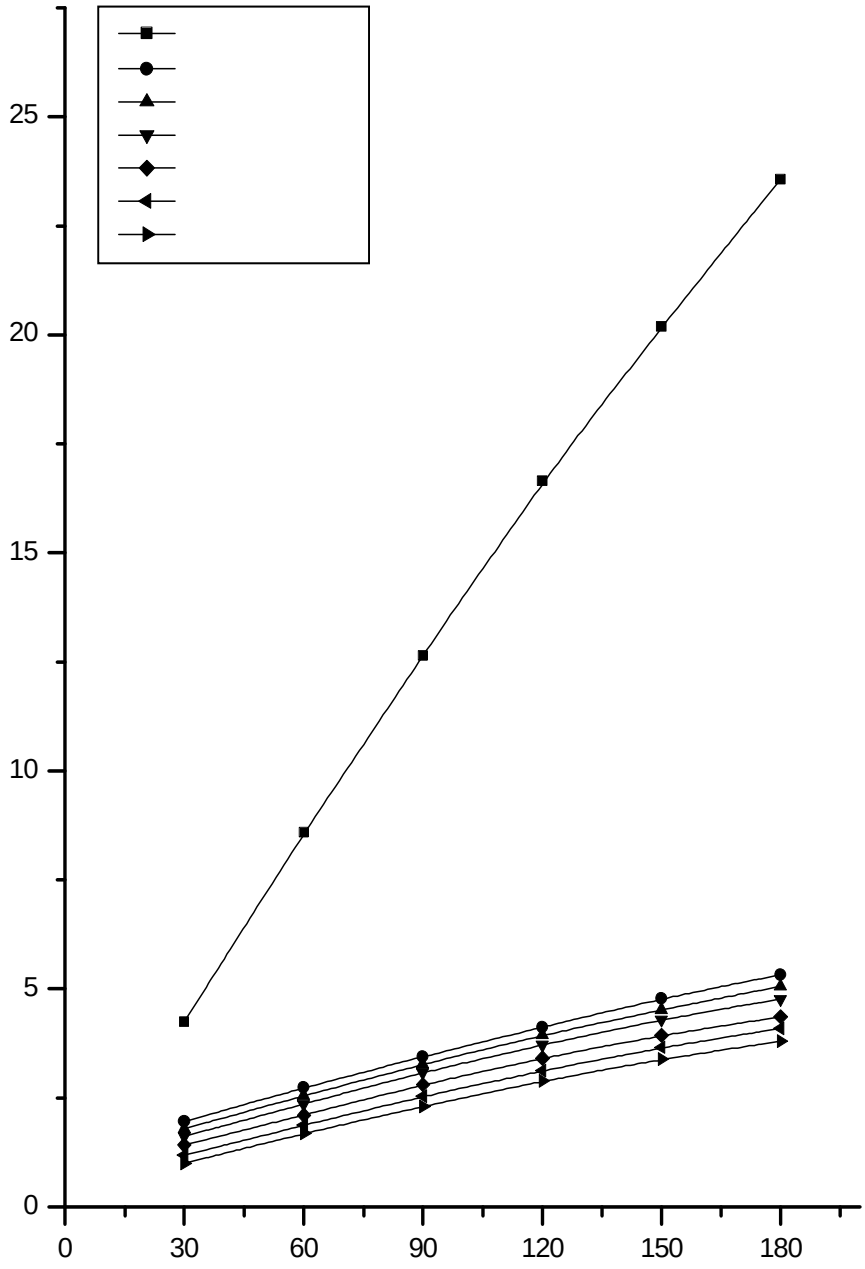
25
20
15
10
5
0
0
30
60
90
120
150
180

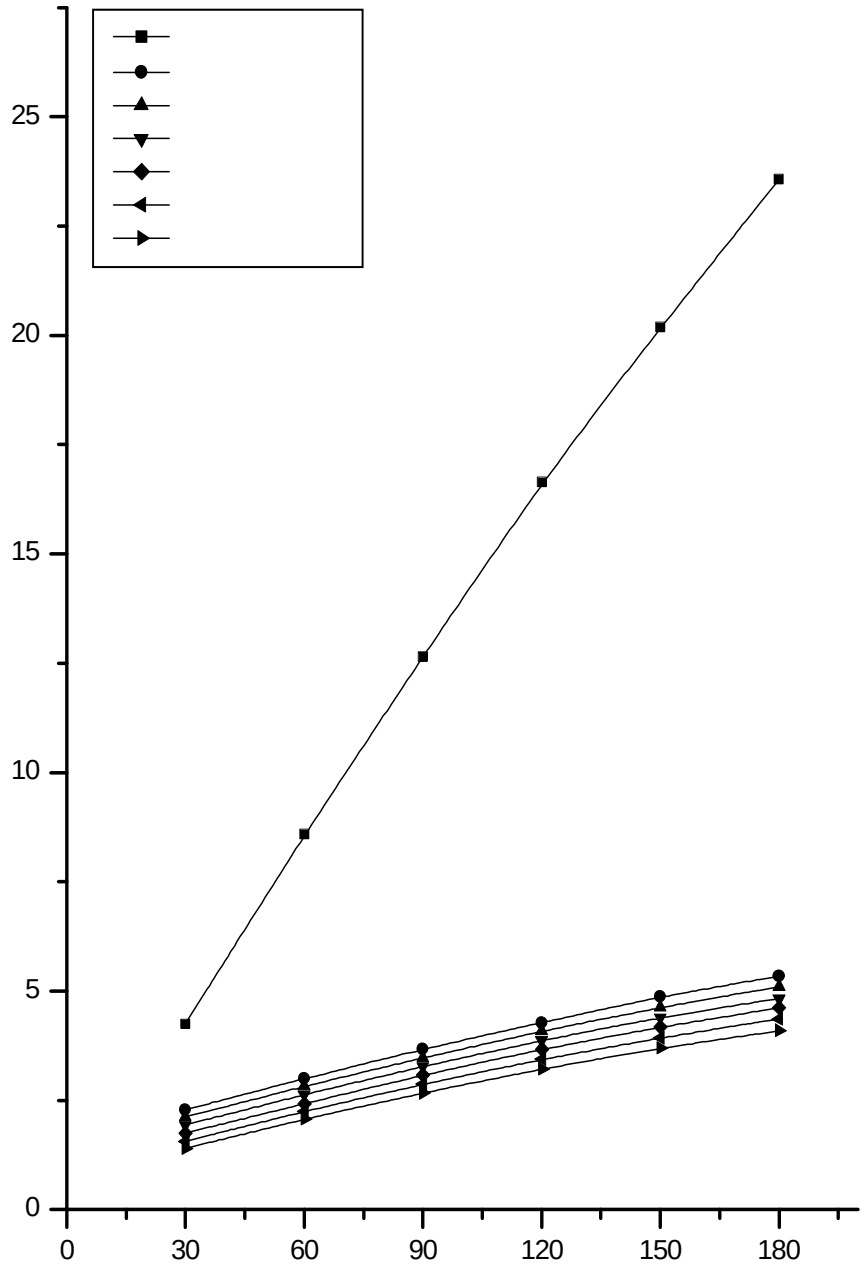
25
20
15
10
5
0
0
30
60
90
120
150
180

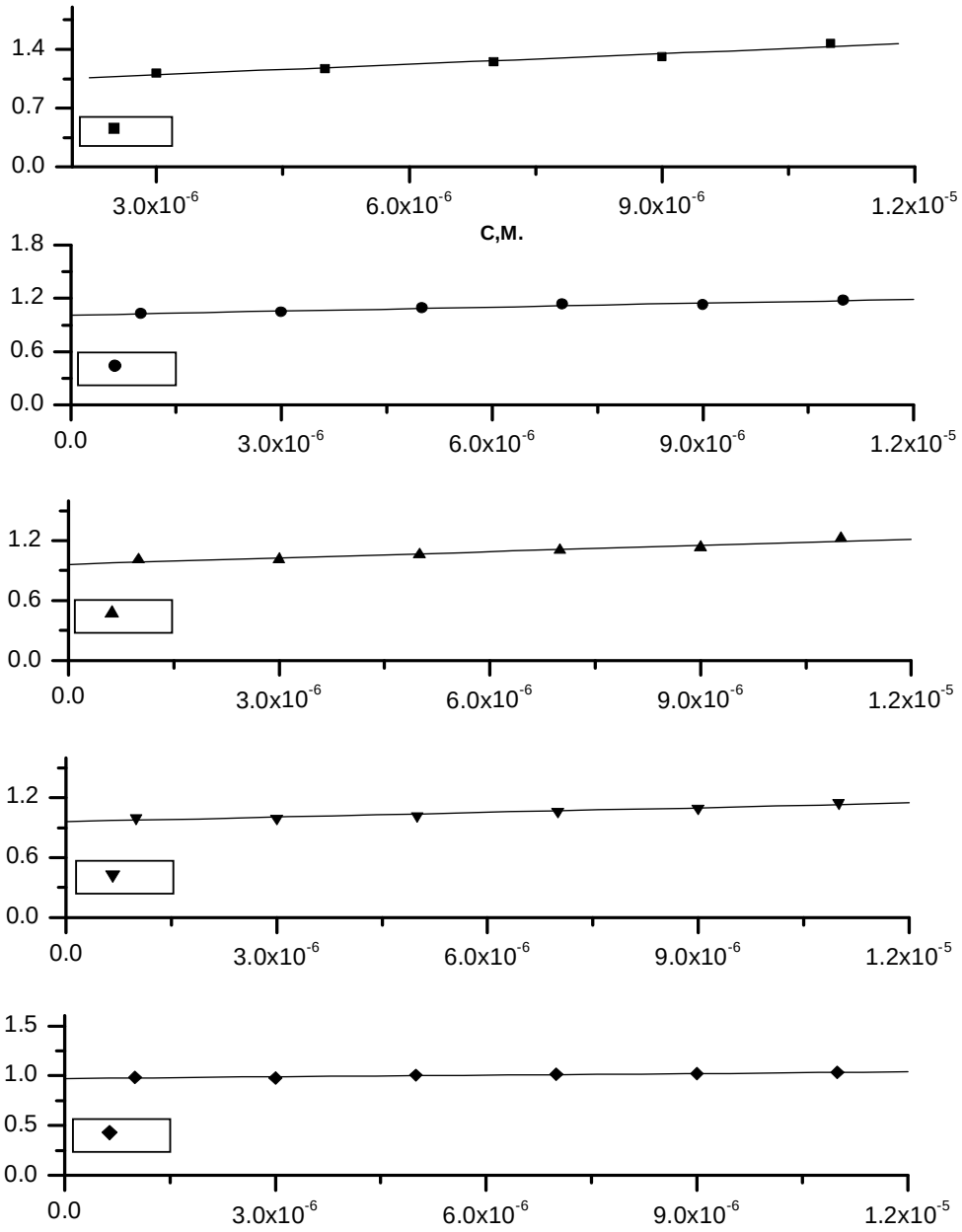
1.4
0.7
0.0
3.0x10-6
6.0x10-6
9.0x10-6
1.2x10-5
C,M.
1.8
1.2
0.6
0.0
0.0
3.0x10-6
6.0x10-6
9.0x10-6
1.2x10-5
1.2
0.6
0.0
0.0
3.0x10-6
6.0x10-6
9.0x10-6
1.2x10-5
1.2
0.6
0.0
0.0
3.0x10-6
6.0x10-6
9.0x10-6
1.2x10-5
1.5
1.0
0.5
0.0
0.0
3.0x10-6
6.0x10-6
9.0x10-6
1.2x10-5

5. Effect of substituted groups:

As shown previously that the inhibition efficiency depends essentially on the electron density at the active centers of the inhibitor molecule.The subsequent step is to follow the effect of substituted group wether increase or decrease the inhibition efficiency through its effect on the active centers ,i.e: electron donating or withdrawing groups .

The substituted groups studied are [OCH_3, CH_3] which are located in para- positions of phenyl ring. The overlap between the inhibitor electron rich centers and empty d-orbitals increases in case of (OCH_3) more than (CH_3) due to the lone pair of electrons located on the oxygen atom of the (OCH_3), H atom in para position has no effect on electron density, Cl and nitro group are electron withdrawing group and their order of inhibition depends on the magnitude of their withdrawing character. Finally, the order of inhibition efficiency of these compounds **(2a-e)** from weight loss technique follows the following order Table (2.1).

$$\textbf{\textit{p}-OCH}_3 > \textbf{\textit{p}-CH}_3 > \textbf{\textit{p}-H} > \textbf{\textit{p}-Cl} > \textbf{\textit{p}-NO}_2$$

6. Electrochemical technique:

Electrochemical techniques are based on current and potential measurements. According to the choice of the technique accurate and confidential data, concerning the corrosion process, can be obtained.

6.1- Galvanostatic polarization technique:

Galvanostatic polarization curves of α-brass in 2M nitric acid in the absence and presence of different concentrations of arylazo curcumin compounds at 30^{o}C are illustrated in **Figs.(45-49)**. The numerical values of the variation of corrosion current density ($i_{corr.}$), corrosion potential ($E_{corr.}$), Tafel slopes (β_a and β_c), percentage inhibition efficiency (%In) and degree of surface coverage (θ) with the concentrations of different arylazo curcumin compounds are given in Tables (2.7-2.10). From these Tables one can conclude that:

1- The cathodic and anodic curves obtained exhibit Tafel-type behavior. Addition of arylazo curcumin compounds increases both cathodic and anodic overvoltages and causes mainly parallel displacement to more negative and positive values, respectively.

2- The corrosion current density (icorr.) decreases with increasing the concentration of arylazo curcumin compounds, which indicates that the presence of these compounds retards the dissolution of α-brass in 2M nitric acid solution and the degree of inhibition depends on the concentration and type of the inhibitor present.

3- The order of decreased inhibition efficiency of arylazo curcumin compounds is: **2a> 2b > 2c >2d>2e**

This is also in agreement with the observed order of percentage inhibition efficiency calculated from weight loss method.

4- The data suggested that these compounds act as mixed type inhibitors i,e enhances both the anodic and cathodic reactions but the cathode is more polarized when an external current was applied.

5- The corrosion potential ($E_{corr.}$) values shifted to less negative values by increasing the concentration of arylazo curcumin compounds.

Table(2.6): Percent inhibition efficiency from galvanosatic polarization of α-brass containing various concentrations of all compounds used in 2M HNO_3 at 30°C.

Concentration (M)	Inhibition efficiency (%In)				
	2a	2b	2c	2d	2e
$1x10^{-6}$	21.38	18.4	16.3	15.5	12.4
$3x10^{-6}$	24.9	23.1	20.8	19.2	18.1
$5x10^{-6}$	29.35	26.3	23.7	21.9	20.3
$7x10^{-6}$	33.12	28.98	25.9	25.3	23.7
$9x10^{-6}$	37.98	34.2	31.32	29.7	28.9
$11x10^{-6}$	40.18	37.2	33.8	32.76	31.1

Table (2.7): The effect of concentration of compound (2a) on the free corrosion potential ($E_{corr.}$), corrosion current density ($i_{corr.}$), Tafel slopes (β_a & β_c) and degree of surface coverage (θ) for α-brass in 2M HNO_3 at 30°C.

Concentration, M.	$-E_{corr.}$, mV	$i_{corr.}$, μA cm^{-2}	β_a, mV dec^{-1}	$-\beta_c$, mV dec^{-1}	θ
0	720	168.63	55	57	-
$1x10^{-6}$	724	132.58	80	68	0.214
$3x10^{-6}$	724	126.64	86	77	0.249
$5x10^{-6}$	725	119.14	90	87	0.293
$7x10^{-6}$	726	112.78	97	97	0.331
$9x10^{-6}$	726	104.59	105	100	0.380
$11x10^{-6}$	727	100.87	122	110	0.402

Table (2.8): The effect of concentration of compound (2b) on the free corrosion potential ($E_{corr.}$), corrosion current density ($i_{corr.}$), Tafel slopes (β_a & β_c) and degree of surface coverage (θ) for α-brass in 2M HNO_3 at 30°C.

Concentration, M.	$-E_{corr.}$, mV	$i_{corr.}$, μA cm^{-2}	β_a, mV dec^{-1}	$-\beta_c$, mV dec^{-1}	θ
0	720	168.63	55	57	-
$1x10^{-6}$	723	137.60	75	66	0.184
$3x10^{-6}$	724	129.68	82	72	0.231
$5x10^{-6}$	725	124.28	91	79	0.263
$7x10^{-6}$	725	119.76	100	92	0.290
$9x10^{-6}$	726	110.96	109	106	0.342
$11x10^{-6}$	727	105.90	122	125	0.372

Table (2.9): The effect of concentration of compound (2c) on the free corrosion potential ($E_{corr.}$), corrosion current density ($i_{corr.}$), Tafel slopes (β_a & β_c) and degree of surface coverage (θ) for α-brass in 2M HNO_3 at 30°C.

Concentration, M.	$-E_{corr.}$, mV	$i_{corr.}$, μA cm^{-2}	β_a, mV dec^{-1}	$-\beta_c$, mV dec^{-1}	θ
0	720	168.63	55	57	-
$1x10^{-6}$	723	141.14	71	67	0.163
$3x10^{-6}$	723	133.55	76	75	0.208
$5x10^{-6}$	724	128.66	92	85	0.237
$7x10^{-6}$	724	124.95	101	103	0.259
$9x10^{-6}$	725	115.82	113	118	0.313
$11x10^{-6}$	726	111.63	134	130	0.338

Table (2.10): The effect of concentration of compound (2d) on the free corrosion potential ($E_{corr.}$), corrosion current density ($i_{corr.}$), Tafel slopes (β_a & β_c) and degree of surface coverage (θ) for α-brass in 2M HNO_3 at 30°C.

Concentration, M.	$-E_{corr.}$, mV	$i_{corr.}$, μA cm^{-2}	β_a, mV dec^{-1}	$-\beta_c$, mV dec^{-1}	θ
0	720	168.63	55	57	-
$1x10^{-6}$	723	142.49	62	58	0.155
$3x10^{-6}$	723	136.25	71	71	0.192
$5x10^{-6}$	724	131.70	83	83	0.219
$7x10^{-6}$	725	125.97	102	104	0.253
$9x10^{-6}$	726	118.55	123	118	0.297
$11x10^{-6}$	726	113.39	139	133	0328

Table (2.11): The effect of concentration of compound (2e) on the free corrosion potential ($E_{corr.}$), corrosion current density ($i_{corr.}$), Tafel slopes (β_a & β_c) and degree of surface coverage (θ) for α-brass in 2M HNO_3 at 30°C.

Concentration, M.	$-E_{corr.}$, mV	$i_{corr.}$, μA cm^{-2}	β_a, mV dec^{-1}	$-\beta_c$, mV dec^{-1}	θ
0	720	168.63	55	57	-
$1x10^{-6}$	722	147.72	59	57	0.124
$3x10^{-6}$	723	138.11	67	66	0.181
$5x10^{-6}$	723	134.40	84	80	0.203
$7x10^{-6}$	724	128.66	103	108	0.237
$9x10^{-6}$	724	119.89	124	126	0.289
$11x10^{-6}$	725	112.64	153	147	0.311

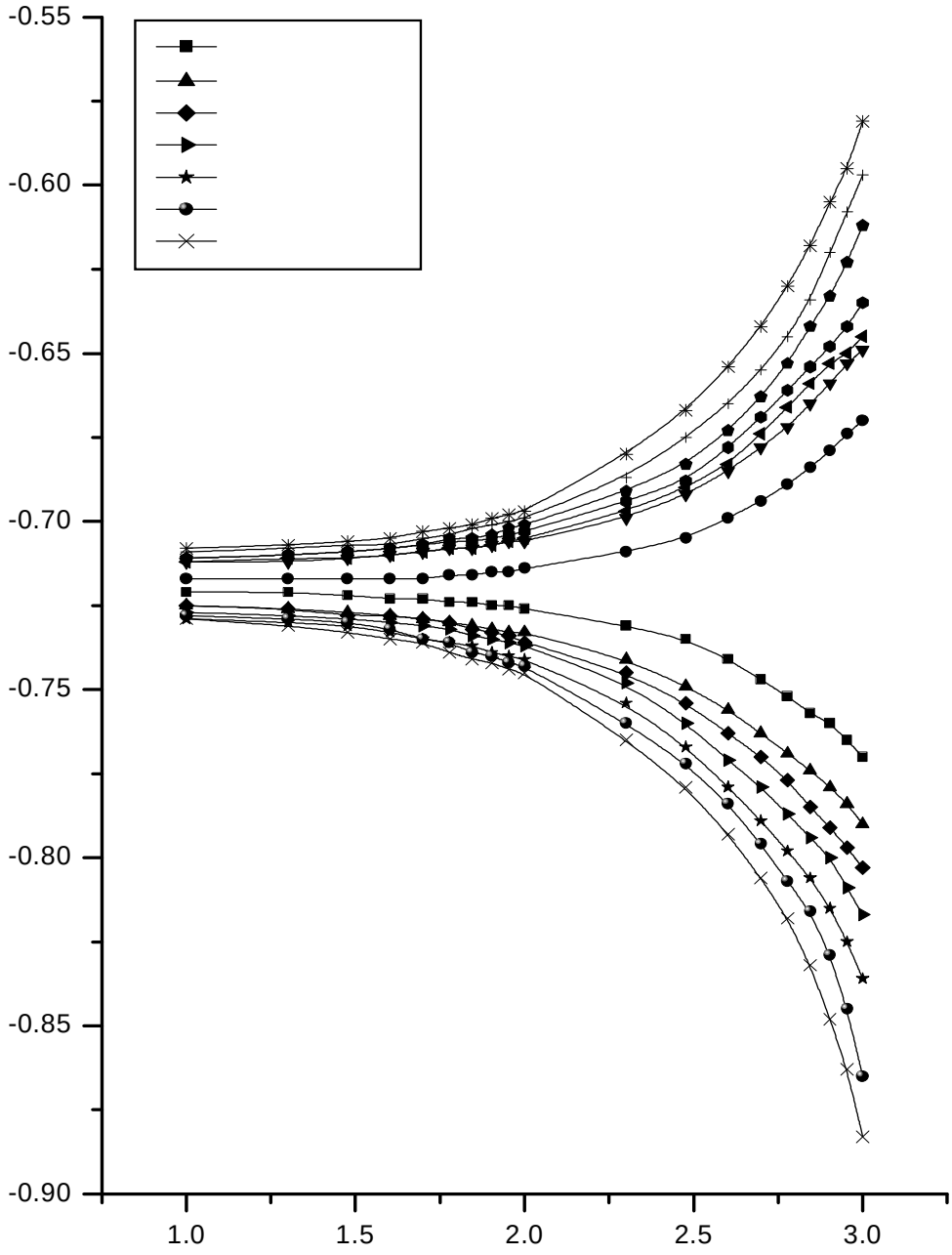
-0.55
-0.60
-0.65
-0.70
-0.75
-0.80
-0.85
-0.90
1.0
1.5
2.0
2.5
3.0

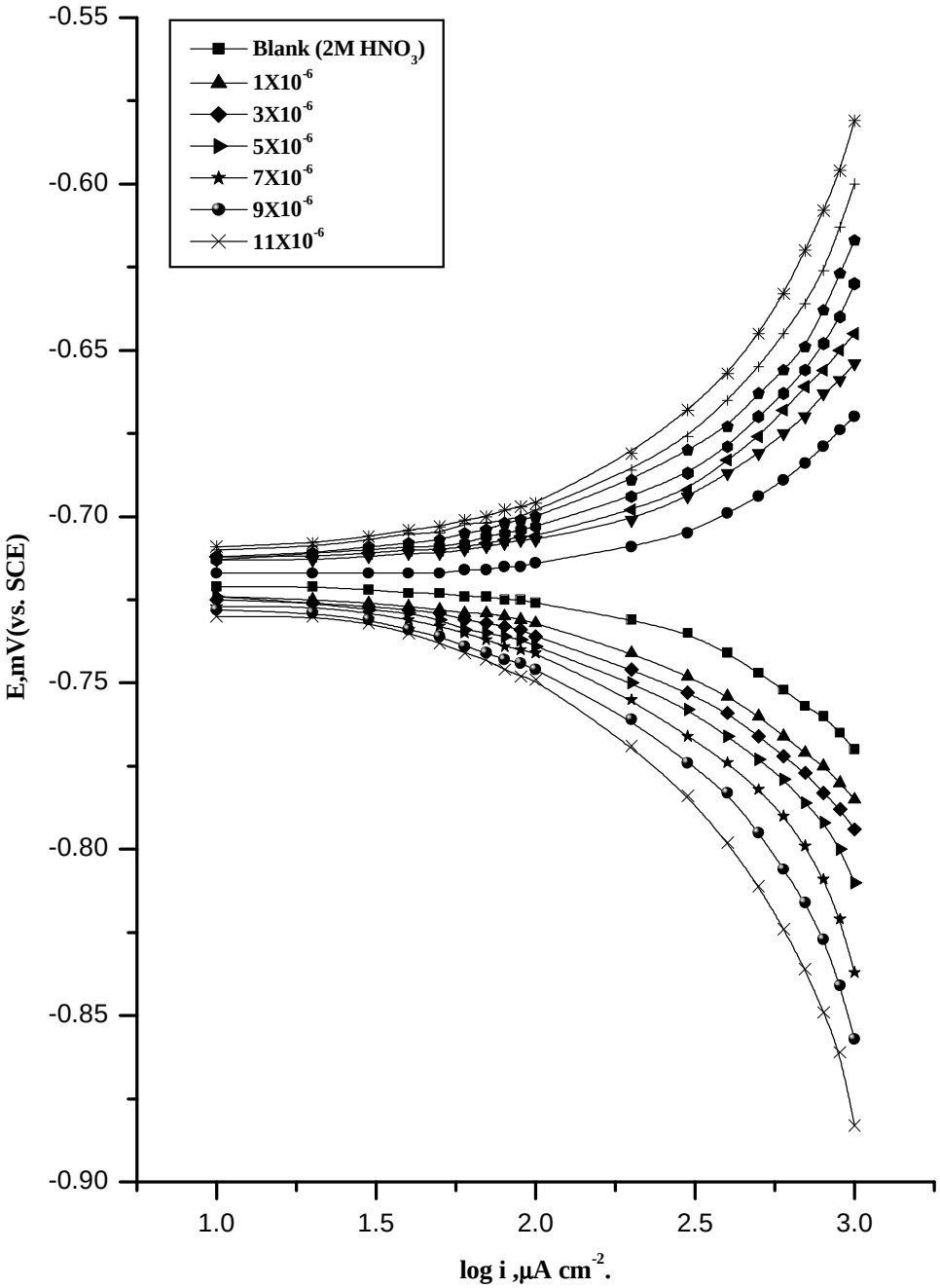

Fig.(46): Galvanostatic polarization curves of α-brass in 2M HNO_3 alone and containing different concentrations of compound (2b) at 30°C.

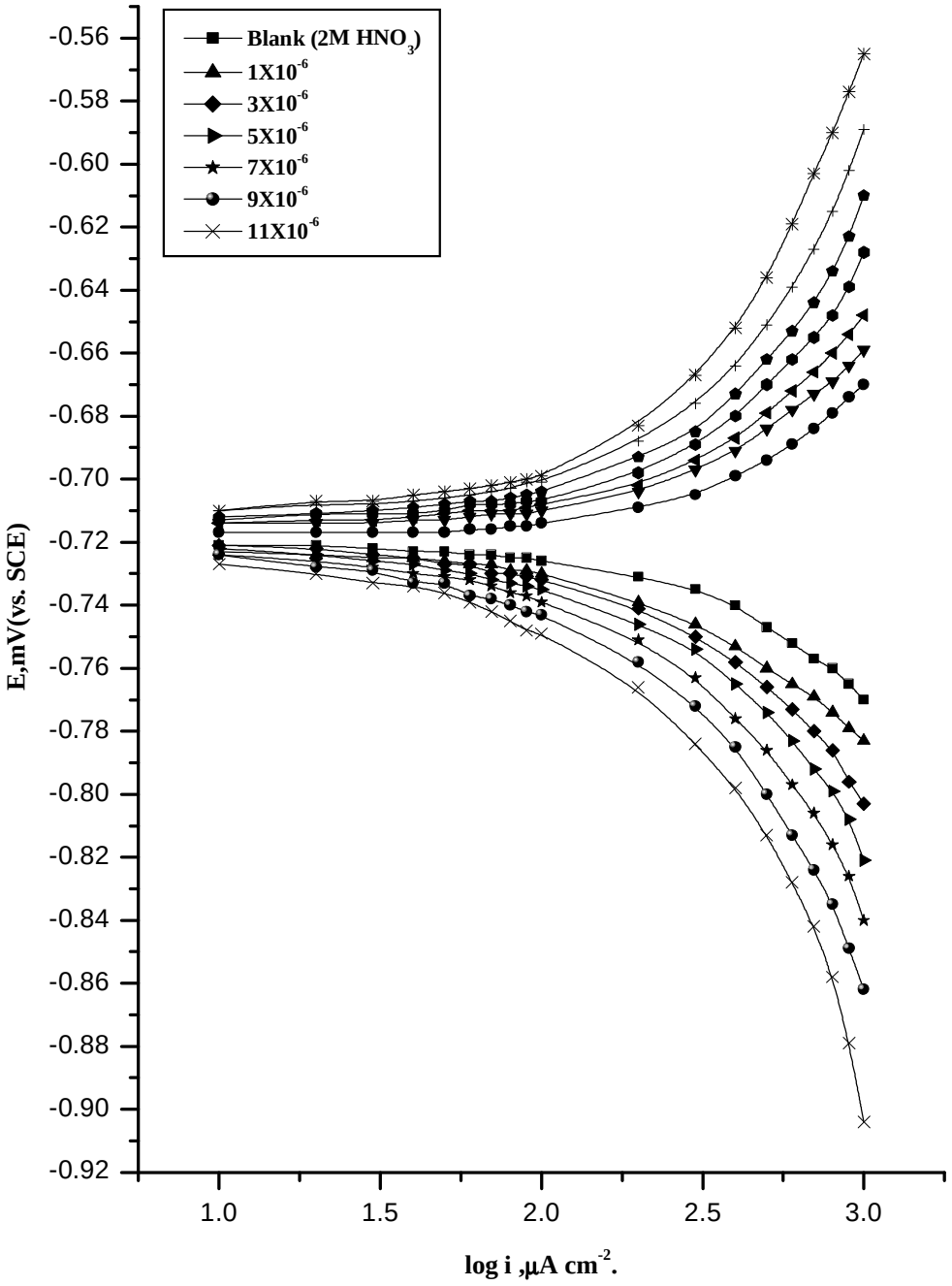

Fig.(47): Galvanostatic polarization curves of α-brass in 2M HNO_3 alone and containing different concentrations of compound (2c) at 30°C.

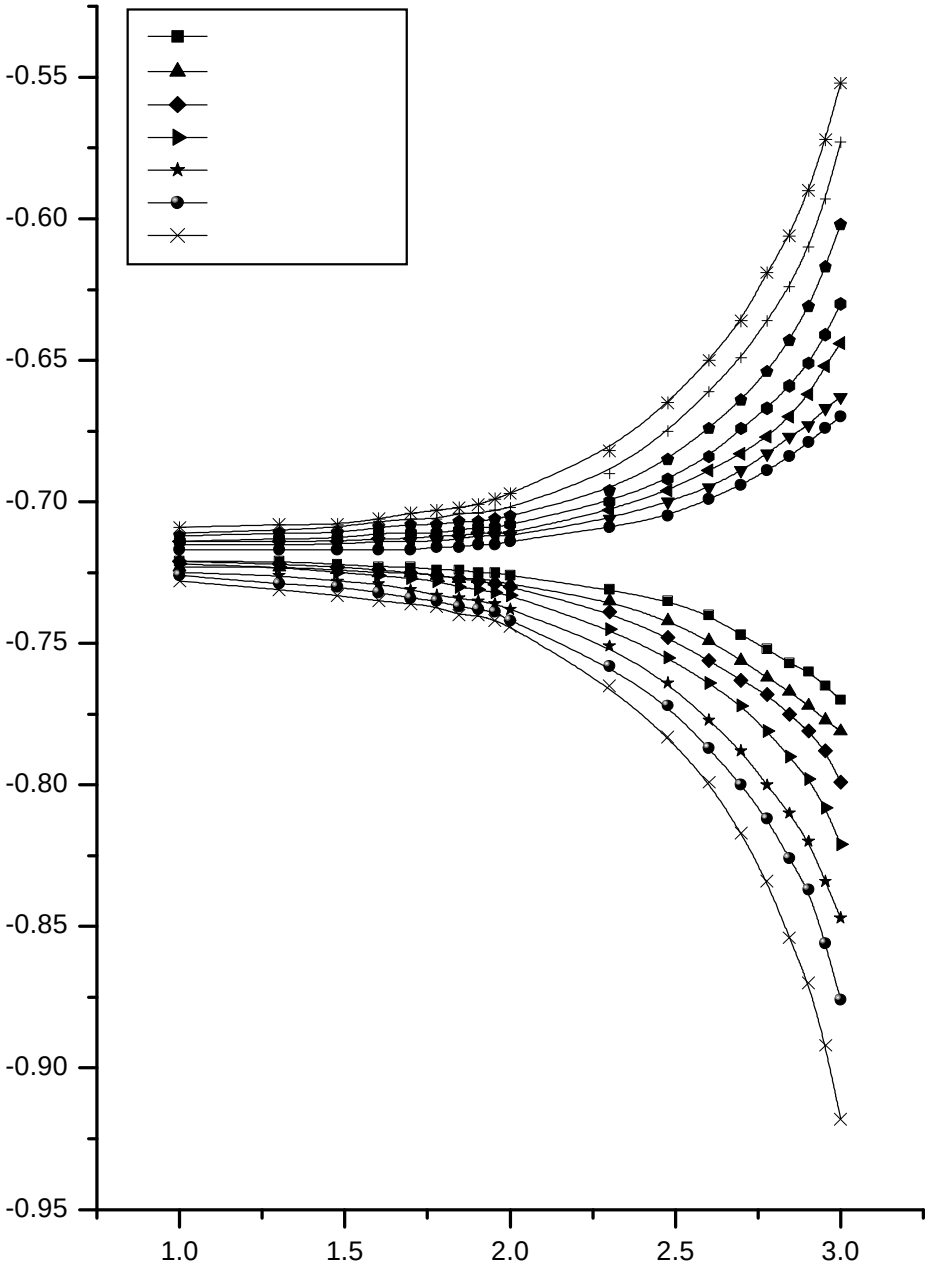
-0.55
-0.60
-0.65
-0.70
-0.75
-0.80
-0.85
-0.90
-0.95
1.0
1.5
2.0
2.5
3.0

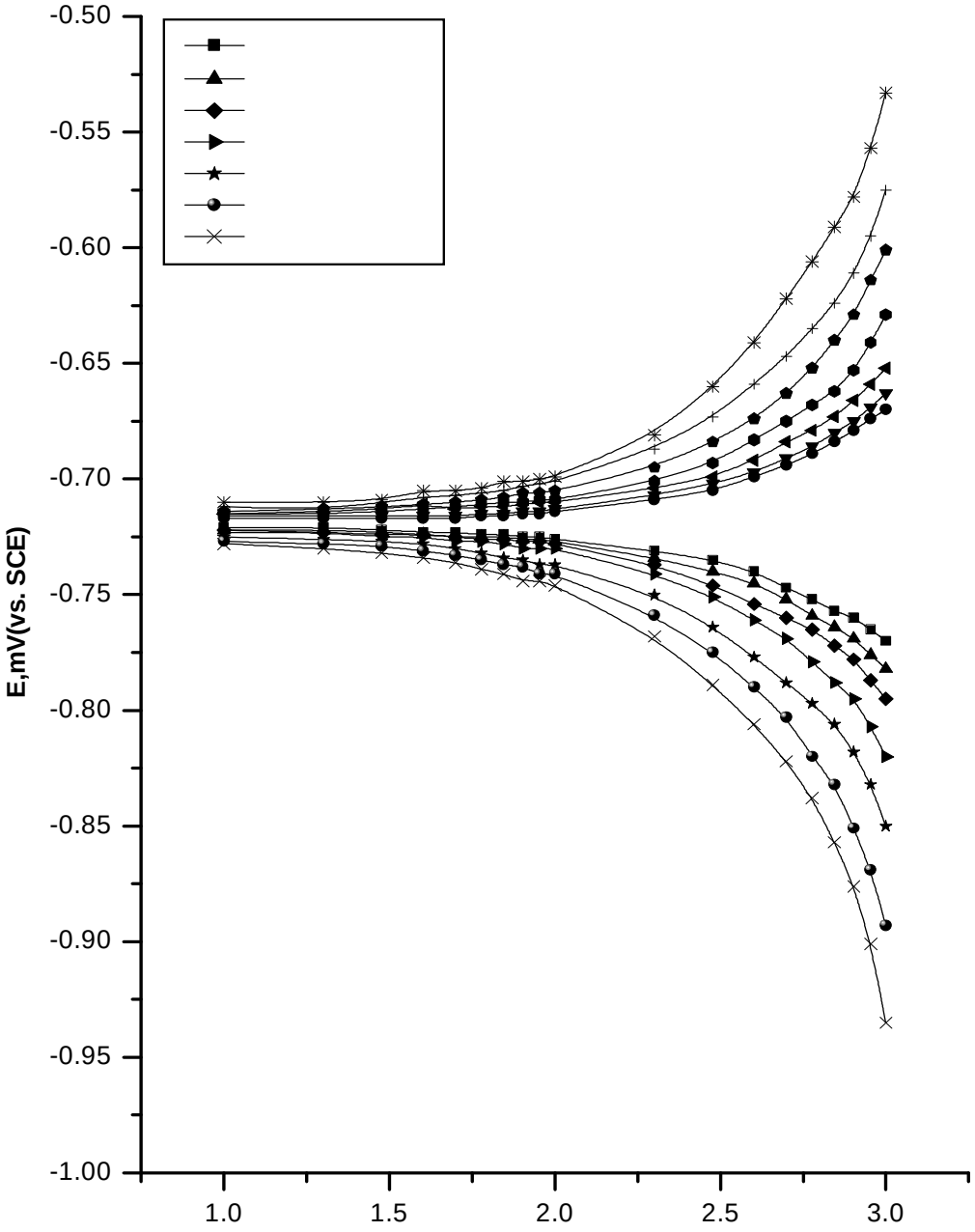
-0.50
-0.55
-0.60
-0.65
-0.70
-0.75
-0.80
-0.85
-0.90
-0.95
-1.00
E,mV(vs. SCE)
1.0
1.5
2.0
2.5
3.0

6.2 Adsorption Isotherms :

Figure (50) represents the relation between θ and log C of the inhibitors **(2a-e)**. The Frumkin's adsorption isotherm is obeyed. From this results it could be concluded that there is a kind of interaction between the molecules adsorbed at the metal surface. This is in agreement with weight loss measurements as shown before .

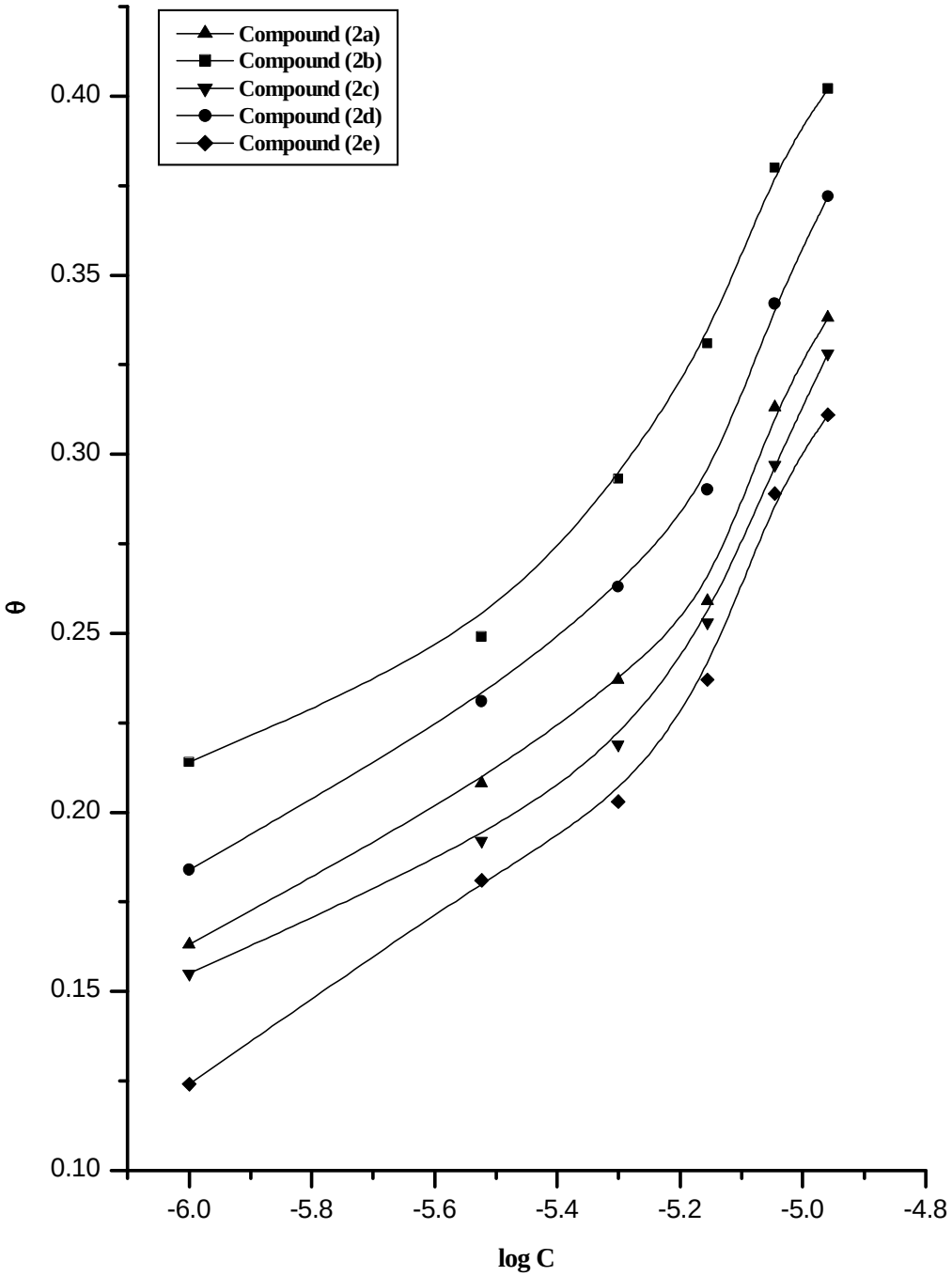

Fig.(50):Log(C) vs. (θ) curves for the diffrent compounds

6.3. Chemical structure and corrosion inhibition of α -brass*:*

Inhibition of the corrosion of α-brass in 2M HNO_3 solution by some arylazo curcumin derivatives is determined by galvanostatic polarization measurements was found to depend on concentration, nature of metal, the mode of adsorption of the inhibitors and surface conditions.

Skeletal representation of the proposed mode of adsorption of the investigated arylazo curcumin derivatives as shown in **Fig.(52)** and clearly indicates the active adsorption centers in the arylazo curcumin derivatives. These compounds can be adsorbed in a flat orientation through the oxygen of two (OH) groups / two (OCH_3) groups and one (N) of the azo group.

The surface coordination is through the nitrogen atoms. It was concluded that the mode of adsorption depends on the affinity of the metal towards the π-electron clouds of the ring system.[168] Metals such as Cu and Fe, which have a greater affinity towards aromatic moieties, were found to adsorb benzene rings in a flat orientation. Thus, it is reasonable to assume that the tested inhibitors are adsorbed in a flat orientation through the N- and O- atoms as shown in **Fig.(52)**. The order of decreasing the percentage inhibition efficiency of the investigated inhibitors in the corrosive solutions was as follow:

2a > 2b> 2c> 2d > 2e

This behavior can be rationalized on the basis of the structure - corrosion inhibition relationship of organic compounds. Linear Free Energy Relationships (LFER) has previously been used to correlate the inhibition efficiency of organic compounds with their Hammett constituent constants (σ).[169] The LFER or Hammett relation is given by.[170-172]

Log R (rate of corrosion) = $-\rho\sigma$

where ρ is the reaction constant. Those constituents which attract electrons from the reaction center are assigned positive σ values and those which are electron donating have negative σ values. Thus, σ is a relative measure of the electron density at the reaction center. The slope of the plot of log (rate) vs. σ is ρ, and its sign indicates whether the process is inhibited by an increase or decrease of the electron density at the reaction center .The magnitude of ρ indicates the relative sensitivity of the inhibition process to electronic effects. **Fig.(51)** shows that curcumin derivatives **(2a-e)** give a good correlation .The large positive slope of the correlation line (ρ = + 0.994) shows a strong dependence of the adsorption character of the reaction center on the electron density of the ring. The strong dependence of the adsorption character of the reaction center on the electron density of the ring may be due to the fact that in this type of derivatives the center of adsorption is conjugated to the ring.

Compound **(2a)** has the highest percentage inhibition efficiency, this due to the presence of *p*-OCH_3 group which is an electron repelling group with negative Hammett constant (σ = -0.27) this group will increase the electron charge density on the molecule. Compound **(2b)** comes after compound **(2a)**, this is due to the presence of *p*-CH_3 group which is an electron donating group with negative Hammett constant (σ = -0.17), Also this group will increase the electron charge density on the molecule but with lesser amount than *p*-OCH_3 group in compound **(2a)**. Compound **(2c)** with Hammett constant (σ = 0.0) comes after compound **(2b)** in percentage inhibition efficiency, because H- atom in *p*-position has no effect on the charge density on the molecules. Compound **(2d)** and **(2e)** come after compound **(2c)** in percentage inhibition efficiencies. This is due to both *p*-Cl and *p*-NO_2 groups are electron withdrawing groups with positive

Hammett constants (σ_{Cl} = +0.23, σ_{NO2} = + 0.78) and their order of inhibition depends on the magnitude of their withdrawing character.

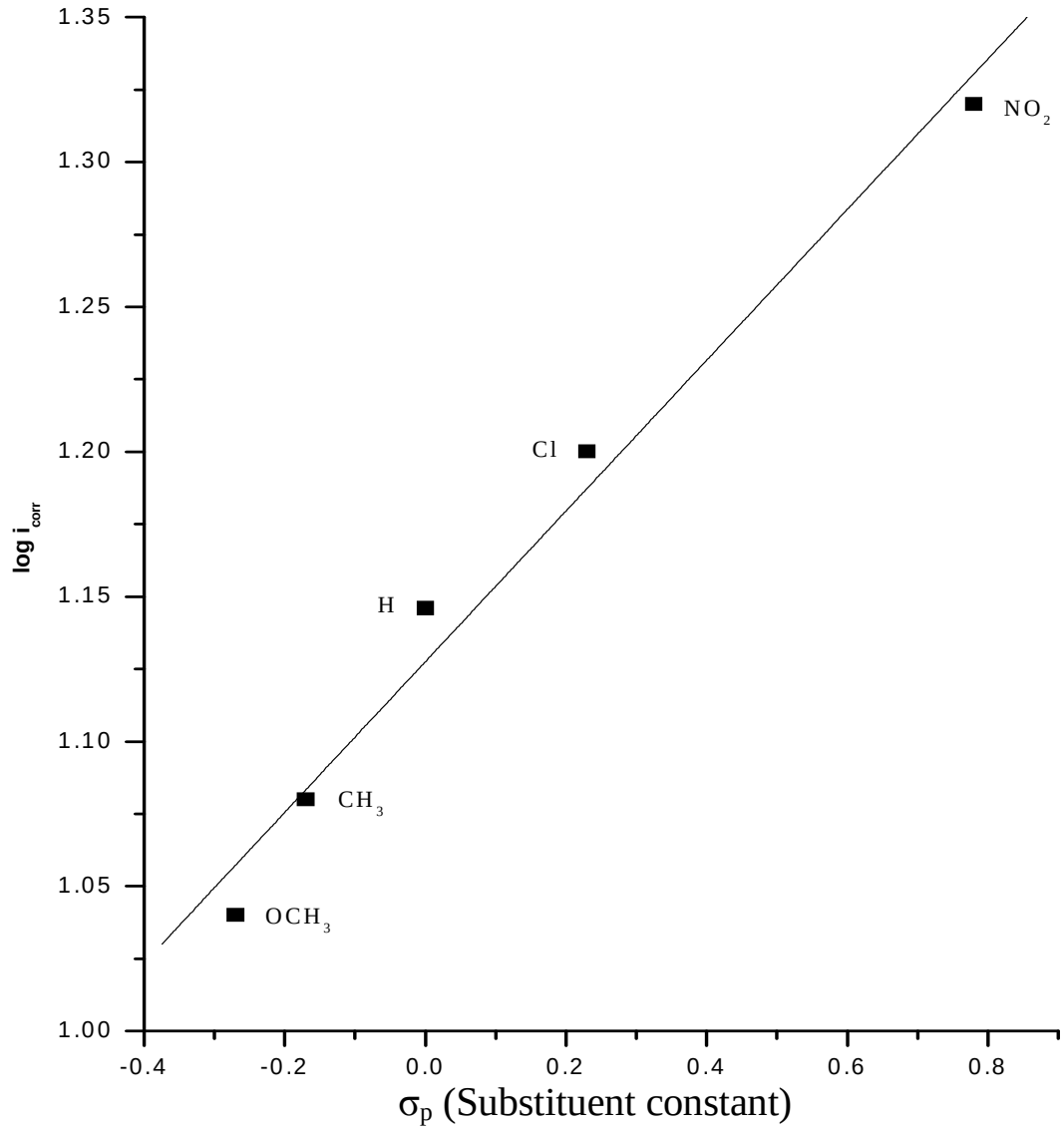

Fig.51. Relation between log corrosion current density, log i_{corr}, and Hammett constants, σ_p of the Substituents from polarization measurements

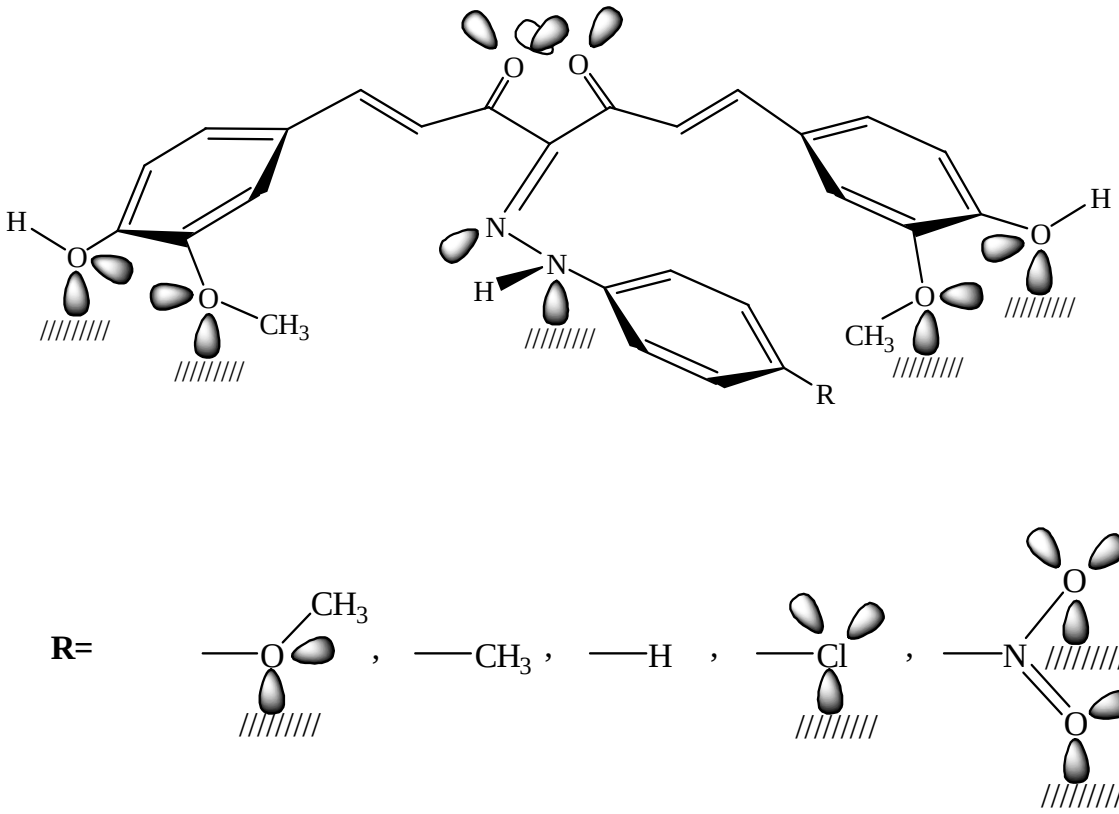

R=

compounds, 2a 2b 2c 2d 2e

Fig.(52): Skeletal representation of the mode of adsorption of curcumin Compounds.